Low frequency measurements on generator insulation

Black, David Franklin

LOW FREQUENCY MEASUREMENTS ON GENERATOR INSULATION

by

David Franklin Black B.Sc.

A thesis presented to the University of Durham, Department of Engineering Science, for the degree of Master of Science.
Research conducted at C.A. Parsons & Co., Ltd., Newcastle Upon Tyne.

JUNE 1977

TO "JIM"

(C.G.G.)

CONTENTS

TABLES

DIAGRAMS AND ILLUSTRATIONS

ACKNOWLEDGEMENT

The author gratefully acknowledges C.A. Parsons & Co. Ltd., Newcastle upon Tyne and the Central Electricity Generating Board for permission to present the work of this research programme for the degree of Master of Science.

The author wishes to thank the following for their support, supervision and encouragement: Dr. E.C. Salthouse (Reader in Electrical Science, Department of Engineering Science, University of Durham), Mr. J.A. Denham (Electrical Research Manager) and Mr. J.W. Wood (Group Leader, Insulation Engineering) both of C.A. Parsons & Co. Ltd., Newcastle upon Tyne. The author is grateful to Mr. J.W. Wood for the information received which led to the preparation of the sections on conventional discharge detection and measuring instruments.

Sincere thanks are also due to Mrs. Marie Malia for her diligence and patience in typing and correcting the final manuscript.

The author wishes to thank Mr. C.G. Garton for his continued interest and encouragement shown during the present experimental work and also for his informal 'lectures' on the physics of dielectrics.

Last but by no means least, I would like to thank my wife Lesley for her continued help, patience and encouragement during the work.

ABSTRACT

This thesis describes an experimental arrangement which has proved successful in the measurement of one of the most significant quantities as regards the deterioration of insulation, namely discharge energy loss/cycle. The arrangement was used at very low frequency (0.1 Hz) and recorded discharge energy loss/cycle in thermally aged sections of 500 MW stator bars with micaceous insulation.

The purpose of thermally ageing the stator bar sections was to create both large and small voids within the insulation, the intention being:

(1) To measure the change of discharge energy loss/cycle with ageing time of the sections.

(2) To differentiate between both the large and small voids created in the sections.

Whilst it was possible to show the increase of discharge energy loss/cycle with ageing time, it was not possible, with the present experimental arrangement, to detect voids of differing dimensions. This was because of surface discharge across the guard electrode interspace, and lack of precision in the measurements. However, it is believed that a proposed system will be more successful. The present experimental arrangement responds to both large and small amplitude discharge pulses and is more sensitive than conventional integrating instruments used at power frequencies.

Tan δ due to discharge was measured on the stator bar sections at both 50 and 0.1 Hz, but on differing experimental arrangements. Apart from the initial ageing times of the specimens, varied approximately linearly over the range investigated, although they differed by a constant amount. Some of the difference was accounted for by only

measuring half the discharge energy loss/cycle because of commutation noise from the VLF generator, the other being unaccountable and due to the measurements of similar, but not necessarily equal quantities on different experimental arrangements.

During the experimental work, discharge inception voltage was found to be invariant with frequency.

1. INTRODUCTION

Until recently the demand for electricity has increased year by year. Accompanying this increase in demand there has been a corresponding increase in the size of electrical generators. Machines installed recently are rated at 500-660 MW but 1300 MW machines are being designed and 2000 MW machines are envisaged for the not too distant future. The reliability of such machines depends on, among other factors, the quality of the insulation system employed and its ability to maintain its insulating properties for the life of the machine. Lacotta and Fozard[1] have pointed out that the costs associated with the failure of such a machine, or breakdown of auxiliary high-voltage motors has lead to the development of test techniques which can be used to assess the quality of the stator insulation. Their reasons for this are:

i. "the high cost of outages"

ii. "the increased electrical and mechanical stresses on the insulation"

iii. "the newer types of insulation being introduced"

iv. "the greater reliance that is placed on these large units for base-load generation".

The methods commonly used to test the stator insulation include d.c. insulation resistance measurements at high and low voltages and a.c. measurements of the insulation loss angle over a range of applied voltages. More recently the use of insulation tests at low frequency (0.1 Hz) has been advocated to overcome some of the short comings of the traditional test methods. This thesis is concerned with the development of such tests and with discharge measurements at low frequency in particular.

1.1 Stator insulation

The types of coil used in the stator of large electrical machines include half coils, basket coils and hairpin coils. Half coils are used when the full coil would be too large to handle. The coil for a 500/660 MW machine is some 7.5m long and weighs some 250 Kg. Basket (or diamond) coils form a two layer winding. They are formed by hand or using a pulling machine, and are used on salient pole generators, synchronous capacitors and motors with outputs between 1 and 500 MW. Hairpin coils are restricted to machines with outputs between 1 and 15 MW.

The conductor stack is an important part of the coil. A well consolidated conductor stack is both mechanically and electrically sound and provides a structure suitable for the application of the main wall insulation. The conductor stack consists of single insulated copper strips which are transposed in the 'Roebel' fashion so that each strip successively occupies each position in the stack along the coil. Each strip in the stack is wrapped with a single half lapped layer of insulating tape. Nowadays the tape is epoxy resin impregnated mica on a glass backing material.

The insulated conductors are assembled together according to the design specifications of the machine, into a stack, pressed and consolidated to a given size under carefully controlled temperatures, pressures and pressing times. The outside surface of the stack thus formed is the resin impregnated backing material which is a glass cloth made from a lime alumino-boro-silicate glass. The ends of the stack which extend beyond the slot portion, i.e. the end winding region, are jig formed and insulated by hand wrapping tape forms of non-micaceous and micaceous materials. This section of the bar is

subjected to much lower electrical stresses than the slot portion, and hence damage by electrical discharges is minimal.

1.1.1 Main wall insulation

The consolidated conductor stack is wrapped with either sheet or tape comprised of resin bonded mica on paper, terylene or glass cloth. The wrapped bar is pressed at specified temperatures and pressures and consolidated on to the stack; the overall size of the bar, which is determined by the specific design of machine, is controlled by 'stops' in the press. The applied pressure is designed to give up to 25% compression of the insulation which ensures adequate resin flow, optimum mechanical and electrical properties.

The design of stator insulation systems is based mostly upon observation on generators that have been in service for long periods of time. Most problems encountered have been of mechanical rather than electrical origin.

The stator conductors must be fitted tightly into the slot by wedging securely to prevent bar bounce, hence the insulation must have the required properties. The conductors, on the other hand, should have enough freedom to allow for expansion and contraction due to the temperature differentials which can develop between the conductors and the stator core. Direct liquid cooling of the stator windings has reduced the copper temperatures to a relatively low level, and the copper to iron differential is insignificant.

The stator end windings must be restrained to withstand the electromagnetic forces on the end connections. These forces result in axial and tangential movement. All the component parts of the insulation system must be capable of withstanding the resultant relative motion and variation in pressure, without being damaged by abrasion.

It can be seen, therefore, that while electric strength is important, it is the mechanical strength that dictates the design requirements.

1.2 Stator insulation systems

The materials used to insulate the stator, apart from having to withstand the stresses mentioned, have to be capable of being formed round a section of copper in the shape of a coil before being inserted into a slot. They also have to be worked to close tolerances necessary in electrical machines. The materials, therefore, have to be of first class quality and have to operate satisfactorily for long periods under exacting conditions. Shellac or bitumen bonded mica are the traditional materials, but synthetic resin-bonded mica flake is now widely used. Some details of these materials are given below.

1.2.1 Mica

There are two types of interest electrically; these are muscovite and phlogopite. Muscovite is widely used for its electrical qualities. Mica is formed from a complex silicate structure involving layers of oxygen atoms grouped around silicon, aluminium or other metal atoms. These are held together by layers of potassium atoms.

The highest quality micas are clear and transparent, and these vary in colouration (muscovite is generally ruby or green, phlogopite, amber).

Muscovite is stable at temperatures up to 600°C and loss tangent in the range 10^{-3} - 10^{-4} over a wide range of frequencies at room temperature. However, loss tangent and conductivity increase rapidly at high temperatures and this limits the maximum usable temperature. The relative permittivity is in the range 5.5-7.0, and its electric strength for a thickness of approximately 0.1mm lies in the range 1 - 2 x 10^5V/mm. However, intrinsic electric strengths 10^6 V/mm have been noted. Mica is resistant to erosion by prolonged discharge attack - greater than any

other flexible material.

Mica, whether as built-up flake or mica paper, is used for the main insulation of generator stator windings. It is chosen because of its electrical, thermal, mechanical, and discharge resistant properties.

1.2.2 Mica paper

The manufacturing convenience of using uniform and homogeneous materials has led to the development of paper-like materials. This is made by exfoliating the smaller mica flake material into very small plate-like particles approximately 1 μm thick. These are then formed into sheets by settling from suspension in a paper-making machine. Exfoliation is accomplished by heating to 800°C to start disintegration. This is followed by either quenching in water, mechanical disintegration and screening, or quenching in sodium carbonate solution and treating with dilute sulphuric acid, so that the carbon dioxide forces the laminae apart and completes the disintegration. There is another process which employs high pressure water jets to break up the mica mechanically.

The cohesive force between the platelets gives the mica paper the strength to permit handling. The tear strength is too low for most purposes until treated with a binding resin. The resin effects the maximum usable temperature and also effects its dielectric loss. The thickness of mica paper produced is generally in the range 50 μm - 0.25 μm thick. The discharge resistance of mica paper is comparable with mica flake.

1.2.3 Bitumen-asphalt

Bitumen was one of the first materials to be used, and is still used as a bonding agent for mica flakes. Bitumen is a thermoplastic material which becomes fluid when hot, and solid but reasonably flexible when cold.

Many new materials are available with good dielectric properties, but none have been found to match all the properties of bitumen.

1.2.4 Shellac

Shellac was another material which was in early use as a bonding agent, it dissolves in alchohol to form shellac varnish.

1.2.5 Synthetic resins

In 1930, synthetic resins began to replace the traditional thermoplastic materials such as shellac and bitumen.

1.2.6 Epoxy polyester

As epoxy and polyester resins were considered the most likely synthetic resins to replace shellac and bitumen as binders for high-voltage insulation, the properties required of such a system were:

1. High thermal stability - low loss at elevated temperature.
2. Good resistance to electrical discharge.
3. Good bond strength between backing material, mica and copper.
4. Resistant to moisture.
5. High mechanical strength.
6. Thermo-setting instead of thermoplastic.

The polyester group was the first to be used in the electrical industry, since they were the most easily controlled.

However, as a mica binder, the epoxy groups are superior to the polyester groups for the following reasons:

1. They are less permeable to moisture.
2. Their loss tangent is lower at the operating temperature of the electrical machine.
3. They have low shrinkage on curing.
4. They have no adverse reaction with copper.

While epoxies were preferred they were more difficult to control and therefore development of these resins has been slower.

1.3 Mechanisms of insulation failure

It has been recognised that there are several ways in which a solid dielectric can breakdown, namely:-

1. Intrinsic or electromechanical
2. Streamer
3. Thermal
4. Erosion, Electrochemical, Surface tracking.

1.3.1 Intrinsic breakdown

This may be defined as the electrical strength of the material itself when all the known secondary effects have been eliminated. These include thickness of the material, nature of the electrode system, duration of stress, waveform and previous treatment.

Several theories of ultimate breakdown strength, based on solid state physics, have been proposed, but neither the experimental data nor theories account for it satisfactorily. A review of these is given by Cooper[2]. Breakdown in certain materials, i.e. soft rubber or irradiated polythene, appear to be the result of electromechanical failure. Compression decreases the thickness which in turn increases the stress, and if the elastic modulus is low enough, breakdown is achieved.

Garton[3] assumed that if (d_o) is the initial thickness of the material of Young's modulus (Y) which decreases to a thickness (d) when subject to an applied voltage (Vs), then the electrically developed compressive stress is in equilibrium if

$$\varepsilon_o \varepsilon_r \frac{Vs}{2d^2} = Y \log_e \left(\frac{d_o}{d}\right) \qquad \text{------} \quad 1.1$$

Differentiating with respect to d^2, it is seen that $d^2 \log_e \left(\frac{d_o}{d}\right)$ has a maximum value of <0.6. Further increase of (Vs) beyond this value causes the material to collapse. Under these conditions, therefore, the highest apparent electric strength is given by

$$E_o = \frac{Vs}{d} = 0.6 \left(\frac{Y}{\varepsilon_o \varepsilon_r}\right)^{\frac{1}{2}} \qquad \text{------} \quad 1.2$$

1.3.2 Thermal breakdown

This was extensively investigated by Whitehead[4]. An electrical field, applied to a dielectric at room temperature, produces little conduction current. However, as the temperature of the insulation increases, thermal dissipation from the surfaces occurs and the final result depends on the heat dissipated in relation to heat generated. The main effects of energy loss, causing the temperature to increase are:-

1. Electronic conduction currents (I^2R loss)
2. Ionic conduction $\sigma_o \exp\left(-\frac{V}{kT}\right)$
3. Dipolar loss
4. Discharges, surface or internal.

The equation for the continuity of heat is

$$\sigma E^2 = C_v \frac{dT}{dt} + \text{div (K grad T)} \qquad \text{------} \quad 1.3$$

i.e., Heat generated = heat absorbed + heat lost.

From this equation, two results may be implied, i.e., Impulse Breakdown and Long Term Breakdown.

For Impulse electric stress there is insufficient time for heat loss to occur, i.e.,

$$\sigma E^2 = C_v \frac{dT}{dt} \qquad \text{------} \quad 1.4$$

Considering a ramp rise of voltage to produce an electric field at

a time (t_c), these being the critical values for breakdown, then it may be proved that

$$E_c = \left(\frac{3C_v K_b T_c^2}{\sigma_o U t_c}\right)^{\frac{1}{2}} \exp\left(\frac{U}{2K_b T_o}\right) \quad \text{------} \quad 1.5$$

where U = constant for dielectric

K_b = thermal conduction

This shows that (E_c) is independent of (t_c) the critical temperature. For long time thermal breakdown we have,

$$\sigma E^2 = K \text{ div (grad T)} \quad \text{------} \quad 1.6$$

i.e. Heat generated = Heat loss.

For this condition, there are two extremes, thin or thick samples of dielectric. For a thick dielectric sample, the electrode-dielectric contact has negligible thermal resistance, whereas for a thin dielectric sample the electrode contact is considered most important.

It can be proved that for a thick sample under a.c. stress that

$$V_c^2 = 8 \int_{T_a}^{T_m} \left(\frac{kT}{\sigma}\right) dt \quad \text{------} \quad 1.7$$

where V_c = Critical voltage

T_m = Temperature at dielectric centre

T_a = Temperature at electrode boundary

From the equation it is seen that V_c does not depend on thickness.

1.3.3 Electro-chemical failure

Dielectric deterioration is due to ions arising from the dissociation of impurities or ionisation of the insulating material. The ions lose charge on arrival at the electrodes after an electrode reaction. The products are generally chemically or electrically harmful to the insulation. Impurities in the dielectric, and moisture are the sources of ions. Therefore, to minimise electro-chemical deterioration, it is important to avoid contamination during manufacture. Leakage currents

in solid insulation increase rapidly with temperature, and electrochemical deterioration may be more rapid at elevated temperatures.

Garton[5] developed a theory, which makes it possible to calculate the concentration of ions from the variation of loss angle of the dielectric with voltage. This was for thin films of the impregnant between layers of solid dielectric.

1.3.4 Surface tracking

If carbon deposits are produced by some means in such a way that they form together, a continuous conducting path may result, and this would cause failure of the insulating surface. This path may be formed by high energy discharges from a high potential electrode. If the insulating surface is contaminated, i.e. because of condensation and deposits of dust, surface discharge may be quite severe.

At lower voltages, the formation of continuous films of low conductivity between electrodes occurs. The flow of current through a moisture film causes it to evaporate. The break in the film causes a spark between the two receding edges, and if the current in the spark is large enough, a carbonised channel may be formed. If these channels become numerous and continuous, the concentration of stress in the undamaged parts leads to rapid failure.

1.3.5 Erosion breakdown

If an insulating material fails after long service, it is generally due to erosion by discharges. All insulation systems contain gaseous inclusions. A common situation is where an air gap is in series with a solid dielectric. This gap occurs in cracked insulation, at the surface, or at the edges of electrodes. The dielectric strength of the air gap is lower than that of the solid, and consequently breakdown occurs at a voltage considerably lower than that required to puncture

the solid.

The minimum voltage at which continuous discharge occurs is known as the discharge inception voltage. Its value depends on the pressure and composition of the gas (Paschen's law), the shape of the electrode, electric field, and the condition of the adjacent insulation. When discharge occurs in the internal voids of the insulation, a large number of electrons ranging in energy from zero to greater than 14eV arrive at the anode. Similarly a large number of positive ions move towards the cathode. A theory suggested by Garton[6] is that bond breaking is probable by the bombardment of positive ions, causing the breakage in CH_2 groups from the polymer chain, in the case of polythene. The effect is a slow erosion of the material and in consequence a lengthening of the gas gap, with a corresponding reduction in solid insulation thickness to withstand the applied stress. Organic materials are especially susceptible to decomposition by discharges, whereas inorganic materials are not quite so sensitive. For example an epoxy resin system has shown to be superior to natural resin mica splittings system at a nominal stress of 4kV/mm.

Tests in hydrogen at normal working pressure and temperature have confirmed this superiority, and support the introduction into service of this insulation at higher electrical stresses than those employed for natural resin systems.

1.3.6 Streamer breakdown

There are two types of concern, one that produces breakdown in approximately 20 years, i.e. 'service' breakdown, and one that occurs after one minute. Both are important. It is necessary to understand the mechanism of short-time breakdown to ensure that partial breakdown of the insulation has not occurred during any test that may be performed.

This would certainly effect its prospective service life.

Streamer breakdown is the propagation of the breakdown channel through the material, and is named after a similar effect in air.

Breakdown of solid insulation is preceded by failure of the ambient medium. When an a.c. voltage is applied to a solid dielectric between electrodes, a fraction of this voltage appears across the insulation. The remaining voltage will be supported by the ambient medium. If, however, the latter breaks down under the applied stress, a small charge will be deposited instantaneously at a particular site, and consequently the full voltage will be applied across it. The system may be considered as a point-plane arrangement, i.e. an earth plane and high-potential discharge channel. The local field produced is much greater than the intrinsic breakdown field and the formation of a discharge channel in the ambient medium results.

The factors that effect this type of breakdown are intrinsic electric strength and its variations in temperature and time, electrode geometry, surface conductivity, ambient medium and waveform.

1.4 Insulation tests on large machines

The reliability of insulation in high voltage electrical machines is of the utmost importance. Even though a machine has been properly designed and the insulation tested, there is no guarantee it will not fail in future service. Insulation deteriorates whether in service or not. As far as stator insulation deterioration is concerned, four basic processes are involved, and although these are defined separately, they could in practice act together in various combinations. These are:-

1. Electrical: Both surface and internal void discharges result in tracking and erosion of the insulation respectively.

2. Mechanical: Both vibration and differential expansion of the core cause abrasion of the stator insulation.

3. Chemical: Insulation ages and cracks by oxidation of organic materials in air, however, the working medium in stators is hydrogen. Degradation does occur, but the exact processes are not understood.

4. Thermal: Heat generated within or next to the insulation causes degradation of the insulation bond.

One of the most effective ways of detecting faulty insulation is to perform a high voltage test.

The following are desirable in any test method:-

a. The non-destructiveness of the test, and hence the correct distribution of the electrical stresses in the system under test.

b. The ability of the test to detect the fault.

High potential or over-voltage tests on insulation assume a definite relationship between applied test voltage and insulation life. This assumption requires that the same processes are responsible for the deterioration and possible failure of the insulation at all levels, especially at the test and service voltages. Such a condition is difficult to achieve in practice.

There are in practice two main tests for assessing the condition of insulation; these are the 50 Hz over-voltage test and the d.c. test. The 50 Hz over-voltage test on insulation of high voltage machines is a form of quality control, to prove the 'soundness' of the insulation. However, during the test, discharges on surfaces and in voids may reach a level that is potentially dangerous to the insulation under test, whereas the discharge level during service may be quite harmless.

D.C. tests have the ability to discover certain faults in the insulation.

Mandatory insulation tests carried out during manufacture of the machine are:

1. Insulation resistance tests.
2. High-voltage tests.

1.4.1 Insulation resistance tests

The insulation resistance is measured with a low direct voltage applied, usually 1-2.5 kV, to ensure that the winding is dry and clean. This test is applied both before and after the high-voltage tests to ensure that the tests have not damaged the insulation.

1.4.2 High-voltage a.c. tests

It is general practice to do these tests at different stages during the manufacture of the machine, to ensure that each process has been carried out correctly. If a failure does occur, then it can be repaired quickly at a relatively low cost. When a machine is being manufactured, tests can be made at the following stages:

a. After the coils have been manufactured but before being wound in the machine.
b. After being wound into the machine. In the case of a turbo-generator with half coils, the bottom-of-slot coils would be tested before the top-of-slot coils were wound into position.
c. After connection in their respective phase groups.
d. Before running-tests.
e. After running-tests.

Test (e) is carried out in accordance with BS 5000 Pt2 Nov 1973.

Test (a) is made at a substantially higher voltage to ensure that the winding will meet the final test. Also, should there be any weak-

nesses in the windings these will be discovered during the winding stage. BS 5000 Pt2 Nov 1973.

High voltage tests should mostly be 1000 V + (2 x rated voltage) with a minimum of 2000 V.

When a machine has passed its works test, then at site, a voltage of 85% of the test voltage should be applied, and if repairs have been done, only 75% of the original value need be applied.

A direct voltage may be applied instead of the alternating voltage, especially at site where high-voltage equipment is not available. This voltage should be 1.41 x 0.85 of the final rms voltage.

1.4.3 Other insulation tests

Other insulation tests have been devised, but none of them have replaced the high-voltage test. Some have now supplemented this test to give a further guide to the consolidation and reliability of the insulation. Some of these tests, and the modern instruments used for the purpose, are now briefly discussed.

1.4.4 50 Hz loss tangent and capacitance tests

This test indicates the degree of consolidation and hence void content of an insulation system. The characteristic required is a 'low and flat' loss tangent/applied voltage curve which extends beyond the rated voltage of the machine. If the capacitance of a large number of coils of similar dimensions is measured, then the capacitance of each should fall within certain limits, giving a check on the insulation. These measurements are made using a Schering Bridge or a Transformer Ratio-Arm Bridge, which gives a direct measurement of loss tangent ($\tan\delta$) and capacitance. When possible these measurements are made with guarded electrodes at least 3.5 cm long.

1.4.5 ERA discharge detectors

These instruments measure discharge in voids of the insulation. Several papers have been written concerning their use.[7,8] When a voltage is applied across the insulation under test, the voids break down under the applied stress, and the discharges are displayed on an oscilloscope and compared with a calibration pulse. The measurements on the Mk. 1 and Mk. 2 detectors are made in millivolts or volts and on the Mk. 3 in decibels, from which they can be converted to mV from a chart.

However, these discharge detectors do have the following deficiencies, when measuring discharges in rotating machine insulation.

1. During the test, only the maximum discharge magnitude is measured, i.e. only the largest pulse is taken and compared with the calibration pulse. The remaining many, and possibly important discharges are ignored.
2. The results, obtained in pico-coulombs, are independent of the voltage amplitude.
3. With detectors Mk. 1 and Mk. 2, all discharges, i.e. internal and external, occur together on the trace and cannot be distinguished. This has been shown experimentally with samples both in and out of oil, the oil being used to suppress the surface discharges.
4. With the Mk. 3 detector it is possible to distinguish between the internal and external discharges, but in many cases the external discharges can be so large that they mask internal discharges. Therefore, these detectors are generally used in 'noise free' enclosures, free from electrical surges etc.

5. At site the background level must be established before any tests are made, as the background noise can be so high as to make measurements meaningless.

1.4.6 Dielectric loss analyser (DLA)

This instrument is relatively new in the electrical industry and was specifically designed for use with h.v. rotating machine insulation.[8,9]

Any insulation has two forms of loss:

(1) The dielectric or material loss due to the type of insulation used.

(2) The gaseous or discharge loss due to the ionisation of the voids in the insulation as the voltage is increased.

The loss is displayed in the form of a parallelogram on an oscilloscope screen, the area inside the loop being determined by the number of voids discharging in the insulation. The instrument is easy to use and does not need a discharge-free enclosure. The results are expressed in Joule/μF/cycle, thus taking into account the electrical size of the equipment being tested.

A criticism of the instrument is that true balance may not be maintained over the entire test voltage range, and so the instrument will respond to both solid and discharge loss.

1.4.7 D.C. Tests

This method has been the subject of many papers, and considerable controversy.[10,11] The advantages of this method of test may be summarized as follows:

Advantages

(a) only physically small equipment is needed to test electrically large rotating machinery;

(b) it will discover faults, i.e., cracks in the insulation;

(c) the leakage currents can be maintained, thus giving the degree of contamination.

Disadvantages

(a) the stress distribution with d.c. is completely different from that with a.c. and therefore unrealistic conditions are imposed on the insulation of a.c. machines, especially at slot exits;

(b) failures have occurred in the overhang sections of the machines when tested with d.c. due to surface contamination, i.e. dirt and moisture. This is because d.c. tests are governed by the surface resistivity and a.c. tests by the permittivity of the insulation.

1.4.8 Low frequency

A method has been developed in which a voltage of low frequency (0.1 Hz) is applied to the insulation.[12] This method has all the advantages of a.c. testing with the added advantages of d.c. testing. This method is relatively new.

1.4.9 VDE 0530 Pt 1.66

From all the tests detailed above only the h.v. tests are subject to a British Standard, but several customers have their own required values for loss tangent and a German Specification VDE 0530 Part 1.66 lays down limits for h.v. coils. Part of this states, 'The maximum increase in tan $\delta/0.2\ U_n$ shall not exceed the corresponding increase before heat application by more than 0.004. The increment in (tan δ) over each $0.2\ U_n$ interval shall not exceed 0.009. For rated voltages >10.5 kV but <17 kV these values should not be exceeded'. U_n is the rated voltage of the machine. This test measures the quality of new

insulation but it does not guarantee it under service conditions.

1.5 Ageing of insulation

Ageing of insulation is a complicated process, and its measurement in a machine is equally difficult. Numerous papers have been written on the subject but after some 60 years of work there still appears to be unknown or immeasurable factors affecting the process. Many observers have tried to compare the ageing of various machines, operating at different sites, with each other, but this is extremely difficult unless actual conditions are taken into account and can be allowed for. What these factors are is still unknown. It would, therefore, seem logical only to compare the ageing of an insulation system of a particular machine with itself over a period, and not with any other.

The following is an attempt to explain briefly one condition which causes the deterioration or ageing of insulation and the methods employed to detect it.

A coil manufactured with thermoplastic materials 'swells' on heating, causing the main insulation to part from the conductor stack. This is the most important area of the coil since high stresses appear there, causing electrical discharges in the voids so formed, and erode the bonding materials by chemical action. Also completely eroded are such cellulose-based materials as cotton, silk, and paper, leaving behind only some bonding agent, loose dust and the mica flakes. The conductor stack, having now been weakened, can vibrate and if it is a multi-turn coil can cause an interturn failure which subsequently turns into an earth fault.

A coil insulated with the thermo-setting synthetic resins and

using glass cloth as a backing material with either micapaper or mica flake is more resistant to these conditions, because at elevated temperatures the whole coil, i.e., insulation plus copper, moves as one. Consequently, the possibility of the bond breaking between the first layers of insulation and the conductor stack is less and the formation of voids is less likely, other than those voids introduced during manufacture. Hence there is less chance of the conductor stack breaking loose, vibrating and causing an interturn fault. To detect such deterioration is difficult and therefore, it is necessary to carry out two tests, one which detects any weaknesses in the main insulation wall, and the other which detects any weaknesses in the conductor insulation or reveals voids in the area of the conductor stack.

A winding generally consists of three phases, each phase containing a number of coils connected in series, and therefore any test applied at the terminals is applied to all the coils. It also has been shown that loss tangent/maximum discharge measurements, applied in this manner, only give an indication of the average condition of the winding, and that the existence of a single 'bad' coil will be masked by the remainder and go undetected. Therefore, for all these tests to be beneficial, it is necessary to split the winding into individual coils. The only method of discovering weak coils is to apply a high voltage to the winding, of sufficient potential to find a weak coil but not high enough to cause permanent damage. Work has been carried out testing machines in this manner and satisfactory results have been obtained with a voltage of $1\frac{1}{2}$ x rated voltage of the machine, this being based to some extent on the fact that sound insulation has a voltage breakdown value of at least four times the rated voltage.

In short, tests are available which give an indication of the average condition of the winding and also the condition of the main wall insulation.

2. DISCHARGES IN INSULATION

A partial discharge is one which does not bridge metal electrodes. Generally, a dielectric is present on one or both electrodes, this may be solid, liquid or gas, Partial discharges occur in cavities of solid dielectrics, here both the electrodes are shielded from the discharge. Surface discharges also come into this category since, at least one electrode is shielded by a solid dielectric. This is also true of discharges from a sharp point at high voltage - here the discharge is shielded from one electrode by a column of non-ionised gas. The magnitudes of these discharges are generally small, but nevertheless can cause progressive deterioration and ultimate failure of an insulation system. It is necessary, therefore, to detect their presence in some form of non-destructive test.

Partial discharges come into the category of gas discharges, in which gas molecules are ionized by electron collision. The electrons so formed, gain momentum in an electric field, these cause further ionisation of molecules, so that finally an avalanche of electrons is formed. The avalanche of electrons causes current to flow through the gas.

Figures. 2.1 and 2.2 give a classification of discharges. However, a simple classification is not always possible. For example, in Fig. 2.2a, an intermediate state between surface and internal discharge is indicated. If the interspace becomes smaller and eventually is closed at the sides, the discharge becomes internal. In figure 2.2b a combination of surface and corona discharge is shown.

2.1 Deterioration of dielectrics

Internal and surface discharges cause damage to dielectrics, the damage may be due to several processes such as:-

a. Ion and electron bombardment causing heating of anode and cathode, erosion of these and chemical processes at the surface (polymerization, cracking, gassing).

b. Formation of chemical products in the ionized gas, such as nitric acid and ozone.

c. Ultra-violet rays or soft X-rays.

The cause of damage depends on the type of dielectric.

For example, Mason[14] has shown that thermal degradation is the principal mechanism in polythene.

2.1.1 Internal discharges in plastics

These have been extensively studied by Mason[14], in which he distinguishes three stages of deterioration:-

(a) Uniform surface erosion occurs, which may be caused by thermal degradation, soft X-rays or ultra-violet radiation. Thomas[15] has shown that electrons are trapped below the surface, so that ions laid down by consecutive discharges cannot neutralize them. The trapped charges cause a high electric field in the dielectric, which may reach the intrinsic strength and result in surface erosion.

(b) Discharges become concentrated near the periphery of the cavity, which may be due to the field concentration in this region. The discharges become concentrated and a number of deep pits are formed at the periphery of the cavity. As the length of the pits grows, the energy of the discharges increases, and carbonization of the pits may occur.

(c) The stress at the top of the pit approaches the intrinsic electric strength of the dielectric over a few microns. The dielectric breaks down over this distance, the field concentration moves on to the new tip, and narrow channels propagate through the dielectric initiating complete breakdown.

Surface erosion and pit forming take the major part of the time-to-breakdown. This time may be a few hours at high stress (10-20 kV/mm) or several years at a lower stress, say 3-5 kV (50 Hz). The third stage, the propagation of channels leading to breakdown, may occur in a few cycles.

2.1.2 Internal discharges in impregnated paper

The deterioration by discharges in impregnated paper insulation has been studied by Robinson.[16] Discharges in voids adjacent to the conductor attack the insulation and penetrate the first paper layer. The penetration occurs at the edge of the void, as in the case with cavities in plastic insulation. After coring the first few paper layers, surface discharges occur along the layers and carbonized tracks are formed, these follow the weakest points in the insulation. At the foot of the carbonised track local overheating takes place, which finally leads to thermal breakdown.

2.1.3 Internal discharges in mica[17]

There are two types of mica, these being Muscovite and Phlogopite. Mica is a crystalline structure of silicate layers held together by minerals cations, principally, Al^{+++}, Mg^{++}, K^{+}, and are characterised by a perfect basal cleavage along the potassium layer or C01 plane. The basic sheet silicate consists of tetrahedrally coordinated oxygen atoms around the silicon atom giving SiO_4 in which the Si^{++++} is electrostatically screened. The sheet is built up so that the tetrahedra share corner oxygens and so form a hexagonal network (Fig. 2.3 and 2.4). The shared corner oxygen atoms are in a basal plane (O_B) with the tetrahedral apex oxygen atoms (O_A) facing the same direction, but at right angles to this plane. So that subsequent layers can be built up stably, they are joined together in a mirror image on both

sides of the tetrahedra by cations of such valancy as satisfy the layer charge. The mirror images of the O_A atoms are held together by Al^{+++} or Mg^{++} cations - the centres of hexagonal symmetry of the O_A atoms being occupied by a OH^- ion. The ions and the O_A atoms form a compact two-dimensional network. The nett composition of the silicate layers is $O_2\ (OH)\ Si_2O_3\ _n$. The two planes of O_A atoms and OH ions face each other so that sites of octahedral coordination are created, these sites are occupied by tri or divalent cations. In Muscovite mica, the sites are occupied by two thirds Al^{+++}, whereas in Phlogopite all the sites are occupied by Mg^{++}.

In the ideal structure described, all the tetrahedral sites are occupied by Si^{++++} cations, resulting in an electrically neutral silica layer. In Muscovite and Phlogopite micas, elemental substitutions occur. One third of the Si^{+++} sites are occupied by Al^{+++}, thus giving the silicate layer a nett negative charge - this can be satisfied by the coplanar K^+ cations. The overall silicate structure is:-

Phlogopite Mica,

$$\left[O_3(Si\ 3/_2 + Al\ 1/_2)\ O_2\ (OH)\ Mg_3\ (OH)\ O_2\ (Si\ 3/_2 + Al\ 1/_2)\ O_3\ K\right]_n$$

Muscovite Mica,

$$\left[O_3\ (Si\ 3/_2 + Al\ 1/_2)\ O_2\ (OH)\ Al_2\ (OH)\ O_2\ (Si\ 3/_2 + Al\ 1/_2)\ O_3K\right]_n$$

Ryder [17] showed that mica erodes by low energy discharges, and this is due to the removal or dislocation of the metallic cations from the surface layers. Energy dispersive X-ray analyses (E.D.A.X) confirm this (Fig. 2.6b). The removal of the metallic cations from the surface layers of the mica resulted in a loss of crystalline stability. The re-arrangement of bond lengths and angles of the atoms, caused changes in the surface chemistry and produced mechanical stress. This stress was relieved by surface cracks occurring along impurity

boundaries, macroscopic crystal boundaries or step contours.

Potassium cations are preferentially lost from the structure, these being the mostly weakly bound in phlogopite mica. This resulted in the mica defoliating, exposing each new layer to discharge attack. Leaching of the potassium cations by nitric acid, caused by discharges in air, aided the removal of metal ions. Continued discharge attack resulted in greater cation loss, and final collapse of the crystalline structure; the result being, the formation of silica. The silica formed a variety of nodular and dendritic growth, the scanning electron microscope (S.E.M.) photograph in Fig. 2.6a shows this. The growths caused stress enhancement and greater localised discharge attack. An example of this is seen in the upper right hand corner of Fig. 2.6a, where a flake of phlogopite mica has developed into a silica dendrite and filamentary puncture had occurred around its base to a depth of 300 μm. The lower left hand corner of Fig. 2.6a shows that material has been eroded from the surface.

Ryder[17] concluded, therefore, that mica deteriorated with low energy discharges by a process involving the loss of their metallic cations. This loss caused complete collapse of the crystal structure, finally resulting in the formation of silica. Dendritic formations of silica caused enhanced discharge attack and greater localised damage. The lost cations from the mica were found as metallic salts in localised areas on the surface.

2.1.4 Surface discharges

Deterioration by surface discharges has been studied because it is useful for the assessment of discharge resistance of materials. The processes are similar to internal discharges, Ogilvie[18] found this to be true in the case of polystyrene.

2.1.5 Corona discharges

Corona discharges usually occur around bare conductors and do not attack insulation in the same way as internal or surface discharges. Only indirect action by ozone formed by corona may deteriorate neighbouring dielectrics.

2.1.6 Rate of deterioration - voltage life

Internal discharges

Many variables affect the rate of deterioration in dielectrics. The deterioration increases with number of discharges and therefore it is proportional to the frequency of the applied voltage. It is also dependent on the amplitude of this voltage. The deterioration also depends on the intensity of the discharge and the nature of the dielectric.

Frequency

As the number of discharges increases proportionally with frequency, the life of a dielectric is inversely proportional to frequency, unless the frequency is so high that thermal breakdown occurs.

If d.c. is applied the number of discharges is small and the voltage life is many times that at a.c.

Stress

As the number of discharges increases with increasing stress in the dielectric, the formation of pits occur more rapidly. It can, therefore, be appreciated that propagation channels are more rapidly initiated at a higher stress. The effect of stress upon voltage life is very significant. Mason[14] and Davis[19] have shown that voltage life for polythene decreases as the 7th to 9th power of the stress.

Discharge magnitude

The discharge magnitude increases with the depth of cavity and its area, voltage life is affected by depth of the cavity, not its surface area. Consequently, the correlation between discharge magni-

tude and voltage life is uncertain (Kreuger)[13] only with very large discharges is the voltage life short. In that case the large discharge magnitude is certainly indicating large cavity depth.

Cavity depth

Kreuger[13] has shown voltage life is shorter if the cavity is deeper.

Thickness of dielectric

The thickness of the insulation is of minor importance. The time for treeing to occur is the same for all insulation thickness, if the stresses are identical. The penetration of trees leads to breakdown in a few cycles and has, therefore, little effect on the total time-to-breakdown.

Type of insulation

Different dielectrics have different resistance to discharge. Mica and glass have good discharge resistant qualities. Polythene, PVC and Polystrene are less resistant, whereas rubber and tetrafluorethylene are easily attacked by discharges.

Self-extinction of discharges

A complicating factor in the study of voltage life is that discharges in cavities and surfaces sometimes extinguish because of semiconducting layers formed by the discharges (Rogers)[20].

2.1.7 Deterioration of micaceous machine insulation in service conditions

Section 2.1.3 applies to experimental work on small samples of micaceous insulation tested in air. However, the working medium in a machine is hydrogen and although degradation of the mica does occur in hydrogen, it is much less pronounced than in air.

The deterioration mentioned was due to electrical and chemical effects. However, when the insulation is in service conditions it must be able to withstand high mechanical forces and thermal cycling. For example, vibration may cause the insulation to wear by fretting. Differential expansion of the core and conductor can result in the insulation being torn. Another complicating factor is that excessive heat generated next to, or within the insulation itself can degrade the mica-resin bond; this applies to both thermoplastic and thermosetting insulation systems.[1,21]

It can be appreciated, therefore, that the deterioration and ageing of insulation in service conditions depends on many interacting processes as outlined above; these may act singly or in unison. For example, thermal cycling can cause differential expansion causing void formation in the insulation. Electrical discharges within the voids can cause both electrical and electrochemical deterioration. A combination of these processes is generally regarded as insulation ageing and deterioration.[21]

2.2 Breakdown of gases

Since all solid insulation inevitably contains air-gaps in the form of defects or voids, it is necessary to review some of the basic processes involved in a gaseous discharge. The voltages, currents and type of breakdown depend upon the gas, electrode separation, gas pressure and current supplied by the external circuit.

Considering the case when the gas becomes markedly conducting and examining the current-voltage characteristic for an increasing d.c. field applied to parallel plate electrodes, Fig. 2.7a, at low field strengths ohmic conductivity is obtained, due to electron emission from

the electrodes (caused by external radiations). Eventually this current saturates, because all charge carriers created are collected. In the transition region, a second process provides more carriers and finally, at the highest fields, breakdown occurs, this is shown in Fig. 2.7a. To initiate and maintain uniform field d.c. breakdown between cold electrodes in a gas, two processes are involved.[22]

(i) Electrons moving away from the cathode multiply by impact ionization of the gas.

(ii) The cathode must supply a constant flow of initiating electrons, these are produced by collision ionization of the metal by ions.

Townsend showed the multiplication followed the law

$$\frac{dn_x}{dx} = \alpha n_x$$

Where n_x is the number of electrons passing through unit area per unit time, at a distance x from the cathode. Townsend's first coefficient α, is a constant of proportionality equal to the average number of ionizations per unit distance of travel by one electron. Hence for a uniform field

$$I = I_o \exp(\gamma d) \qquad \text{- - - - - - - - - 2.1}$$

Where I is the current passing due to an initial flux I_o of electrons, d is the electrode separation.

To obtain breakdown, additional electrons must be created by some secondary process usually assumed to be positive ion bombardment of the cathode.*

*There is no cathode in a gaseous discharge. The secondary ionization process is thought to occur by photoionization.

$$I = I_o \exp(\alpha d)/[1 - \gamma \exp(\alpha d) - 1] \qquad \text{-------} \quad 2.2$$

I_o is due to external radiation, γ is Townsend's second coefficient, defining the production of electrons from the cathode.

This gives the breakdown condition

$$\exp(\alpha d) - 1 \doteq \exp(\alpha d) = 1 \qquad \text{-------} \quad 2.3$$

Detailed theory and experiment show that both γ and αd are functions of V and Pd, V is the breakdown voltage and P the pressure. For a given system V is a function of Pd alone. Typical Paschen curves are shown in Fig. 2.7b. At high pressure the breakdown is localized in the form of a spark, whereas at pressures below atmospheric it is a non-localized 'glow discharge'.

It can be seen from Paschen's curve that V is high at high pressures and separations because the mean free path of the charge carriers is low. A noticeable feature is that V is also high at lowest pressures and separations, this is because there are too few ionizable molecules present in the gas.

The breakdown strength of a gas at moderate vacuum is poor and so when a gas gap is present in a solid dielectric it becomes it weakest feature.

2.3 Calculation of inception voltage in an air-solid dielectric[23]

A solid dielectric containing an air-gap or a void may be represented by two capacitors in series with one another, ignoring the effect of the parallel capacitance of the bulk dielectric (Fig. 2.8).

The two capacitors are assumed to have very high volume resistivity compared to their capacitive reactance. If a sinusoidal voltage

is applied to this arrangement, the voltage will be distributed in accordance with the thickness and the dielectric constant of each capacitor.

If one of the capacitors is in the form of an air-gap C_v and the other some solid dielectric C_s, then the voltage across the air gap C_v can be calculated by capacitance division as follows:-

$$V_v = \left[C_s/(C_s + C_v) \right] V \qquad \text{- - - - - - - -} \quad 2.4$$

If C_s is a dielectric having thickness t_s and dielectric constant ε_r, and C_v is air having thickness t_a and dielectric constant 1, then

$$C_v = \frac{\varepsilon_o A}{t_a} \quad \text{and} \quad C_s = \frac{\varepsilon_o \varepsilon_r A}{t_s}$$

Where A is the area. Substituting into 2.4 and simplifying gives

$$V_v = \left(\frac{1}{1 + \frac{t_s}{\varepsilon_r t_a}} \right) V \qquad \text{- - - - - - - -} \quad 2.5$$

Where V is the total voltage applied to the dielectric. If the ratio t_s/ε_r is represented by β, the equation becomes:

$$V = V_v \, (1 + \beta/t_a) \qquad \text{- - - - - - - -} \quad 2.6$$

This equation can be applied to the edge of a curved electrode or similar electrode configurations, providing the electric field remains sufficiently uniform.[23]

If the ionization voltage V_i is substituted for V_v the equation becomes:

$$V = V_i \, (1 + \beta/t_a) \qquad \text{- - - - - - - -} \quad 2.7$$

V_i = ionization voltage in air at N.T.P. for any given air-gap distance t_a.

Substituting values for V_i and t_a for breakdown voltage between plane parallel electrodes for various distances and values of β, a

family of curves result as shown in Fig. 2.9a. It is noted from the curves that as β increases, the minimum inception voltage and the air-gap distance at this minimum increases. When β = o, the curve follows Paschen's law.

If β_{min} from Fig. 2.9a is plotted as a function of air-gap distance, a near linear relationship is obtained, Fig. 2.9b.

Therefore, if t_s and ε_r are known for various materials, V_i may be obtained. Dakin[24] obtained the following empirical expression:

$$V_i = 720 \left(\frac{t_s}{\varepsilon_r}\right)^{1/2} \qquad \text{- - - - - - - -} \quad 2.8$$

A similar result was obtained by Mason.[25]

Both Dakin[24] and Halleck[23] found this relationship to hold for a number of dielectrics having various thicknesses t_s and relative permittivities ε_r.

Fig. 2.9b shows that for some given voltage and value of β there would be a critical air-gap distance, over which no discharge would occur.

Dakin[24] found only slight differences in the inception voltage with 0.8 mm radius and square-edge electrodes. Halleck[23] showed that the inception voltage was not influenced by the radius of curvature at the edge down to approximately 0.8 mm. Below this, the inception voltage is lowered by a maximum of 10% to 20% for square-edge electrodes. The range of error largely depends on the value of β. Therefore, within these limitations, the inception voltage can be calculated in electrical quantities.

2.4 The discharge model

The main electrical partial discharge quantities may be separated

into individual quantities and integrated quantities. Individual quantities are - apparent discharge magnitude q_a (pC), repetition rate n (pulse s^{-1}), and energy of a single discharge E (Joule); integrated quantities are - mean current I (microamp), quadratic rate D (Coulomb^2 s^{-1}), and discharge power p (Watt). In addition inception voltage V_i, and extinction voltage V_e are of importance.

These quantities form the basis of discharge measurements, and are related to the quantities involved in an individual discharge. The theoretical relationship may be developed from a discharge model circuit which may be taken to represent a single discharge within the specimen[26]. The concept of a discharge model may also be used to evaluate the response of the basic types of partial discharge measuring circuits to a single discharge.

The discharges result from ionization in internal gaseous cavities in solid dielectrics,[4,6,22] and these cause instantaneous drops in voltage, ΔV, across the terminals of the specimen. After each discharge a transient 'compensating current' pulse occurs to re-distribute the charge between the capacitances constituting the test circuit. This is followed by a slower 're-charge pulse', from the test voltage source to restore the original terminal voltage. The concept of a discharge model with definite capacitances allows the magnitude of the charge and energy exchanges during single discharges to be calculated theoretically, in relation to the terminal voltage step ΔV. Since the capacitances of such cavities are unknown, the actual charges dissipated in them are indeterminate, q_a apparently lost by the specimen being accepted as the discharge magnitude. However, the energy dissipated in the cavities during single discharges can be determined, under certain conditions, from the measured charge q_a and the discharge inception voltage, V_i.

Moreover, discharge energy is the significant quantity, as regards insulation damage.

The basic problem in discharge measurement is transmitting small voltage pulses from the specimen at high voltage to a suitable measuring instrument, with minimum and known attenuation. The magnitude of the discharges to be measured may vary from pico-coulombs to micro-coulombs; their repetition frequency from $100s^{-1}$ to $10^6 s^{-1}$.

2.4.1 The d.c. discharge model[26]

Here, a continuously increasing direct voltage is applied to the model (Fig. 2.8), it is assumed in the following calculations that after the discharge, the voltage across the cavity is zero.

C_a is the capacitance of the solid dielectric, C_v is the capacitance of the enclosed void and C_s is the total capacitance in series with the void. When a voltage V is applied to the terminals of the sample, the voltage developed across C_v is

$$V_v = \left(\frac{C_s}{C_s + C_v} \right) V \qquad \text{- - - - - - - -} \quad 2.9$$

If V is large enough to cause ionization of the void C_v

then $V = V_i$, giving

$$V_v = \left(\frac{C_s}{C_s + C_v} \right) V_i \qquad \text{- - - - - - - -} \quad 2.10$$

The stored energy in the circuit before breakdown of C_v is given by

$$Q = \left[C_a + \left(\frac{C_s C_v}{C_s + C_v} \right) \right] V_i \qquad \text{- - - - - - - -} \quad 2.11$$

After breakdown of the cavity and assuming it to be completely discharged, then the charge is

$$Q = \left(C_a + C_s \right) \left(V_i - \Delta V \right) \qquad \text{- - - - - - - -} \quad 2.12$$

From conservation of charge

$$Q' = Q$$

The drop in potential across the circuit is therefore

$$\Delta V = - \frac{V_i C_s^2}{(C_a + C_s)(C_s + C_v)} = - \frac{V_v C_s}{C_a + C_s} \quad \text{------ 2.13}$$

The apparent charge transfer measured at the terminals is

$$q_x = C_x \Delta V$$

where
$$C_x = C_a + \left[C_s C_v / (C_s + C_v) \right] \quad \text{------ 2.14}$$

from
$$q_x = \frac{C_x C_s^2 V_i}{(C_a + C_s)(C_s + C_v)} \quad \text{------ 2.15}$$

The actual charge transfer is $q = C_v V_v$

$$q = \left(\frac{C_v C_s}{C_s + C_v} \right) V_i \quad \text{------ 2.16}$$

Equating actual and apparent charge transfer i.e., equations (2.15) and (2.16) then

$$q_x = q \frac{C_s C_x}{(C_a + C_s) C_v} \quad \text{------ 2.17}$$

Generally $C_a \gg C_s$ and therefore $C_a = C_x$

$$\therefore \quad q_x = q \left(\frac{C_s}{C_v} \right) \quad \text{------ 2.18}$$

If ε_v and ε_s are the relative permittivities of the void and series capacitances and t_v and t_s their thicknesses, then equation (2.18) can be expressed as

$$q_x = q \left(\frac{\varepsilon_s t_v}{\varepsilon_v t_s} \right) \quad \text{------ 2.19}$$

This equation indicates that the thicker the insulation relative to the void depth, the lower the apparent charge transfer q_x.

The energy of the discharge measured at the terminals is

$$E_x = \frac{1}{2} q_x V_i \qquad \text{------} \qquad 2.20$$

The energy within the void is

$$E = \frac{1}{2} q V_v \qquad \text{------} \qquad 2.21$$

Using equations (2.10) and (2.17), we have

$$E = \frac{1}{2} q_x \left(\frac{C_a + C_s}{C_s C_x}\right)\left(\frac{C_v C_s}{C_s + C_v}\right) V_i$$

and from (2.20)

$$E = E_x \left(\frac{C_a + C_s}{C_s + C_v}\right)\left(\frac{C_v}{C_s}\right) \qquad \text{------} \qquad 2.22$$

Generally $C_x = C_a$, $C_a \gg C_s$ and $C_v \gg C_s$

therefore $E = E_x$ ------ 2.23

Hence, the measured energy at the terminals of a test sample is approximately equal to the actual discharge energy and is independent of sample dimensions. However, this is not true of apparent charge transfer q_x, which does depend on sample thickness i.e., reducing with increasing thickness of insulation according to equations (2.18) and (2.19).

2.4.2 The a.c. discharge model[27]

A sinusoidal voltage applied to the discharge model produces an identical voltage across the cavity which, if sufficiently high, causes it to break down electrically. This is known as the discharge inception voltage, V_i. This depends upon the electric strength of the contained gas, the relative permittivities of the gas and the dielectric, and the shape of the cavity.[14,28] With this value of voltage, V_i, applied across the specimen terminals, a discharge will first occur at one peak of

the applied alternating voltage, and reduce the voltage across the cavity to a low value. This causes a momentary fall in the terminal voltage - e.g. at point(a)in Fig. 2.10(2).

After the first discharge, the cavity recharges with reverse polarity during the falling part of the voltage cycle and is considered to reach a voltage V_i at the zero of the terminal voltage wave. In practice, this is unlikely, because the cavity is not completely discharged and the terminal voltage has to change by more than its peak amplitude to restore the cavity voltage to V_i again in the reverse direction Fig. 2.10(1). Succeeding discharges thus occur in the quarter cycle before each peak of the applied voltage; a stable condition is reached with two discharges per cycle.

At higher voltages, several discharges occur in each half cycle and may begin before the voltage zero. The change in voltage across the specimen determines the restoration of potential across the cavity. All discharges occurring between a positive and subsequent negative peak are of one polarity, whilst those in the opposite sequence of the cycle are of reverse polarity. Residual cavity voltage after a discharge reduces the interval before the next discharge of the same polarity, but causes a longer delay before the first discharge of opposite polarity.

However, 'ideal' cavities in which internal discharge conditions remain constant do not exist in practice. The cavity breakdown voltage may change as a maintained discharge proceeds, due to heating and residual ionization, and it may also differ if the cavity is adjacent to an electrode for positive and negative discharges. Variable conductivity of the surface walls of the cavities also affects the

area discharged. These factors can cause the discharges to be erratic even when voltage is maintained at inception.

The discharge sequence of Fig. 2.10(2) is for that of a single discharging cavity. The discharges, excluding any residual charge and polarity effects, are equally spaced with respect to the voltage scale, and their number per cycle roughly proportional to the voltage applied. In practice a small increase in voltage across the specimen, above inception increases the number of discharges many times. These are grouped toward the peak of the voltage wave, and are due to many similar discharging cavities.

2.5 Calculation of discharge energy loss in a dielectric

The energy dissipated by discharges in voids of dielectrics can be calculated in two different ways.[29] Either the sum is taken of the energies dissipated in the single discharges, or the sum of the energies taken out of the supply at the single discharges. The latter sum may consist of positive or negative contributions, because energy can be stored and returned to the supply at a later discharge. The first sum consists of positive contributions only. However, due to conservation of energy, both sums give the same result over a sufficient number of cycles.

The sum of energies taken from the supply is

$$\sum q_a V \qquad \text{- - - - - -} \quad 2.24$$

where V = instantaneous voltage applied to the dielectric

q_a = apparent loss of charge in the individual discharge.

V and q_a may be positive or negative, if they are of different sign, energy is returned to the supply.

Considering now the energy dissipated in the single discharges; it is assumed that the void completely discharges whenever the voltage across it reaches $V^{\pm}$ (Fig. 2.10(1)). The dielectric or specimen being tested may be considered as a three capacitor arrangement (Fig. 2.8). C_a represents the total capacitance of the dielectric, C_s the solid dielectric in series with the void and C_v the capacitance of the void itself. The energy dissipated in the discharge is:-

$$\tfrac{1}{2}CV^2 = \tfrac{1}{2}V^2 \left(C_v + \frac{C_s C_a}{C_s + C_a}\right) \qquad \text{------- 2.25}$$

$$= \tfrac{1}{2}V^2 \left(C_v + C_s\right) \text{ for } C_a \gg C_s$$

$$= \tfrac{1}{2}V \left(\frac{C_v + C_s}{C_s}\right) VC_s$$

now $V\left(\frac{C_v + C_s}{C_s}\right) = V_i$ and $VC_s = q_a$

$$\therefore \tfrac{1}{2}CV^2 = \tfrac{1}{2}V_i\, q_a \qquad \text{------- 2.26}$$

where

V_i = inception voltage of the first discharge

q_a = apparent loss of charge from the specimen.

The sign of V_i and q_a are always the same, and their product is always positive. V_i and q_a may have a different absolute value for an applied voltage of reversed polarity, the following example illustrates this.

Assume repetitive discharges occurring in the ratio 4:5 at a certain voltage applied to the dielectric (Fig. 2.10). Both expressions (1) and (2) give the same result.[29] Discharges (d) and (g) give negative contributions to equation (1), whereas equation (2) contains

positive terms only. Over a sufficient number of cycles then,

$$\sum q_a V = \tfrac{1}{2} \sum q_a V_i \qquad \text{------ 2.27}$$

3. GENERATION OF HIGH VOLTAGE ALTERNATING WAVEFORMS AT 0.1 Hz

The major difficulty in generating a high voltage sine wave at 0.1 Hz is that a transformer with a high-turns ratio cannot be used as a final output stage. This is because the inductance of a conventional 50 Hz transformer would not support the voltage when applied at 0.1 Hz.

3.1 Generation of non-sinusoidal waveforms

If a sine wave is not required, non-sinusoidal very low frequency (VLF) waves may be generated quite simply. Bossi[30] et al. used high voltage d.c. supplies and by switching suitable time constants in the generator produced square, exponential and triangular waves. In this circuit to obtain an alternating waveform, capacitors C_1,C_2 (Fig. 3.1) are charged by voltages of opposite polarity, obtained by rectifying the high voltage supplied by the transformer T, via an oil switch S. The peak charging current through the diodes D_1,D_2 is limited by the resistance R_c. Here, the time constant of the charging circuit should be much less than that of the load R_c, i.e., R_cC_1 or $R_cC_2 \ll RC$. For the sample capacitance C_x to have negligible effect on the timing of the wave the capacitance $C \gg C_x$.

With this circuit the authors could obtain a maximum rectangular voltage of 150 kV, at the output or a triangular waveform of 30 kV peak which deviated from linearity by 2%. The frequency of these waveforms are easily controlled by the switching time of the oil switch S_1 - periods of 6, 10 and 20s were obtained, corresponding to frequencies of 0.16, 0.1 and 0.05 Hz respectively. During the period of switching, the discharge detection circuit is made inoperative by the switch S_2.

3.2 Generation of sinusoidal waveforms

While it is easier to generate non-sinusoidal waveforms for testing purposes, 0.1 Hz sine waves tests have been accepted and written into specifications in both Britain and the United States.[31]

The problem of generating high voltage sine waves may be solved in two ways:

(i) Employ a high voltage direct coupled amplifier (Miller, et. al).[32],

(ii) Employ a low frequency modulated 50 Hz source, utilizing a conventional high voltage output transformer (ASEA).[33]

With the first method, it is possible to produce a high quality sinusoidal output, the circuit described by the authors[32] could generate 25 kV peak with a 0.3 μF capacitive load. The waveform is produced by modulating two high-voltage d.c. supplies, (Fig. 3.2). The modulation is accomplished by the use of triode valves, operating at high voltage. The grids are supplied by control signals transmitted from the low-voltage control circuit through fibre optic light guides. The noise figure for this instrument is low, 1 pC in 1000 pF. Hence this type of instrument is ideal for discharge measurements at 0.1 Hz[34]. Unfortunately, it is not yet commercially available, and uses thermionic valves which might not be robust enough for field use.

The second method of generating a sine wave at 0.1 Hz is commercially available and was only intended for overpotential testing the insulation of large machines[33] (Fig. 3.3). This generator can supply an 0.7 μF capacitive load at 70 kV peak. Although this generator is capable of supplying greater loads at higher voltage levels than the previous method, it is electrically very noisy, because of the high voltage rotating mechanical switches which demodulate the 50 Hz wave-

form. Consequently, before it can be used for discharge measurements it must be screened and the low frequency high voltage supply filtered.[35] This generator forms the basis of the present work and is, therefore, described in some detail below.

3.3 VLF generator used in the present investigation

The most basic part of the low frequency generator is the voltage multiplier circuit shown in Fig. 3.4a. Consider this circuit with constant amplitude 50 Hz applied. S_1 closes at the beginning of the cycle for 5 mS allowing C_S to charge up to the peak value of the positive applied voltage V. S_1 is then opened leaving a voltage of V on C_s. 5 mS after this S_2 closes, the input voltage is now acting in series with the voltage already on C_S, thus $2\hat{V}$ is developed across C_L, assuming $C_S \gg C_L$. The voltage relating to the various switching sequences are shown in Fig. 3.4b. Now, consider a 100% 0.1 Hz modulated 50 Hz sine wave applied to the circuit in Fig. 3.4a from which it is required to remove the 50 Hz component, thereby obtaining an 0.1 Hz sine wave. The following sequences of events occur, Fig. 3.5. At the beginning of the modulated cycle point 0 switch S_1 closes for 5 mS then opens allowing C_S to charge to the peak value of the 50 Hz applied at that time (A). 5 mS later switch S_2 closes for 5 mS and during the negative peak C_S and C_L charge up to give the point (C) providing $C_S \gg C_L$. Similarly points (D) and (E) along with the charge already acquired add to give (F). This process continues until the point (M) where the first quarter cycle of the 0.1 Hz waveform has developed. After the point (M) the 50 Hz applied wave begins to decrease in amplitude and the load capacitor C_L, having been charged to a maximum by the modulated 50 Hz, cannot lose its charge except through its own dielectric resistance which can be high $\geqslant 10^{10}\,\Omega$. The capacitor C_L, therefore,

transfers some of its charge back to C_S and the voltage across C_L decreases. The process of the load capacitor losing voltage continues until the point O, where the first half cycle has developed.

The negative half cycle is formed exactly in the same way but by arranging for the 50Hz wave to change phase by 180° at the point (O). This is achieved by using a centre tap on the modulating variac. The switches S_1 and S_2 are driven by a common motor in synchronism with the 50 Hz supply, i.e., 1500 rpm. The modulation variac is also driven by the same motor, but from a low speed output at 10s, i.e., 0.1 Hz.

Figures 3.6a and b show the 50 Hz modulated input wave to the high voltage transformer and the 0.1 Hz demodulated output wave respectively. A photograph of the experimental VLF generator is shown in Fig. 3.8.

3.4 Efficiency of the generator

The series capacitor C_S is charged to $2\hat{V}_{in}$ which is applied to the load capacitor C_L. The equivalent circuit therefore, is $2\hat{V}$ acting in series with C_S and C_L. The output voltage $\hat{V}_o$, is given by

$$\hat{V}_o = 2\hat{V}_{in} \Big/ \left[1 + \left(\frac{C_L}{C_S}\right)\right] \qquad \text{- - - - - -} \qquad 3.1$$

if $C_S \gg C_L$, $\hat{V}_o \rightarrow 2\hat{V}_{in}$,

if $C_S = C_L$, $\hat{V}_o = \hat{V}_{in}$

and if $C_S \ll C_L$, $\hat{V}_o \rightarrow 2\hat{V}_{in}\left(\frac{C_S}{C_L}\right)$

Therefore, for maximum output voltage from the generator $C_S \gg C_L$. Fig. 3.7 shows the variation of $(\hat{V}_o/\hat{V}_{in})$ versus $2(1 + \frac{C_L}{C_S})^{-1}$, this is chosen for various values of (C_L/C_S).

4. DISCHARGE DETECTION AND MEASUREMENT AT VERY LOW FREQUENCY

Although there is no absolute basis for predicting the life of insulation from discharge characteristics, it is important to detect

harmful discharges, which may occur in otherwise sound insulation. Discharges are detected using an impedance connected in series with the test object or in series with the coupling capacitor, and the discharge magnitude is determined by measuring the voltage drop across the impedance with a suitable instrument giving a visual indication or permanent record.

Various instruments are used in an attempt to solve this problem. The choice of instrument and method of detection depends on the discharge sensitivity and resolution required. To obtain perfect reproduction of a discharge pulse, an instrument with infinite bandwidth, and linear phase relationship is required. In practice the bandwidth is limited by the choice of detection circuit. Instruments which measure partial discharges can be classified in terms of the bandwidth of the detection circuit and the method of measurement.

Discharge detection at very low frequency (VLF) is, in essence, the same as at power frequency, although measurement of the basic quantities involved are difficult because of the reduced frequency. For a given sample, the average discharge pulse repetition rate per cycle is reduced by approximately 500 times, at 0.1 Hz compared to 50 Hz. The low discharge repetition rates make it difficult to use any of the conventional integrating or averaging discharge measuring instruments without modification. An integrating or averaging instrument requires that the time constant of the detection circuit is greater than the periodic time of the test wave, in this case 10s. The subsequent loss in sensitivity becomes prohibitive. The ERA discharge detector is a conventional instrument which may be used at VLF, but the display is unsuitable, being synchronised at 50 Hz. The resultant non-stationary discharge pulses on the display are difficult to measure. A conventional

oscilloscope is also unsuitable as a display, because of the low repetition rates involved.

For satisfactory measurements at VLF, a permanent record of the discharge pulses must be made. Tape recording is possible, but pulse height analysis is more convenient[27]. In the present experimental work the latter approach was adopted, and achieves the maximum sensitivity possible.

4.1 Principles of discharge detection

There are two equivalent circuits which are used to model discharges.[36] The occurrence of a discharge can be represented by a current generator in parallel with the model capacitance, C_x, or a voltage generator in series with it, as shown in Figs. 4.1a and b. When discharge occurs a circulating current i_1 flows through C_v and R, and i_2 through C_s, C_a and R (Fig. 2.8). The form of i_2 is given by Fig. 4.1c.

$$i_2 = K\left(e^{-t/\tau_d} - e^{-t/\tau_r}\right) = C_s \frac{dV_1}{dt} \qquad \text{------- 4.1}$$

where τ_d is the discharge time constant and τ_r the rise time of the current pulse i_2, shown in Fig. 4.1c. Consequently, an increase in voltage occurs across C_s of approximately

$$V_s = \frac{1}{C_s}\int i_2 dt \doteq V i_1 \qquad \text{------ 4.2}$$

and the voltage on C_a drops by

$$\Delta V_a = \frac{1}{C_a}\int i_2 dt \doteq V i_2 \frac{C_s}{C_a} \doteq \frac{q}{C_x} \qquad \text{------ 4.3}$$

The rate of rise of this voltage is determined by the rate of change of i_2 or i_1, and can be obtained from the above equation if τ_d and τ_r are known. However, in most cases $\Delta V(t)$ may be taken as a step voltage of amplitude q/C_x.

There are basic circuits[27,37,38] used for detecting a discharge from lumped parameter test objects under d.c., a.c. or impulse conditions. These are shown in Fig. 4.2a, b, and c. C_x represents the tested object, C_k is a high voltage capacitor used either as a blocking or coupling capacitor. Z_d is the detector impedance across which the voltage due to discharge develops and Z is the impedance of the ht. supply. Circuit A is generally used when one terminal of C_x is unavoidably earthed, C_k being chosen to prevent excessive power frequency voltage appearing across Z_d, while having a low impedance to frequencies of interest contained in discharge pulses. When circuit (B) is used, C_k serves as a return path for high frequency current flowing through the test piece and detector impedance. Sometimes stray capacity to earth is relied upon to provide C_k. The circuit has the advantage that if C_k is $\gg C_x$ extraneous disturbances from either the supply or busbar system are reduced in the ratio of C_x/C_k approximately. Similarly, with the bridge circuit external discharges may be balanced out.

The detection impedances of interest consist of R, RC, RLC, and transformer coupled (band-pass) elements. The response of detection circuits with the different types of impedance are outlined in Figs. 4.4-4.7. Provided stray elements are reduced to negligible proportions in circuits A and B, then these two are equivalent for the same element values. (This can be checked by inserting either of the equivalent discharge models for C_x). The discharge is represented by a step voltage generator of amplitude ΔV in series with C_k, except where otherwise stated. All the expressions developed are for $\tau_d \ll \tau_r$, the recharge time from the supply. The expressions in the following section are then obtained.

4.1.2 Resistive and inductive detection impedances $Z_d = R_d$

Two conditions are of interest, either $\tau_d \gg \tau_r$ or $\tau_d \ll \tau_r$. If $\tau_d \ll \tau_r$ the voltage V_d measured across R_d will have the same form as i_2, see Fig. 4.4, and the apparent discharge magnitude may be found from the volt time integral of i_d, as, $q_d = q\frac{C_k}{C_x+C_k}$. If $\tau_d \gg \tau_r$ then the discharge may be considered as a step voltage equivalent source, though the actual waveform will have a rise time determined by i_2.

If then $V_d(t)$ is the voltage appearing across Z_d when a single discharge occurs within the test object

$$V_d(t) = \Delta V e^{-t/C_d R_d} \qquad \text{------} \qquad 4.4$$

where $C_d = \frac{C_x C_k}{C_x+C_k}$

The amplitude of the exponentially decaying pulse is $\Delta V = q/C_x$.

The volt-time integral of the pulse, that is the area under the volt time curve gives the apparent discharge magnitude measured.

$$q_d = \frac{\Delta V}{R_d}\int_0^T e^{-t/R_d C_d}\, dt = \Delta V\, C_d,\ T \gg \tau_d \qquad -- \qquad 4.5$$

Hence, both the initial amplitude of the discharge pulse appearing across R_d and its volt-time integral enable q to be evaluated.

$Z_d = C_d$ in parallel with R_d

$$V_d(t) = \Delta V\left(\frac{C_p}{C_d}\right)e^{-t/R_d C_d} \qquad \text{------} \qquad 4.6$$

where $C_p = \frac{C_x C_k}{C_x+C_k}$, $C_d = C_p + C_d$

Consequently, the initial amplitude of the exponential pulse is:-

$$\Delta V\left(\frac{C_p}{C_d}\right) \doteq q/(C_x+C_d) \qquad \text{------} \qquad 4.7$$

Also $$q_d \doteq \frac{\Delta V C_p}{C_d R_d} \int_0^T e^{-t/R_d C_d} \quad \text{------} \quad 4.8$$

$$= \Delta V C_p = q \ , \ C_k \gg C_x \quad \text{------} \quad 4.9$$

Thus if there is appreciable capacitance across R_d this

(i) reduces V_d by a factor C_p/C_d

(ii) increases τ_d from $C_p R_d$ to $(C_p+C_d)R_d$.

(iii) leaves q_d still approximately equal to q provided $C_k \gg C_x$.

The measuring circuit arrangements and responses in the cases of $Z_d = C \,//\, R$ are given in Fig. 4.5.

$\underline{Z_d = L_d}$

If R is the resistance of the coil then the response may be evaluated from $$i_d(t) = \Delta V \left[e^{-p_1 t} - e^{p_2 t} \right] \Big/ \left[L (p_1 - p_2) \right] \quad \text{------} \quad 4.10$$

where $p_{1,2} = -\Omega \pm (\Omega^2 - \omega_o^2)^{1/2}$, $\Omega = R/2L_d$, $\omega_o^2 = 1/L_d C_d$

$$C_d = \frac{C_x C_k}{C_x + C_k}, \quad \omega = (\Omega^2 - \omega_o^2)^{1/2} \ , \ \omega_1 = (\omega_o^2 - \Omega^2)^{1/2}$$

These give depending upon the value of R,

<u>Overdamped</u>, $$R \gg 2 \left(\frac{L_d}{C_d} \right)^{1/2} \quad \text{------} \quad 4.11$$

$$V_d(t) = R i(t) + L_d \frac{di(t)}{dt} \quad \text{------} \quad 4.12$$

$$= \Delta V \, e^{-Rt/2L_d} \left(\frac{\Omega}{\omega} \operatorname{Sinh} \omega t + \cosh \omega t \right) \quad \text{------} \quad 4.13$$

<u>Critically damped</u>

$$R = 2 \left(\frac{L_d}{C_d} \right)^{1/2} \quad \text{------} \quad 4.14$$

$$V_d(t) = \Delta V \, e^{-Rt/2L_d} \, (1 + \Omega t) \quad \text{------} \quad 4.15$$

Underdamped

$$R_d \ll 2\left(\frac{L_d}{C_d}\right)^{1/2} \qquad \text{- - - - - -} \qquad 4.16$$

$$V_d(t) = \Delta V \; e^{-Rt/2L_d} \left(\frac{\Omega}{\omega_1} \sin \omega_1 t + \cos \omega_1 t \right) \text{- - - -} \qquad 4.17$$

Examples of the voltage waveforms are shown in Fig. 4.6. In these cases each of the voltages is proportional to ΔV and the maximum value ($t = 0$) gives ΔV directly i.e.

$$V_d = \Delta V = q/C_x \qquad \text{- - - - - -} \qquad 4.18$$

If q_d is evaluated from the voltage waveform and keeping contributions of correct polarity where oscillations occur then

$$q_d = C_d \Delta V \qquad \text{- - - - - -} \qquad 4.19$$

$$= q\, C_k/(C_x+C_k) \qquad \text{- - - - - -} \qquad 4.20$$

$$= q, \text{ if } (C_k \gg C_x) \qquad \text{- - - - - -} \qquad 4.21$$

It may also be shown that for the case of R_d parallel to L_d the effect is equivalent to a series resistance $R_s = \frac{L_d}{C_d R_d}$.

Where appreciable capacitance, C_s, (stray capacitance between turns of the inductor, for example) exists across the inductance of the detector impedance, the expressions for $V_d(t)$, V_d and q are modified by C_s in the capacitance term giving $C_d = \frac{C_x C_k}{(C_x+C_k)} + C_s$ and by capacitance division of ΔV giving $\frac{\Delta V C_x C_k}{(C_x+C_k)C_d}$. The circuit, however, is evaluated for specific values of parameters. A typical voltage waveform is shown in Fig. 4.6.

4.1.3 Transformer coupled detection impedances

The response of the generalised coupled circuit shown in Fig. 4.7, having only mutual inductance coupling, depends upon the relationships

between the time constants of the primary and secondary circuits τ_1 and τ_2 and between the natural frequencies of these circuits f_1 and f_2 where $\tau_1 = 2 R_d C_d$, $\tau_2 = 2 R'_d C_d$, $\omega_1 = \frac{1}{\sqrt{L_1 C_d}}$, $\omega_2 = \frac{1}{\sqrt{L_2 C_d}}$. The two conditions used in discharge measuring instruments to be described both have $\omega_2 > \omega_1$

and are

(i) $\tau_2 \gg 1/\omega_2$, $\tau_1 \gg 1/\omega_1$ ERA Model II (Hivolt) input circuit

(ii) $\tau_2 \gg 1/\omega_2$, $\tau_1 \ll 1/\omega_1$ ERA Model III input circuit

The voltage appearing at the output (secondary) side of the transformer is given by

(i) $$V_d(t) = qk \frac{n_2}{n_1} \frac{1}{C_x} \frac{\omega^2}{(\omega_2^2 - \omega_1^2)} \left(e^{-t/\tau_1} \cos \omega_1 t - e^{-t/\tau_2} \cos \omega_2 t \right) \quad -- 4.22$$

(ii) $$V_d(t) = qk \frac{n_2}{n_1} \frac{\omega_2^2}{C_x} \frac{\tau_2 \tau_1}{4(\tau_1 - \tau_2)} \left(e^{-2t/\tau_1} - e^{-2t/\tau_2} \right). \quad ----- \quad 4.23$$

where, n_1, n_2 are the transformer turns ratios and k is the coupling factor.

In each case the output voltage is proportional to the discharge magnitude q, and has the forms shown in Fig. 4.7.

4.1.4 The effect of strays on the measurement of discharge intensity

Stray inductance

Stray inductance L_s, due to leads and construction of high voltage capacitors may be typically from 1 to 10 μH and will be represented in the detection circuit A and B as shown in Fig. 4.3. The effect of stray inductance in the case of circuits A & B (which are still equivalent provided C_s is negligible) with $Z_d = R_d$ may be evaluated from the previously given information. The peak voltage across R_d, V_d, will be found to vary from a maximum value of ΔV with R_d very large (overdamped condition) to $\frac{1}{e}$ ΔV at critical damping and correspondingly

lower values with lower values of R_d.

Stray Capacitance

If stray capacitance is present (Fig. 4.3) both across the detector shunt and from the high voltage terminal to earth, the former will not effect the equivalence of circuits A & B, but will reduce sensitivity. Stray capacity from the high voltage terminal, however, upsets the equivalence between circuits A & B and gives errors in calculated discharge magnitudes if not accounted for. It may be seen from Fig. 4.3, that compensating current flows from both C_s and C_k through the detector shunt in circuit A, whereas in circuit B only the compensating current flowing through C_k is measured. Correct calibration will allow for these effects.

4.1.5 Bridge circuits (neglecting strays)[38]

This type of circuit, Figs. 4.8a and b, is usually used to eliminate the power frequency voltage in a.c. testing though not necessarily rejection of external influences at other frequencies. The voltage pulses, due to discharge within the sample, appearing across the detector shunts Z_{d1} and Z_{d2}. are,

$$V_{d_1}(t) = - \Delta V \frac{R_d}{R_d+R_k} e^{-at} \qquad \text{------} \quad 4.24$$

$$V_{d_2}(t) = + \Delta V \frac{R_k}{R_d+R_k} e^{-at} \qquad \text{------} \quad 4.25$$

where $a = C_x + C_k / [C_x C_k (R_d + R_k)]$

R_d and R_k are equal and purely resistive. Since these pulses are of opposite polarity a differential measurement gives

$$V_d = \Delta V \qquad \text{------} \quad 4.26$$

The circuit shown in Fig. 4.8b, with additional blocking capacitance C_{k2}, gives

$$V_d(t) = \Delta V \left(\frac{C_x}{C_d}\right) e^{-t/R_d C_d} \qquad \text{- - - - - -} \qquad 4.27$$

provided that

$$C_{k_2} \ll C_{k_1}, \quad C_d \doteq C_{k_1} \gg C_x$$

Consequently, q may be determined from V_d or the volt-time integral of the voltage across R_d.

4.1.6 Effect of recharge pulse in detection circuits.[27]

The time constant associated with the supply, τ_r is usually much greater than τ_c, the time constant which determines the rate at which current flows into the sample from the blocking capacitance to compensate for the drop in voltage across C_2. Under these conditions, current from the supply, i_r. recharges the sample at a much slower rate than that at which the compensating current i_c flows. If, however, τ_r is of the order of τ_c the recharge and compensating currents through Z_d interfere with one another (Fig. 4.8c). In circuit A the recharge pulse flows in the same direction as the compensating current while in circuit B the currents flow in the opposite directions. In bridge circuits the effect of recharge pulse will not be measured provided the arms are identical.

4.2 Conventional discharge detection, display and indicating instruments used at 50 Hz

Complete instruments involve discharge detection, display and measurement. Discharge detection has been discussed above, but the instrument (Fig. 4.9) connected across the detection impedance has a clearly defined bandwidth and this must be considered when developing a complete instrument.[39] Fig. 4.10 shows the response of a wide band amplifier to a step impulse, the amplifier is assumed to have constant

gain from d.c. to some upper cut-off frequency f_2. Generally, there is some attenuation at low frequencies f_1, thus eliminating power frequencies from the detection circuit. Wide and narrow bands are defined as having a $\Delta f = (f_2 - f_1) > (f_1 + f)/2$ or $< (f_1 + f)/2$ respectively.

For example, the ERA III has a band-pass from 10-150 kHz and is classified as wide band, while an R.I.V. meter with a bandwidth of 3 kHz operating at 1 MHz is classed as narrow band. The response of an idealised band-pass instrument having the characteristics shown in Fig. 4.11, to a step impulse is the difference of the response with low pass bandwidths of f_2 and f_1. With a wide band instrument the high frequency cut-off determines the rise time of the pulse, while the low frequency cut-off determines its decay time. A narrow bandwidth gives a response in which the duration of the major pulse is $\Delta f = \Delta\omega/2\pi$.

The response of instruments having either of the above idealised characteristics to step impulses, are shown in Fig. 4.10b and c.

4.2.1 Measurement of individual quantities

4.2.1a Cathode ray oscilloscope

Oscilloscopes are available having upper cut-off frequency, f_2, of 100 MHz and response down to d.c., $f_1 = 0$. These instruments have been used in conjunction with capacitance coupled ($Z_d = R_d$) and single tuned ($Z_d = L_d$) measuring circuits, a typical measuring arrangement being shown in Fig. 4.12a.. Because of their bandwidth they accurately reproduce the amplitude and waveform of the voltage appearing across the measuring shunts from which q can be evaluated.

The sensitivity of an oscilloscope (in pC) when used with a resistive measuring shunt may be obtained simply from the following formulae due to Krueger[13].

When amplifier noise is the limitation

optimum sensitivity is $$q_{min} = \frac{2\sqrt{N}\, C_d}{0.375} \quad - - - \quad 4.28$$

When circuit noise is the limitation $$q_{min} = \sqrt{KT\, C_d} \cdot \frac{2.5}{\xi} \quad - \quad 4.29$$

In the first expression N is a function of $\sqrt{\text{bandwidth}}$, while in the second it is independent of bandwidth. $\xi = \left(\frac{\gamma_d}{\alpha}\right)^{\alpha/(\alpha-\gamma_d)}$, $\alpha = 1/f_2$.

The noise level of a moderate oscilloscope of say 5 MHz bandwidth might typically be 100 μV. Then for C_d = 100 pF.

$$q_{min} = \frac{\sqrt{2}.10^{-4}.10^{-10}}{0.375} = 0.4 \text{ pC}$$

One disadvantage of using the full frequency range of the instrument is that a large power frequency voltage component may develop across the detector impedance and impair sensitive measurements and recording. Generally, a high pass filter with a cut off at 1 or 10 kHz is inserted between detection impedance and the oscilloscope.

4.2.1b ERA model III instrument[40]

This instrument, shown schematically in Fig. 4.12b is one of three originally developed by ERA for discharge detection and is classed as a wideband instrument; it is used in conjunction with a band-pass from 10 KHz and the gain is greater than 10^6. Various input coupling units are available for matching different ranges of sample capacitance to the instrument. The primary circuit of each band-pass coupling unit is critically damped at frequeneies within the range 15 to 50 KHz by providing a suitable value of primary inductance to match a range of sample capacitances. The secondary is overdamped with a time constant of about 50 ns. The overall sensitivity, which is proportional to $\sqrt{C_X}$ is determined by amplifier noise,

and is 0.005 pC for C_x = 6pF (the lowest acceptance specimen capacitance due to stray capacity), and 15 pC for C_x = 250 μF.

The output voltage waveshape from the instrument and measuring circuit in response to a discharge within the test object C_x is shown in Fig. 4.12c. The resolution is of the order of 30 μs (corresponding to f_1 = 15 KHz) which enables about 180 discharge per quadrant to be discriminated at 50 Hz test voltage frequency.

After amplification, the discharge pulse is displayed on an oscilloscope screen superimposed upon an elliptical time base synchronized with the power frequency test supply. A phase adjustment control (rotate ellipse) enables the top and bottom points of the CRO display to be made coincident with the test voltage peaks.

The instrument has been designed with a continuously variable amplifier gain control and in order to measure the apparent discharge magnitude q it is provided with an internal calibrator.

One of the main advantages of the instrument is that it presents a visible display which, with experience, may be used to distinguish discharges occurring within the test object from those occurring either in the blocking capacitor, the testing transformer or on the busbar system. The indication may also be used to distinguish different types of discharge occurring within the one test object. Typical examples of the discharge pattern obtained when the measuring shunt is in series with the sample for different types of discharge are given in Fig. 4.13 . The possibility of using the instrument in this way results directly from the fact that the bandwidth is wide enough to maintain pulse polarity at the output. This is also true of an oscilloscope, but for recording purposes the ERA III is preferred.

4.2.1c ERA model II instrument

A form of the Model II instrument is commercially available. The instrument employs a bandpass input circuit consisting of an auto transformer which is coupled to the band-pass input circuit, internal to the instrument, by a connecting coaxial cable. This is tuned to the measuring frequency of the amplifier, which is 500 KHz, the bandwidth at this frequency is f = 10 KHz.

A range of transformer coupled input circuits are provided for different ranges of sample capacitances; the total range of specimens which can be accommodated is 7 pF to 0.1 μF. Sensitivity is 0.005 pC for 10 pF and 1.5 pC for 0.1 μF.

Because of the narrow measurement bandwidth, the output of the instrument amplifiers has an envelope of width about $2/10^4$ = 200 μs. The resolution is about 140 μs or 40 pulses per quadrant at 50 Hz test frequency.

4.2.2 Measurement of integrated quantities

4.2.2a Mean current meters[27,41]

The requirements for a satisfactory mean current meter are illustrated in Fig. 4.14 . In this instrument discharge pulses appearing across the measuring impedance, R_d and C_d in parallel are amplified, rectified and then averaged.

The voltage appearing across the measuring impedance is given by equation 4.6, i.e.,

$$V_d(t) = \Delta V\left(\frac{C_p}{C_d}\right)e^{-t/R_dC_d},\ C_p = C_xC_k/(C_k + C_x)$$

If this is averaged one obtains

$$\frac{1}{T}\int_0^T V_d(t) = q_dR_d/T = qR_d/T \qquad \text{- - - - - -} \qquad 4.30$$

Hence, averaging the voltage across a fixed measuring resistance gives an indication proportional to

$$\sum q/_T = I, \text{ or } \sum n/|q| = I \qquad \text{------} \qquad 4.31$$

if all pulses are of the same charge.

There are three requirements for the amplifier which may have a high pass filter between it and the detecting impedance to suppress power frequency voltages. These are:-

i) High upper cut-off frequency to obtain the contribution due to high frequency components in the discharge.

ii) Wideband to enable correct waveforms to be obtained without distortion due to overlapping of consecutive pulses.

iii) Low frequency cut-off to provide lower frequency, particularly power frequency harmonic, rejection.

In practice f_2 = 5MHz, f_1 = 30 KHz or 10 KHz have been suggested. It should be noted that after passage through the high pass filter and amplifier the discharge pulses are distributed so that the volt time integral, i.e., the charge of the pulse above and below the zero line are equal and rectification is therefore necessary. Also that if measuring circuit B is used the compensating and recharge pulses, which have equal charge, are additive across the measuring impedance, while for circuit A they cancel. The time constant C_dR_d should therefore be kept short relative to ZC_d when circuit A is used in order that the charge and recharge pulses do not overlap.

4.2.2b RIV meters[42]

Radio noise meters, or Radio Influence Volt (RIV) meters were used in an attempt to correlate on a national basis in the USA the effects of extraneous electrical fields associated with transients in plant and transmission line systems on radio communications. The type of instrument was essentially a super-heterodyne radio receiver, with detector

circuits designed to have specified time constants and a logarithmic output meter calibrated to measure the radio frequency input voltage at a specified frequency directly in microvolts. RIV meters generally operate over one of two frequency ranges, 0.15 MHz to 30 MHz or 30 MHz to 100 MHz. The measurement is continuously variable within the range and the specifications give bandwidth limits of from 2.5 KHz to 11 KHz approximately for the normal measurement frequency, f_d, of 1 MHz.

The two main meter specifications[43,44] give the response of the instruments to short ($\tau_d \ll \frac{1}{f_d}$) 0.158 μ VS pulses repeated at 100 pps as equivalent to a 1mV rms sine wave of frequency f_d. Based upon this calculation, meters made to either of the specifications should have different responses since their specified detector time constants differ. This may be seen since the instrument acts as a narrowband amplifier, whose amplifier output is proportional to q (since the response is determined by the volt-time integral of a voltage pulse over a resistance) and is of $\frac{2}{\Delta f}$ duration. When passed through the quasi-peak detector circuit, the output capacitor will charge to a certain value while the pulse lasts, then gradually discharges according to the specified detector discharge time constant. This gives a response which depends upon input pulse repetition rate for meters having 1/600 and 1/150 mS detector time constants.

The overall response is determined from[37]

$$V = \sqrt{2}\,\Delta f\, q\, R_d\, k\ (\mu V) \qquad \text{- - - - - -} \qquad 4.32$$

where q is apparent charge in pC, R_d is the input resistance across the meter terminals (including the meter input resistance if not negligible) and k is the factor determining the output voltage variation with pulse repetition rate n.

RIV meters are usually used with a circuit which has an equivalent measuring impedance $Z_d = R_d = 150\Omega$. If this is used as the input resistance then the instrument response may be checked by injecting a known charge q through the resistor. This is done by injecting a fast rise time pulse of amplitude V_o, repeated n times/second, through a known capacitance C_o, of value such that

$$C_o R_d \ll {}^{1}/_{f_d}, \quad q = \frac{1}{R_d} \int_o^{\infty} V_o \, e^{-{}^{t}/_{R_d C_o}} = V_o C_o \qquad \text{------ 4.33}$$

4.2.2c Measurement of discharge power P

A normal Schering bridge with a sensitive detector measures the power loss due to partial discharge, but affordsno means of separating this from normal dielectric loss. This difficulty may be overcome by a modification by Gelez[45] Fig. 4.15a, whereby balance adjustment is made successively with a selective galvanometer or electronic detector, tuned to the test frequency, and with a cathode ray oscilloscope. At the first setting, the total capacitance and loss current (including those due to discharge) are balanced out. The bridge is then readjusted, using the oscilloscope, to balance only the normal loss and capacitance currents, eliminating the basic power frequency component. Two values of power loss in the specimen are then calculated from each of the two sets of bridge readings, their difference giving the power loss attributable to discharges. The effective capacitance change due to the partial discharge current can also be calculated, giving a direct measure of the fractional volume of cavities in the dielectric. The latter is expressed by $\frac{1}{\varepsilon}({}^{\Delta C}/_{C})$ (where ΔC is the apparent change in C).

The sensitivity of this system is limited by residual mains harmonics (since it depends on visual balancing by means of the CRO). A

more complex bridge arrangement has been suggested by Veverka et al[46] to overcome this difficulty without the need for a very pure sine wave supply.

4.2.2d Veverka's methods[46]

The suggested form of the bridge is shown in Fig. 4.15b. The setting up condition is $R_d C_x = R_k C_k$ i.e. the same as the a.c. balance conditions.

Therefore, $V_d = \Delta V e^{-t/R_d C_x}$

and $\int V_d \, dt = R_d q$; that is, the charge magnitude is given by $\frac{1}{R_d}$ times the volt-time integral across R_d.

This relationship is for the compensating charge. For recharge from the supply it may be shown that there will be no voltage across the diagonal of the bridge. Now the energy change ΔE may be equated to qV where V is the instantaneous voltage across the test object. Therefore, to determine the power delivered by the discharge it is possible to use a wattmetrical system. The unbalance voltage due to discharges is fed into a low frequency amplifier, feeding the voltage coil of the watt-meter. The instrument transformer in the diagram is used to balance out the dielectric loss component of the test object.

4.2.2e The 'loop trace' method

The loop trace method, in the form shown in Fig. 4.16b was developed by Dakin[8]. It gives a very convenient method for measuring the partial discharge power and indicating discharge inception voltage (above a certain magnitude of discharge). Dakin's circuit was developed from the simple method illustrated in Figs. 4.16a.

Referring to Fig. 4.17a

$$V = \frac{Q}{C_s} + V_a \qquad \text{------} \qquad 4.34$$

$$Q = VC_s - V_a C_s \qquad \text{------} \qquad 4.35$$

If V_a is a constant during the discharging period then $\frac{dQ}{dV} = C_s$ and during the non-discharging portion $\frac{dQ}{dV} = C_x$

Here C_s represents the total capacitance of solid dielectric in the sample with all air spaces completely short circuited.

If C_s is only slightly $> C_{air}$ it is difficult to measure accurately from the resultant parallelogram. This can be avoided by Dakin's method in which the normal charging current is eliminated together with losses. The method, Fig. 4.16b, employs four capacitance arms. C_d and C_k are capacitors which are relatively large compared with C_{k1} and the sample capacitance C_x (C_d and C_k 0.1 to 1.0 μF). The voltage AB is introduced to the vertical deflection plates of the CRO. Balance is achieved by varying C_k. The loss angle may be balanced (as in Wien Bridge) with resistance r in series with C_{k1} or R_d in parallel with C . The latter is usually preferable in which case the time constant $C_d R_d$ should be chosen as not to discharge C_d during the cycle. The detector used by Dakin employed an audio transformer having a high impedance, 100 KΩ.

During the discharging part of the cycle $\frac{dQ}{dV} = C_s - C_x$ and during the non-discharging period the slope is zero. It is important that there be no harmonics in the test voltage because otherwise it is not possible to balance the bridge. The sensitivity may be found using the relationship $q = C_4 R$ (vertical deflection on oscilloscope in volts), where R is the detector transformer ratio. Dakin states that the charge per cycle sensitivity is better than 5×10^{-10} coulombs (500 pC).

A measure of the discharge energy E is the area of the loop trace,

$= Q\ (1.5708 V_{max} + 0.4292\ V_i)$ Joules per cycle at the test frequency used,

$= H\ (1.5708 V_{max} + 0.4292\ V_i)$ Volt divisions. The values of H,

V_{max} and V_i are as shown in Fig. 4.17d the charge diagram is assumed to consist of a parallelogram plus two half ellipses.[47]

4.3 Discharge measurements at very low frequency

In the preceding sections it was mentioned that conventional display and indicating instruments are unsuitable for use at VLF. In the initial experimental work an estimate was made of the sensitivity that could be obtained using a conventional RC integrator. To appreciate the problem, consider the following argument. The voltage output of an integrator is

$$e_o = \frac{1}{RC}\int_0^T e_i\,dt \quad \text{or} \quad e_o = \frac{1}{RC} e_i T \quad \text{------} \quad 4.36$$

where T = duration of pulse. The discharge pulse from the amplifier output is $\simeq$ 30 μs in complete width, however, the amplitude is only constant for 6 μs. Considering this as the input pulse to the integrator, the output voltage is $e_i\ 6.10^{-6}/RC$. Now RC has to be preferably much greater than the periodic time of the applied wave, i.e. RC $\gg$10s. The highest discharge voltage pulse recorded was 5 V, this corresponded to 3000 pC. It is now possible to estimate the output voltage from the integrator due to single discharge of 3000 pC, i.e., $5 \times 6 \times 10^{-6}/10 = 3\ \mu V$. This figure is very low and poses a problem for the electronics in terms of supply rail stability and circuit noise. By consulting Table 4.3.1 for number of discharges/half cycle in a given voltage level, the total voltage output from the integrator may be estimated for a half-cycle. It was deduced that the output voltage from the integrator was

$$e_o = \left(\frac{6 \times 10^{-7}}{RC}\right) e_i = 6 \times 10^{-7}\, e_i, \text{ where RC = 10.}$$

Since the output voltage of an integrator is proportional to the sum of the input pulses in number and magnitude we have

$$e_o = 6 \times 10^{-7} \sum N_i V_a \qquad \text{- - - - - -} \quad 4.37$$

where N_i = number of pulses in a particular voltage level

V_a = average voltage of the pulse in a particular voltage level = $(V + \Delta V)/2$.

From Table 4.3,

$N_i V_a = 25$, the output from the integrator is therefore

$25 \times 6 \times 10^{-7} = 15\ \mu V$.

Thus, integrating the discharge pulses over the periodic times of the test wave results in a very small voltage output. This voltage is too small to be seen visually on an oscilloscope and would need d.c. amplification. The maximum sensitivity on the oscilloscope used was 50 mV/cm, a signal of 10mV/cm on this scale would be just visible. Thus the d.c. amplifier would need a gain of at least 10 mV/15 μV $\doteq$ 670. The restrictions on the amplifier system are as mentioned:-

(1) good voltage stability in the voltage rails feeding the amplifier (also differential amplifier);

(2) very small ripple on the supply rails, (detector system should be powered by batteries);

(3) very low noise amplifiers with low d.c. drift properties are necessary.

The figure of 15 μV is quite realistic and it was indeed difficult to obtain an integrated signal, due to the causes mentioned. However, using pulse height analysis, sensitive measurements of charge and energy may be made. A typical pulse counting arrangement[27] is shown in Fig. 4.18, voltage pulses developed across the detector impedance are fed through a high pass filter to a wideband amplifier.

The input measuring circuit and amplifier bandwidths should be such as to utilise fully the time discrimination of the counters.

Usually resistance in parallel with capacitance is used as a measuring impedance, the capacitance being made variable to reduce sensitivity, while R_d is varied to keep approximately constant pulse duration. The gain of the amplifiers may be typically 10^5 (10 μv sensitivity) which is then sufficient to give a sensitivity of 0.01 pC in a test specimen of 100 pF, and also provide enough signal to operate the pulse counters. The pulse counter is operated with a discriminator level or pulse height analyser before the counting stages, and pulse inversion is usually necessary since counters operate with one polarity only.

In assessing the accuracy of pulse counts, it is necessary to take account of the fraction of pulses lost due to their occurrence within the discrimination time of the counter, which may be defined as the minimum time difference between consecutive pulses such that the counter counts both pulses. The amount of error involved can be estimated by using Poisson statistics for random events[48]. This law states that, for events occurring at random the probability that a time (t) elapses between consecutive events is given by

$$p = \int_0^t \mu e^{-\mu t} dt \qquad \text{------ 4.38}$$

where μ is the average occurrence of events/unit time. Applying this law to the case of random pulses, and taking τ as the resolution time for the counters, it can be seen that a probability of an interval less than this would be given by

$$p = \int_0^{\tau} \mu e^{-\mu t} dt \qquad \text{------ 4.39}$$

To take account of the bunching of pulses during the 0.1 Hz cycle, μ must be modified.

Integrating equation (9) gives

$$P = 1 - e^{-\mu\tau} \qquad \text{------} \quad 4.40$$

The probability value P is the loss of pulse in a given count. A curve showing the effect of this and also illustrating the effect of bunching is shown in Fig. 4.19.

4.4 Initial experimental investigation, arrangement and results

In order to minimise the electrical noise due to commutation, the high voltage VLF supply was filtered. It is desirable that the high voltage supply should not be filtered excessively because of:-

a) loss of supply voltage across specimen by impedance division

b) too long a supply recharge time constant for the discharge pulses which can also reduce the sample voltage under certain conditions - Widmann[49].

The filter comprised 20 MΩ in series with 3nF, giving 4% (1 dB) loss in 0.1 Hz test voltage across the specimen, whereas 95% (26 dB) of the commutation noise was filtered from the specimen. Further reduction in commutation noise and other electrical interference common to the VLF high voltage supply can be reduced substantially by using a balanced bridge and a precision high frequency differential amplifier (Fig. 4.20). An alternative to this is to employ a logic system developed by Black[50], sensitive measurements in an electrically noisy environment can be obtained with this method.

4.4.1 0.1 Hz discharge bridge and differential discharge detector

One arm of the discharge bridge consists of a discharge-free high voltage capacitor (C_s) terminated in a detection circuit consisting of both variable resistance (R_2) and capacitance (C_2). The other arm

consists of the specimen itself, terminated in a fixed resistance (R_1) and capacitance (C_1) detection circuit (Fig. 4.21). The time constant of the differential detection circuit is $10^4 \Omega \times 10^{-10} F = 1\ \mu s$. However, the lead capacitance of the differential amplifier modifies this to 4 μs. Balance of the bridge is achieved by varying both resistance and capacitance in one arm of the detection circuit. The variable capacitance compensates for the difference in the initial voltage step of the balancing square wave, whilst the variable resistance compensates for the decay time (Fig. 4.22).

For the bridge to be balanced, the voltage amplitudes and decay times in the differential circuit must be equal. As a consequence of this, a balance which is independent of frequency is achieved (provided that the dielectric losses of C_s and C_x are equal).

Now,
$$V_a = \frac{V\, C_s}{C_s + C_2} e^{-t/(C_s + C_2)R_2}, \qquad \text{------- 4.41}$$

$$V_b = \frac{V\, C_x}{C_x + C_1} e^{-t/(C_x + C_1)R_1}. \qquad \text{------- 4.42}$$

For zero output voltage from the bridge $V_a - V_b = o$, or $V_a = V_b$.

The initial voltage step is determined by capacitance division, and for the amplitudes to be equal $C_s/(C_s + C_2) = C_x/(C_x + C_1)$, or expressin in terms of the variable capacitance, $C_2 = C_s C_1/C_x$.

For the decay times to be equal, the exponentials in the above expressions must be equal, i.e., $(C_s + C_2)R_2 = (C_x + C_1)R_1$. Expressing this in terms of the variable resistance, $R_2 = (C_x + C_1)R_1/(C_s + C_2)$. The variable time constant R_2C_2 for balanced conditions must have a value $\left[(C_x + C_1)R_1/(C_s + C_2)\right] \times (C_sC_1/C_x)$, or $R_2C_2 = R_1C_1$,

$$\text{where} \quad = \quad (C_x + C_1)C_s / \left[(C_s + C_2)C_x\right]$$

R_1C_1 = fixed detector time constant,

R_2C_2 = variable detector time constant,

C_s = standard discharge free capacitance,

C_x = specimen capacitance.

By using an oscilloscope with a good differential amplifier as a discharge detector, common mode disturbances could be rejected by 125 times (42 dB) for a bandwidth of 100 kHz. This was determined by injecting a 2 kHz square wave of known amplitude at the top of the discharge bridge (Fig. 4.22a) and varying R_2C_2 until the signal was a minimum at the detector output (Fig. 4.23a). Hence, the ratio of the two signals gives a measure of the common mode rejection in the system.

Thus, the balanced discharge detection circuit is capable of operating in the presence of interference levels that would make the use of a single-input detector impractical. Interference due to commutation in the test circuit may be suppressed in this way (Fig. 4.20).

For optimum rejection[13], the dielectric losses in the test and high voltage standard should be equal, as otherwise the bridge balance conditions are different for every frequency. When the bridge is balanced, a discharge in the test object, of capacitance C_x produces an exponentially decaying voltage pulse across the bridge balance points.

The oscilloscope used for a discharge detector was modified to produce a single electrical output representative of the differential signal observed on the oscilloscope screen (Fig. 4.24). Because of a small amount of 5 MHz oscillatory pulses (due to commutation) in the output of the differential amplifier, a low-pass filter having a high frequency (3 dB) cut-off of 100 kHz was used to completely attenuate it. As the resolution (t) between successive pulses varies approximately as

the reciprocal of the bandwidth of an amplifier ($t = {}^{1}/_{\Delta f}$), 10^{5} ps^{-1} should be resolved. However, as far as pulse height analysis is concerned this is an inaccurate figure. For the pulse height analyser to measure no error in discharge magnitude, the output pulse from the filter due to a single discharge must be allowed to approach zero voltage.

The detector time constant, being much larger than that of the amplifier plays the major role in determining the output pulse width (Fig. 4.23b). However, the pulse width is the sum of the individual responses. To determine the time (t) for complete charging or discharging of an RC circuit, a value of 5 RC is generally taken. On this basis, the time for the output pulse (t_o) to approach zero voltage is calculated from

$$t_o = 5 \left[R_d C_d + (2\pi\Delta f)^{-1} \right] \qquad \text{------} \quad 4.43$$

where R_d, C_d are the detector capacitance and resistance respectively, Δf is the bandwidth of the amplifier. Substituting in the appropriate values of $R_d C_d$ = 4 μs, Δf = 100 kHz ($R_f C_f$ = 2 μs) in the above equation gave a value of t_o = 30 μs. Therefore, the maximum number of pulses that can be resolved without error in amplitude is ${}^{1}/t_o = 3.10^{4}$ ps^{-1}. The theoretical value of total pulse width (t_o) was in good agreement with the experimental one (Fig. 4.23b).

For maximum amplification, the discharge decay time constant (t_p) of the pulse should exceed the time constant (t_a) of the amplifier. Since, $t_a = 1/(2\pi\Delta f)$ = 1.5 μs and t_p = 4 μs, these conditions are fulfilled, i.e. $t_p > t_a$. However, under these conditions, the front of the pulse which had a 0.5 μs rise time at the input of the 100 kHz filter was found to be attenuated and having a rise time of = 3 μs.

This agreed well with filter theory that gives a value t_r (10% - 90%) = 0.35/(Δf, 3 dB), Δf = 100 kHz (Fig. 4.23b).

4.4.2 Pulse height analysis and measurement

Before pulse height analysis, the amplitude distributions of both charge (q) and energy (Δe) from the specimen were monitored. The experimental arrangement is shown in Fig. 4.24. This is similar to the final experimental arrangement and is explained in detail in the following section. Also included in this section will be the calculation of discharge energy loss/cycle and calibration of the similar systems. Referring now to the initial experimental work, the sensitivity controls on the differential amplifier were kept constant, and at a level that could cope with the largest pulse occurring without saturating the differential amplifier output. The maximum of each distribution was determined, and it was decided to pulse height analyse in ten equal pulse window levels. Unfortunately, only a single channel pulse height analyser was available, and the pulse window level had to be adjusted for each new measurement. The results are shown in Tables 4.4.2 and 4.4.3, and are plotted in histogram form in Fig. 4.25. The count of the pulses in each window level was taken over ten times the periodic time of the low frequency test wave (100s) and ten times above the commutation noise which was $\doteq$ 4 pC. These measurements were taken with 10 kV peak applied to the specimen stator bar section.

The integrated discharge energy in the specimen using the developed instrumentation was found to be 1.7 J/μF/cycle $\pm$ 12% - see Table 4.4.3 This compared favourably with a figure of 1.5 J/μF/cycle $\pm$20% when the specimen was tested at 50 Hz with a conventional dielectric loss analyser (DLA). The same voltage was applied to the specimen in each case, namely 10 kV peak. Although experimentally the two methods of measurement were quite different, the figures for discharge energy loss/cycle

are in good agreement. This and previous experimental work[35] tends to indicate that discharge energy loss/cycle is approximately the same at the two frequencies.

4.5 Final experimental arrangement and measurement technique

To obtain a good differential measurement it is required that the dielectric losses of the standard and specimen be almost identical; this is difficult to achieve in practice. One way to accomplish this is to test two identical specimens at the same time. In this way it is possible to achieve a very high rejection from high frequency noise on the test supply[13]. However, this is not the only requirement, the detector or differential amplifier must also have a very good common mode rejection ratio over a wide frequency range - this is difficult to meet.

In the final experimental arrangement, therefore, a simple 'straight' discharge detector was used, thus avoiding the complications of a differential one. The high voltage VLF supply was doubly filtered with two RC sections, comprising 9 MΩ and 0.01 μF respectively and because a two-section h.v.filter was employed, it was possible to perform reasonably sensitive measurements (Fig. 4.27). Before making discharge measurements, it was necessary to evaluate the level of discharge in the system with a discharge free capacitor in place of the specimen. The commutation noise in the system was found to be ≙ 200 pC in 150 pF with 20 $k\hat{V}$/0.1 Hz applied.

Because of the prohibitively long time involved in single channel pulse height analysis over a range of test voltages, a simple low resolution multi-channel pulse height analyser[51] was designed and constructed, this will now be discussed in detail. (A photograph of

the instrument is shown in Fig. 4.26).

4.5.1 Measurement

A measurement of total average discharge energy loss/cycle at 0.1 Hz was made using an analogue multiplier in conjunction with a simple low resolution pulse height analyser (PHA) - this is shown in Fig. 4.28. With this it was possible to measure the instantaneous power or energy taken from the VLF supply due to a discharge in the specimen - this in turn gave the loss of energy in the specimen itself.

The energy measuring system comprised:- the discharge detector, input amplifier, multiplier, high voltage potential divider and PHA. A fraction of the low frequency test waveform ($\lambda V \sin\omega t$) and the individual discharges (q_a) from the detector are multiplied together by an analogue device, the output of which (Δe) is the instantaneous value of charge times voltage, i.e., $\Delta e = (\lambda V \sin\omega t)\, q_a$. Energy may be taken from or returned to the supply by the specimen. It is possible to distinguish between energy supplied to the specimen and that returned by it on a polarity basis. Charge-voltage pulses taken from the supply are positive, whereas those returned are negative. This may be deduced by considering the phase of the applied voltage with respect to that of the discharges and taking the product of the two. Hence, if the charge-voltage pulses are integrated over a sufficiently long period of time and the difference taken, this is a measure of discharge energy loss in the specimen. However, only positive charge-voltage pulses were observed during the experimental work.

4.5.2 Calibration

The system was calibrated (for a particular sample) by simultaneous injection of known charge and voltage at the respective points

Fig. 4.28). For example, a known charge $V_o C_x$ i.e., (q_o) was injected into the specimen, this passed through the measuring system and formed the X-input of the multiplier. Simultaneously, a known direct voltage (V_{dc}) was applied to the bottom of the high voltage potential divider which formed the Y-input of the multiplier. Hence, the height of the voltage pulse from the multiplier was $V_{dc} q_o$. i.e., energy. Whereas it is necessary to do a charge calibration for every different specimen, it is not necessary to do a voltage one. The high voltage potential divider had an attenuation of $1.0 \times 10^4 \pm 3\%$.

The multiplier had a frequency response of 1 MHz and could cope with voltages of $\pm$10 V peak at the inputs. The electronic noise from the output of the multiplier was 10 mV p-p and this set a limit to the smallest signal that could be multiplied. For example, to see the output from the multiplier clearly, signals of 0.8 V and 0.02 V were required on their respective inputs. The voltage dynamic range of the multiplier was, therefore, taken to be 10 x 500 i.e., 5.10^3. The percentage error of the full output was 1%. Therefore, the multiplier used had good sensitivity, accuracy, voltage dynamic range and frequency response.

4.5.3 Calculation

The PHA gives the number of energy pulses in a particular level (over ten cycles of the low frequency wave), summation and averaging was performed arithmetically. Hence the total average discharge energy loss/cycle in the specimen is

$$\frac{\lambda}{AT_p} \sum_{o}^{AT_p} (V \sin \omega t \quad q_a) \qquad \text{- - - - -} \quad 4.44$$

where λ = attenuation factor

V = instantaneous voltage applied to the specimen.

A = integer $\geqslant 10$

T_p = periodic time of the low frequency wave.

q_a = apparent discharge magnitude.

The counters in the PHA were divided into five equal energy levels, i.e. e_1, $2e_1$, $3e_1$, $4e_1$, and $5e_1$ (Fig. 4.33). To calculate the total average integrated energy loss/cycle at 0.1 Hz, hereafter referred to as total De(0.1) for brevity, the following calculations were involved. The De(0.1) in a particular channel level (e_c), averaged over ten cycles of the low frequency wave is.

$$e_c = (ne_1 + \tfrac{1}{2}\beta e_1)N_c/10 \qquad \text{------} \quad 4.45$$

where n = integer (1→5).

N_c = number of pulses in a given channel level

i.e., N_1-N_2 etc.

e_1 = minimum discriminator energy level for counter 1.

βe_1 = channel energy separation

Since the counters are equally spaced in energy levels,

e_c in each channel level/cycle is, $e_{c1} = 0.15\ N_1e_1$,

$e_{c2} = 0.25N_2e_1$, $e_{c3} = 0.35N_3e_1$, and $e_{c4} = 0.45N_4e_1$ - from equation 4.45

where $N_{1\to4}$ = respective channel level counts.

The total De(0.1) in the specimen is, therefore, the sum of these individual quantities, hence

$$\sum_{j=1}^{4} e_{cj} = \frac{\lambda}{AT_p} \sum_{o}^{AT_p} (V \sin\omega t\ \ q_a) \qquad \text{- - - - -} \quad 4.46$$

A sample recording sheet used for this purpose is shown in Table 4.5.3.

4.5.4 Experimental instrument for determining discharge energy loss/cycle

Section 2.5 explains the basic principle involved in the measure-

ment of total De(0.1). The present section is concerned with the description of the experimental instrument for its determination.

The observed low repetition rate discharge pulses at 0.1 Hz made it possible to construct a low-resolution pulse height analyser (PHA) as a final store and recording stage for the energy pulses taken from the supply. The PHA is in effect being used as a sensitive integrator with an infinite time constant. An analogue integrator and visual display at VLF is impractical. To integrate the relatively small numbers of discharge pulses at 0.1 Hz over a time interval much greater than the periodic time of the applied wave, requires the use of very large time constants. Therefore, in this application, the analogue integrator is very insensitive.

In the instrument to be described, the PHA records the energy pulses taken from the VLF supply in five amplitude selective electromagnetic pulse counters. The number of pulses within any range of pulse magnitudes is determined by subtracting the sum of the upper channel count from the adjacent lower channel count.

Because of the low repetition rate of the discharge pulses, and the relatively high time constant in the discharge detection circuit of 15 μs, it was possible to use general purpose 741 operational amplifiers in the majority of the instrument design. It was also permissible to use electromechanical counters as final digital displays. The resolution time of the five counters were extended by the use of binary dividing circuits to 160, 80, 40, 40, 40 - ps^{-1} respectively. Since the pulse repetition rate decreases with amplitude, the counters in the lower levels were increased in resolution time by a greater amount.

Discharges from the specimen are developed across VR_x which is the

variable input attenuator for the voltage follower A_1 (Fig. 4.29). The initial amplitude of the discharge pulse developed across the terminals of the input amplifier, depends upon the ratio of the sample capacitance C_x, to that of a stray capacitance C_s. The stray capacitance C_s is variable, depending upon the position of the wiper on VR_x. The input capacitance of the amplifier is negligible. The decay time constant of the discharge pulse is then approximately, $(C_x + C_s)R_x$. Specimen capacitances(C_x) of $\doteq$ 150 pF were used in the experiments and a value of R_x was chosen to be 100 kΩ , this gave a detector time constant of 15 μs. The value of R_x was a compromise between completely attenuating the test frequency and maintaining optimal sensitivity of the following amplifiers. Optimal sensitivity is obtained if the time constant of the amplifier is made equal to that of the signal.[13]

The output of A_1 is fed directly into the Y-input of the analogue multiplier (Fig. 4.30). A fraction of the VLF test waveform fed through A_2 forms the X-input of the analogue multiplier. The high voltage capacitor divider C_4,C_5 attenuates the test frequency by 4×10^3 at the input of A_2. VR_1 (Fig. 4.29) is a fine adjustment control and with this it is possible to set the amount of attenuation in the X-input of the multiplier accurately. In this case it was set to 10^4 $\pm$3%. A_2 and its associated components must not introduce any significant phase shift in the test waveform applied to the multiplier, otherwise error will be introduced in the multiplication of q_a and V. The only source of phase error in this case would be in the relative value of C_5, R_3. The phase error is then $\theta = \tan^{-1}(X_c/R)$ $= \tan^{-1}(6.4 \times 10^4/10^6)$ giving $< 4^\circ$ or $\doteq$ 1% error.

The two signals having been multiplied together, are reduced in gain by 10 times at the output of the multiplier - this is necessary because of the wide voltage dynamic range of the device. The lost

gain is recovered through A_4 (Fig. 4.31). A_5,T_1 provide a sufficiently low output impedance source capable of driving five energy pulse height discriminators connected in parallel.

The five parallel connected energy pulse height discriminators consist of monostable circuits A_{7-11} (Fig. 4.34) which develop at their outputs, pulses of constant width and amplitude. The width of the output pulse is controlled by R_{25-29},C_{13-17}, 100 μs in this case. An output only occurs when the incoming energy pulse (Δe) exceeds the voltage discrimination level set on each circuit, these voltages are preset by VR_{8-12} to e_1, $2e_1$, $3e_1$, $4e_1$ and $5e_1$. A continuously variable control VR_7, (Fig. 4.31) allows these preset levels to be altered simultaneously to any amplitude range of energy pulses. The voltage discrimination level (VR_7) could be varied up to a maximum of 5V. This, in conjunction with the input attenuator VR_x, could accommodate any amplitude range of energy pulses experienced in the experimental work.

The 100 μs pulse from the discriminators is insufficient to operate the electromagnetic counters, and consequently must be lengthened in time. The binary dividers B_{1-5} (Fig. 4.34) perform this lengthening in time of the counters. The binary dividers can not drive the electromechanical counters directly, and therefore transistors T_{3-7} serve this purpose.

The energy pulses taken from the VLF supply are averaged over the cycles of the 0.1 Hz, i.e., 100s. It is convenient, therefore, to have a built-in device that only allows the instrument to function for this period of time, A_3, RL perform this function (Fig. 4.29). The pilot bulb (L) indicates the count time interval.

The stabilized d.c. supplies used to power the instrument are shown in Fig. 4.35 and 4.36. It is particularly important that the voltage fed to the voltage discriminator level control is well stabilised, otherwise error in pulse height discrimination would occur. To achieve the required amount of voltage stabilization, a commercial regulator is used following a series regulator (Fig. 4.35).

4.5.5 Sensitivity of the instrument

The energy of an individual discharge is $E_d = \frac{1}{2} q_a V_i$, if the voltage across the cavity falls to zero. If there are n equal discharges/cycle, the total power loss would be $\frac{1}{2} n f q_a V_i$. This may be equated to $\Delta \tan \delta$, or $(\tan \delta)_d$ as measured on a Schering bridge.[13]

Hence,

$$\frac{1}{2} n f q_a V_i = 2\pi f C_x \Delta \tan \delta \, V_i^2 \qquad \text{- - - - - - -} \qquad 4.47$$

$$\therefore \qquad \Delta \tan \delta = \frac{n q_a}{4\pi V_i C_x} \qquad \text{- - - - - - -} \qquad 4.48$$

q_a = apparent discharge magnitude

$\Delta \tan \delta$ = minimum rise in $\tan \delta$ which may be discerned. For an average bridge this is $\doteq 10^{-4}$.

As an example, consider a specimen C_x of 1nF in capacitance. Single discharges of 6×10^3 pC would just be detectable at $V_i = 5$ kV r.m.s. - according to the above formula. Detection of smaller discharges at voltages just above V_i would only be possible if many sites

were discharging. Thus, loss tangent measurements obtained from a Schering bridge, or by any integrating instrument, i.e., the dielectric loss analyser (DLA) are insensitive when only few discharges/cycle are present. It is also impossible for these instruments to distinguish between very large discharges in the presence of many small ones.

The developed instrument responds to both large and small amplitude pulses. It is also more sensitive than a Schering or DLA bridge in that it responds to single pulses. The increased sensitivity is obtained by using the PHA as an integrator. In the experimental arrangement used, it was possible to detect 14 pC in a specimen of 134 pF under calibration conditions, V_{dc} being equivalent to an applied test voltage of 5 kV r.m.s. Relating this to a value of $\tan \delta$, and replacing the test voltage for the inception voltage in equation 4.48, $\tan \delta$ 10^{-7}. This is an improvement of 10^{3} in sensitivity for an average bridge, and 10 times for the most sensitive.

4.6 Calibration of discharge measuring instruments and circuits

IEC Recommendations require calibration of both the measuring instrument and the complete detection circuit used for discharge measurements. The suggested methods of calibration are outlined below. Since the Recommendations themselves apply essentially to lumped parameter test objects, the calibration method and its application to partial discharge testing also only applies to this type of object. However, it is accepted that such a calibration be performed in the case of distributed parameter test objects, as a minimum requirement.

4.6.1 Instrument calibration

An instrument calibration is required to determine the instrument

indication corresponding to a discharge of known apparent charge and repetition rate, and also to determine either pulse resolution or the effect of different pulse repetition rates depending upon whether the instrument measures an individual or an integrated discharge quantity. In addition to this a complete determination of the instrument response over its working range of pulse amplitude and repetition rate is required to establish its suitability of measurement in this range. The instrument is calibrated together with the detector impedance and connecting cables since these are essential parts of the instrument. It is suggested that the calibration be repeated as necessary to check that the desired response characteristics are maintained.

4.6.2 Calibration of instruments measuring apparent charge q

Calibration of an instrument for the measurement of apparent charge q of single partial discharges is carried out by passing short current pulses of any convenient but known charge magnitude, q_o, through the instrument (or through the detection impedance Z_d). Such pulses may be produced by means of a generator giving rectangular step voltages of amplitude V_o, in series with a small known capacitance C_o should be small so that the duration of the current pulse through C_o is small compared with the response time of the instrument (or with $1/f_2$, where f_2 is the upper limit of the frequency response). The decay time of the step voltage should be long compared with this response time. Under these conditions this calibration pulse is equivalent to a discharge of magnitude $q_o = V_o C_o$.

As a source of calibration pulses with short rise times small, battery operated, pulse generators are in common use, employing either

transistors or relays with mercury wetted contacts.

4.6.3 Calibration of instruments measuring I or D

Instruments for measuring average discharge current I, or quadratic rate D, are calibrated by injecting pulses in the same manner as described and the same requirements should be met. In addition the pulse repetition rate, n, must be known. If the pulses are derived from a rectangular voltage generator of fundamental frequency, f_o, and if both positive and negative current pulses are used, the repetition rate n_o will be equal to $2f_o$. Under these conditions the instrument reading corresponds to an average discharge current $I = 2f_o.V_o.C_o$, or to a quadratic rate $D = 2f_o.(V_oC_o)^2$.

4.6.4 Calibration of RIV meters

RIV meters are calibrated for partial discharge measurement purposes by injecting pulses in the same manner as described and again the same requirements should be met. In addition, however, the value of C_o should be such that the time constant of the pulse at the meter terminals is $\frac{1}{f_d}$. Under these conditions for a pulse repetition rate of 100 ps^{-1} the RIV meter indication should be laid down in the appropriate specification (i.e. within the specified limits) for pulses of volt-time integral 0.158 μVS.

The variation of meter indication, K, with the repetition rate of repeated pulses (normalised with respect to the indication at 100 ps^{-1}) can also be determined by adjusting the repetion rate of the generator and again should be within specification.

4.6.5 Calibration of the instrument in the complete test arrangement

The calibration of the instrument in the complete test arrangement

is made to determine the factor by which the indication of the instrument has to be multiplied to give the desired quantity under the actual test conditions, with the test object connected. This factor is affected by the circuit characteristics, especially by the ratio of the test object capacitance to that of the coupling capacitor, C_x/C_k. Hence the calibration should be repeated for each new test object, except in cases when tests are made on a series of practically identical test objects. The calibration need only be made at one or a few values of the measured quantity. This calibration can be used to check the minimum discharge intensity which can be measured.

4.6.6 Calibration of test arrangements for measurement of q_o, I, D or RIV.

4.6.6a IEC Method

Calibration of instruments measuring q, I, D or RIV in the complete test arrangement should be made by injecting short current pulses into the terminals of the test object, as shown in Fig. 4.37 at a suitable repetition rate (IEC recommend twice test power frequency in ps^{-1}). In the case of test circuit A, shown in Fig. 4.2b, it is important to note that if the calibration pulses are applied between the high voltage terminal and earth, errors are likely to be introduced. In the same case, errors will also be caused by any stray capacitance C_{oe} to earth from the junction point of C_o and the step voltage generator unless these are negligible in comparison with C_o itself, since this causes a charge $V_o C_{oe}$ to flow through Z_d in the opposite direction to the calibration charge.

The calibration pulses are obtained in the same manner as described and should meet the same requirements. In addition to these requirements, the value of calibrating capacitor C_o must be less than

about 0.1 C_x, unless this capacitor remains connected during a test. The calibration pulse is then equivalent to a discharge magnitude $q = V_o C_o$.

4.6.6b Alternative methods

An alternative method of calibrating test circuits with very low capacitance test objects ($C_x < 10$ pF) is to inject a square wave from the generator directly in series with C_x as shown in Fig. 4.37a (ii) the calibration pulse then being equivalent to $q_o = V_o C_x$.

Another way of obtaining calibration pulses is by means of a corona discharge reference source, such as the point discharge gap or the wire discharge gap. As yet, however, no corona reference has been found which gives constant discharge magnitude consistently and such sources must themselves be calibrated.

Yet another method, indirect calibration, is used with some instruments measuring apparent discharge magnitude and this involves injection of charge into an element of the low voltage part of the measuring circuit, as shown for example in Fig. 4.37b (i), by a generator having the same characteristics as discussed previously. The square wave is often, as in the ERA Model II and III instruments, obtained from a mains driven relay thereby synchronising the calibration pulses with the test voltage frequency.

In either of the basic circuits A and B, Fig. 4.2, indirect calibration produces an indication equivalent to an actual discharge of magnitude,

$$q = V_o C_o \quad \frac{(C_x + C_k)}{C_k}$$

5. MEASUREMENTS ON STATOR BAR SECTIONS

In assessing the quality of single stator bars it is desirable to measure the amount of energy dissipated by discharges in the insulation. The object of the present experimental work was to measure this energy and attempt to detect voids of differing dimensions in thermally aged stator bar sections, and to evaluate the performance of the specially designed instrument. Hereafter the stator bar sections will be referred to as the specimens.

5.1 Preparation and thermal ageing of unrestrained specimens

Two 60 cm sections of 500 MW stator bars, the specimens, were prepared for measuring both maximum tan δ due to discharge loss only at 0.1 Hz and tan δ at 50 Hz, i.e., the difference between discharge and solid loss, hereafter these two quantities will be referred to $\delta_2 m$ and δ_1 respectively. The total average discharge energy loss/cycle, i.e., total De(0.1), over a range of test voltages was also measured.

The measuring electrode of each specimen was 14 cm long, giving capacitances of 168 and 178 pF respectively. The specimens were fitted with 3 cm long guards, the measuring and guard electrodes being applied with conducting paint. The specimens having been prepared, were then thermally aged in an oven at a constant temperature of 180°C. Every 48 hours, they were withdrawn from the oven and allowed to cool completely. The thermal shock which the specimens experienced, caused the insulation to delaminate. The specimens were aged for approximately 260 hours in total.

5.2 Measurement of δ_1 and $\delta_2 m$ in the thermally aged specimens

At the end of each 48 hour ageing interval, a measurement of both δ_1 and $\delta_2 m$ was made on the aged specimens.

A measurement of δ_1 was made using a Schering bridge (shown in fig 4.15a) over the test voltage range of 10-20 $k\hat{V}$ -10 $k\hat{V}$ being the discharge inception voltage of the specimens, δ_1 is given by the relationship.

$$\delta_1 = (\tan \delta - \tan \delta_o) = (C^1R_2^1 - CR_2) - - - \quad 5.1$$

where $\tan \delta = C^1R^1{}_2$ - solid plus discharge loss angle, and

$\tan \delta_o = C R_2$ - solid loss angle

Having obtained the values of $C R_2$ and $C^1R^1{}_2$ from the Schering bridge, at balance, for various ageing times of the specimens, equation 5.1 is used to obtain the values of δ_1.

The measurement of $\delta_2 m$ in the specimens was obtained using the experimental arrangement shown in Fig. 4.28. Here, total De(0.1) was measured from 10-20 kV peak, in intervals of 2 $k\hat{V}$; the results are shown in Table 5.2.1 Having obtained total De(0.1) for each value of test voltage for the aged specimens, it is then possible to express this in terms of an equivalent δ_1 - the maximum value of this was computed, i.e., $\delta_2 m$ for comparison with δ_1, the results of which are shown in Table 5.2.2 Calculation of this quantity is explained in section 5.4. The necessary calibration procedure involved is explained in Section 4.5.2.

5.3 Frequency independence of discharge inception voltage

Since an electrical discharge occurs in a time interval approximately 10^{-9}s, frequency effects in V_i are not to be expected until the test frequency approaches this time interval.[52] Buffler and Helszajn[53], have shown excellent correlation between partial discharge inception voltage at 60 Hz and power breakdown at 450 MHz, this was obtained by the relationship $P \propto V_i^2$, where P is the break-

down power and V_i is the inception voltage. This information was obtained when the authors were designing a microwave circulator. The dielectric materials used in the experimental work were ferrite and polystyrene crossed linked with teflon.

Both Mason[54] and Rodgers[20] use a model to explain the possible variation of discharge inception voltage with test frequency; they assume surface conductivity of the cavity walls of the void to be responsible. Whilst surface conductivity on the walls of the cavity with discharge activity no doubt effects the discharge sequence, it is unlikely to be responsible for significant changes in discharge inception voltage, that is the first discharge occurring in the cycle as the voltage is gradually increased across the void. Discharge inception voltage is substantially independent of frequency because the voltage across the void is initially determined by the permittivities of the system.

During the present experimental work V_i, at 0.1 Hz, was found to be 10% higher than that at 50 Hz. The inception voltage (V_i), at 0.1 Hz, was more difficult to determine than at 50 Hz, because of the reduced frequency and commutation noise from the VLF generator. Nevertheless, it was established that V_i at the two frequencies differed by no greater amount than 10%. A subsidiary experiment conducted at 1200 Hz on micaceaous insulation also showed V_i to be essentially the same as at 50 Hz. Since micaceous insulation has an extremely high volume resistivity, frequency dependence due to discharge activity is not to be expected.

5.4 Presentation of results at 0.1 Hz

The power (P) dissipated in a dielectric with associated parallel resistive loss (R) is V^2/R, and since $\tan \delta_o = 1/\omega CR$, the power (P), therefore, may be written as

$$P = V^2 \omega C_x \tan \delta_o \qquad \text{------} \quad 5.4$$

where V = Applied voltage to the dielectric or specimen

ω = Angular frequency of the applied voltage

C_x = Sample capacitance below discharge inception

tan δ_o = Loss angle of the specimen below discharge inception

This is the power dissipated in the solid part of the specimen. The part due to discharge only, at 0.1 Hz, is (tan δ - tan δ_o), i.e. δ_2.

Now discharge energy loss/cycle (E) is

$$E = 2\pi C_x^* \delta_2 (V-V_i)^2 \qquad \text{------} \quad 5.5$$

where $C_x^* = C_x + \Delta C$, i.e., solid capacitance plus that due to discharge ($C_x^* \doteq C_x$).

V_i = Discharge inception voltage

δ_2 = Loss angle due to discharge only

Clearly, E is a function of $(V-V_i)^2$. Therefore, if discharge energy loss/cycle is plotted versus $(V-V_i)^2$, a straight line graph is obtained - providing C_x and δ_2 remain sensibly constant with applied voltage. For good quality insulation this condition should hold, since the insulation may be thought to contain only small voids of approximately uniform dimensions. Briefly, for good quality insulation, discharge energy loss/cycle increases to no greater than $(V-V_i)^2$. However, if the insulation contains fissures or other weak long paths, inert at moderate stress but discharging over progressively longer paths as the stress increases, the discharge energy loss/cycle may be no longer proportional to $(V-V_i)^2$. Therefore, plotting discharge energy loss/cycle as a function of $(V-V_i)^2$ makes analysis more amenable.

Later, comparison is made with δ_1 and $\delta_2 m$, 20 kV peak being applied to the specimen in each case. To calculate δ_2 over a range of test voltages and $\delta_2 m$ at 20 kV peak, equation 5.5 is re-arranged to give

$$\delta_2 = E/\left[2\pi C_x (V-V_i)^2\right] \qquad \text{------} \quad 5.6$$

and $$\delta_2 m = 10^4 E/2\pi C_x \qquad \text{------} \quad 5.7$$

where E is the total De(0.1) in Joule, C_x is the specimen capacitance in picofarad and $(V-V_1)^2 = 10^8$ in Volt.

The results in Table 5.2.2, for $\delta_2 m$, are obtained via these equations. The decrease in C_x with ageing time of the stator bar section was accounted for in calibration.

5.5 The variation of total De(0.1) versus $(V-V_i)^2$ with thermal ageing time of the specimens

The increase and variation of total De(0.1) versus $(V-V_i)^2$ for the two specimens is shown in Figs. 5.1 and 5.2; only initial, intermediate and final ageing times are shown for clarity.

Before discussing the experimental results obtained, an examination is made of the possible ways in which total De(0.1) might increase with $(V-V_i)^2$, these are:-

(a) If total De(0.1) increases linearly with $(V-V_i)^2$, this implies that there is no large increase with voltage in either the number of separate discharging sites, or in their average length.

(b) If total De(0.1) increases linearly with $(V-V_i)^2$, at low voltages and then ceases to increase at high voltages, this indicates that all the voids in the insulation are being discharged and no new discharge sites are available.

(c) If the rate of change of De(0.1) with $(V-V_i)^2$ increases with voltage, this implies that the insulation contains fissures or long weak paths, inert at moderate stresses, but discharging over progressively longer paths as the stress increases.

Referring now to the present experimental work, the results of which are plotted in Figs. 5.1 and 5.2. The purpose of thermally ageing the specimens was to create both large and small voids within the insulation, the intention being:-

(1) To measure any increase of total De(0.1) with ageing time of the specimens.

(2) To differentiate, if possible, between both the large and small voids created in the specimens (Fig. 5.10a, b and c).

The first of these was easy to measure. Figs. 5.1 and 5.2 show that for all ageing times the total De(0.1) in the two specimens increases, but is always proportional to $(V-V_i)^2$ on average. The best straight lines through the experimental points show this. Unfortunately, this indicates that small voids cannot be separated from the larger ones, the reason for this being two-fold

(1) Surface discharges across the guard-electrode interspace of the specimens made it difficult to correlate measured inception voltage with the physical parameters - this is explained more fully in section 5.8.

(2) Errors - since the measurement and calibration of total De(0.1) was a function of (C_x, V_s, V_{dc}, N , T)

where C_x is the specimen capacitance

V_o is the square wave calibration signal

V_{dc} is the d.c. calibration signal

N is the count number error

T is the count time interval.

total De(0.1) could not be measured to a greater precision than $\pm$ 15%. Here, C_x, V_o, V_{dc} = $\pm$ 3%, N = $\pm$ 10%, T = $\pm$ 5%.

This, as the error bars in Figs. 5.1 and 5.2 indicate, made it difficult to assess, particularly at higher test voltages, whether total De(0.1) was increasing or decreasing with respect to $(V-V_i)^2$. All that could be done was to draw the best straight lines through the experimental points - thus implying total De(0.1) is proportional to $(V-V_i)^2$ for all electrical stresses and ageing times; this is difficult to appreciate. However, it is believed that voids of differing dimensions could be detected, if the measurements were completely automated and vi-

sually displayed. This is explained in Section 6.0.

5.6 The variation of δ_1 and δ_{2m} with thermal ageing time of the specimens

Table 5.2 gives the measured values of δ_1 and δ_{2m} for the thermally aged specimens recorded over the same ageing period; these are shown graphically in Figs. 5.3 and 5.4. Although δ_1 and δ_{2m} both increase with ageing time, δ_1 is larger than δ_{2m} and apparently increases at a greater rate. The variation of δ_1 and δ_{2m} with ageing time is linear - that is, apart from the initial reading at T = 0, before the bars were thermally aged. The only explanation offered for this is the initial thermal shock which they experienced.

As for the greater increase of δ_1, it was difficult to obtain a sensitive balance on the Schering bridge at the higher ageing times, and therefore the experimental error involved was larger. The greater increase of δ_1 over δ_{2m} was, therefore, considered insignificant.

The low measured value of δ_{2m} compared with that of δ_1 may be accounted for in two ways; the first being due to measuring only half the energy pulse distribution, because of commutation noise from the VLF, generator. No great precision could be placed on exactly half the energy pulse distribution being lost during any one interval of test voltage. By examining the pulse count, which was approximately Gaussian distributed over various test voltage ranges, the maximum error expected was $\pm$ 10%. The second reason for the comparably low measured value of δ_{2m} is because of the differing experimental arrangements. No real figure can be associated with this, unless it is assumed that δ_1 and δ_{2m} are equal at the two frequencies. It is reasonable to expect δ_1 to be higher because of the method of measurement. A Schering bridge is used to measure δ_1 which does not separate solid

loss from discharge loss. The instrument developed for use at 0.1 Hz measures the loss due to discharge only.

Earlier work[35] showed that discharge energy loss/cycle by the loop trace method was approximately the same at the two frequencies. The experimental error involved here was no greater than 20%. However, a perfect correlation between δ_1 and $\delta_2 m$ in the present experimental work should not be expected, since the methods of measurement are completely different. To expect perfect correlation similar quantities must be measured, i.e., tan δ due to discharge loss only with the same experimental arrangement. Unfortunately, the resolution of the constructed instrument made this impossible.

5.7 The variation of discharge energy pulse/cycle before and after thermally ageing the specimens with applied test voltage

Discharge energy pulse/cycle versus total average channel energy as a function of applied test voltage to the specimens before and after thermal ageing is illustrated in Figs. 5.1 to 5.8 - see Tables 5.7.1 and 5.7.2 for the recorded data. For clarity of illustration, this data is shown as being continuous in the figures rather than its more correct discrete histogram form, which could make display comparatively difficult.

From Figs. 5.5 and 5.7 both the specimens before ageing increase and vary in the same way, both having a maximum lower channel count of $\doteq 100\mu J$. The specimens at the end of their thermal ageing programme also show similar characteristics (Figs. 5.6 and 5.8). Here again both have a maximum lower channel count of $\doteq$ 40 pulse/cycle, but with a total average channel energy of $\doteq 600\mu J$. The increase of the total

average channel energy for the aged specimens is because of the greater number of discharging voids present, compared with that of the specimens before ageing.

The same number of pulses/cycle for the specimens before and after ageing occurs because the discharge energy pulse maximum is used as a reference level for counting in the PHA. This encompasses the same pulse/cycle distribution for the specimens before and after ageing, the only difference being that the pulses increase in energy - experimentally this was the case.

5.7.1 Counting errors

Two sources of error were involved in counting. One source of error was due to commutation noise from the VLF generator, the other was due to the resolution time of the counters. Unfortunately, due to commutation noise, the counters had to be biassed such that a 50% loss of pulses occurred. The figure of 50% was determined by examining the distribution of pulses in given levels. This was monitored over the whole test programme. The other source of loss involves the counters. The highest average pulse repetition rate/cycle observed in the lowest counter above commutation noise was 84 ps^{-1}. This was measured with 20 $k\hat{V}$/0.1 Hz applied to a section of stator bar at the end of its thermal ageing programme. Equation 4.40 ($P = 1 - e^{-\mu\gamma}$) is plotted in Fig. 5.9 for various resolution times of the counters involved in the experimental work. Therefore, with the pulse repetition rates found experimentally, and the resolution of the counters involved, it was necessary in certain cases to apply correction factors.

5.8 Correlation of discharge energy and inception voltage with void dimensions in the specimens before and after thermal ageing

To analyse the void dimensions and content in the thermally and

non-thermally aged specimens, complete sections were cut away.

Selected small areas of the specimens were examined under the microscope and photographed at ten times magnification, reduced photographs are shown in Figs. 5.10a, b and c.

The non-thermally aged specimen is well consolidated and has practically no void content. However, the specimen which had been severely thermally aged at 180°C, for a period of 260 hours, in an unrestrained condition, was delaminated (Figs. 5.10b and c).

In the following sections, an attempt is made to correlate the measured discharge energy; and inception voltage (V_i), with the void dimensions of the thermally aged specimens.

5.8.1 Calculation of inception voltage

The capacitance (C_s) of a solid section of insulation in which a series void or air gap of capacitance C_v is present, is given by

$$C_s = \frac{\varepsilon_o \varepsilon_r A}{(t_s - t_g)} \qquad \text{------} \qquad 5.8$$

where, t_s is the thickness of the total solid insulation, and, t_g is the thickness of the air gap. The capacitance of the air gap being:-

$$C_v = \frac{\varepsilon_o A}{t_g} \qquad \text{------} \qquad 5.9$$

The voltage developed across the air gap or void (V_v) is simply

$$V_v = \left(\frac{C_s}{C_s + C_v}\right) V \qquad \text{------} \qquad 5.10$$

whereupon substitution of the respective physical quantities becomes

$$V_v = \frac{\varepsilon_r V}{(t_s - t_g)} \Big/ \left[\frac{1}{t} + \frac{\varepsilon_r}{(t_s - t_g)}\right] \qquad \text{------} \qquad 5.11$$

$$\text{or } V_v = V \,/\, \left(1 + \frac{t_s}{\varepsilon_r t_g}\right) \text{ for } t_s \gg t_g \qquad \text{----} \qquad 5.12$$

The largest void volume found in the thermally aged specimen was approximately, (0.1 x 10 x 5) mm^3 - these figures are for gap, width and length respectively (Fig. 5.10c). The breakdown voltage (V_b) for the 0.1 mm air gap was found from Paschen's curve to be $\doteq 10^3$V. However, to attain this value of V_b, the voltage at the test terminals of the specimen must be greater; this depends upon the thickness and the permittivity of the solid insulation in which the air gap is situated. Hence, the inception voltage (V_i) measured at the test terminals is found by equation 5.12. Here, $t_s = 5_{mm}$, $t_g = 0.1$ mm, and $\varepsilon_r \doteq 5$, giving a value of $V_i \doteq 10$ kV peak. This was confirmed experimentally. From Figs. 5.1 and 5.2, V_i remained reasonably constant throughout the thermal ageing programme - that is, from T = 0 to T = 260 hours.

The void content of the non-thermally aged bar was extremely small, the largest void being approximately 30 μm in thickness (Fig. 5.10a). This gives an inception voltage of 17 kV peak. It becomes difficult, therefore, to accept the measured inception voltage for the non-thermally aged specimens as being real - surface discharges across the measuring electrode and guards are presumably being measured. The measured inception voltage for the thermally aged specimens is obviously real - the physical dimensions in Fig. 5.10c confirm this.

5.8.2 Calculation of discharge energy

Knowing the approximate values of V_b and C_v for the void in question, the energy (E_v) dissipated in it can be found from equation 2.25

$$E_v = \tfrac{1}{2}V_b^2(C_v + C_s)$$

where, $C_v \doteq 4.5$ pF, $C_s \doteq 0.5$ pF, $V_s \doteq 10^3$

$$\therefore E_v \doteq 2.5\ \mu J$$

However, it is known[14,55] that when a cavity breaks down electrically, only small fractions of the total area are involved, and conse-

quently small capacitance discharged. A more realistic approach, than that adopted above, is to measure the total fractional capacitance (ΔC_x) discharged in the thermally aged specimens directly from the Schering bridge, i.e., $\Delta C_x = (C^1_x - C_x)$. For the two specimens ΔC_x was found to be 7 and 10 pF respectively, - see sample tan δ recording sheet Table 5.5. From this it is possible to estimate the amount of energy dissipated, at 50 Hz, during a single discharge in the thermally aged specimens by the following

$$E_x = \tfrac{1}{2} V_b^2 \Delta C_x \qquad \text{------} \qquad 5.13$$

where V_b = mean breakdown voltage of the voids.

Here ΔC_x = 10 pF, $V_b \doteq 10^3$

$\therefore \quad E_x \doteq 5\ \mu J$

The foregoing confirms that even when large voids exist in insulation, the whole area is not actively involved. For example, the largest void found from physical dimensions was $\doteq$ 4.5 pF, yet on measuring the total incremental change in capacitance (ΔC_x), due to discharge on the Schering bridge at 50 Hz, was $\doteq$ 10 pF for the whole specimen.

6. CONCLUSIONS

VLF discharge detection and measurement techniques have been used in an attempt to evaluate the condition of stator bar insulation. While the VLF generator used in the present experimental investigation was electrically very noisy, it was possible, however, to perform reasonably sensitive discharge measurements on machine insulation. This was achieved by filtering the high voltage VLF supply and carefully screening the necessary components and the discharge detection circuit.

The initial experimental investigation indicated that discharge energy loss/cycle was approximately the same at 50 and 0.1 Hz, to within $\pm$20%. Although the two methods of measurements were completely

different. The 50 Hz measurement of discharge energy loss/cycle was obtained using a conventional instrument, the dielectric loss analyser (DLA), the 0.1 Hz measurement being obtained by a specially developed instrument.

In the final experimental investigation it was decided to use a less complicated system and to dispense with both the complex differential discharge detection system and the commercial single channel PHA. In place of the differential discharge system a 'straight' discharge detector was employed, the high voltage VLF supplying being filtered by a greater amount to maintain the same discharge sensitivity. A simple multichannel PHA was designed, constructed and used instead of the single channel commercial PHA, thus reducing measurement time to a minimum. The constructed instrument was used to measure total average discharge energy loss/cycle at 0.1Hz, i.e., total De(0.1) over a range of test voltages for various ageing times of the specimens. To simplify analysis of results, and possibly indicate a method of detecting small voids from the larger ones in the insulation, total De(0.1) was plotted as a function of $(V-V_i)^2$. The developed instrument responds to both large and small amplitude discharge pulses. It is also more sensitive than a Schering or DLA bridge in that it responds to single discharges. The increased sensitivity is obtained by using the PHA as a recording instrument. The improvement in sensitivity was 10^3 for an average bridge, and 10 times for the most sensitive.

It was found that the distribution of energy pulses taken from the VLF supply was similar for the specimens both before and after ageing, the only difference being a shift toward the higher energy levels for the thermally aged bars.

The maximum value of total De(0.1) for the ageing times of the specimens was converted into an equivalent tan δ discharge and compared with a value measured on the Schering bridge at 50 Hz. Whilst the variation of these quantities with ageing time of the specimens were approximately the same, they differed by a constant amount. Some of the difference was accounted for by only measuring half the total De(0.1) because of commutation noise from the VLF generator, the other being unaccountable and due to the measurements of similar, but not necessarily equal quantities on different experimental arrangements.

During the experimental work total De(0.1) was found to be proportional to $(V-V_i)^2$ for all electrical stresses and ageing times. Whereas it was possible to show the increase in total De(0.1) with ageing time, it was not possible, with the present experimental arrangement, to detect voids of differing dimensions. This was because of surface discharge across the guard electrode interspace, and lack of precision in the measurements. However, it is believed that the system now to be described will be more successful. Figure 6.1 shows the proposed system. Here, the discharge energy pulses are counted and averaged electronically - that is, a voltage proportional to the total De(0.1) is developed. This is applied to the Y-input of a recording device. The X-input is simply obtained by squaring a known fraction of the test voltage and taking the peak value of it. The result of this is a continuous plot of total De(0.1) versus $(V-V_i)^2$, or more correctly in this case versus V^2, as the test voltage increases at a stipulated rate. Total De(0.1) versus $(V-V_i)^2$ was measured over a test voltage range of 10-20 kV peak, for a particular ageing time, intervals of 2kV - each measurement taking 100s. Hence one complete set of measurements taking 600s. The visual display of this however, need not be presented at this rate. With the advent of micro-

processors, this information could be stored during the test, then displayed on a conventional oscilloscope at 50 Hz, - thus comparative measurement and analysis would be obtained with ease.

APPENDIX

Discharge repetition rate/second/$\frac{1}{2}$ cycle (Ni)	Va	VaNi
15	0.75	11.2
3	1.25	3.7
3	1.75	5.2
1	2.25	2.2
1	2.75	2.7
		$\sum$ 25.

INTEGRATOR OUTPUT VOLTAGE/

HALF CYCLE

TABLE 4.3.1.

V + ΔV	+ ve ½ cycle No/100s	-ve ½ cycle No/100s	Average integrated charge/½ cycle (pC)	
			+ve	-ve
0.5 + 0.5	150	170	12375.0	14025.0
1.0 + 0.5	25	38	3437.5	5225.0
1.5 + 0.5	27	18	5197.5	3465.0
2.0 + 0.5	12	13	297.0	3217.5
2.5 + 0.5	13	10	3932.5	3025.0
3.0 + 0.5	7	12	2502.5	4290.0
3.5 + 0.5	2	3	825.0	1237.5
4.0 + 0.5	4	2	1870.0	935.0
4.5 + 0.5	4	2	2090.0	1045.0
5.0 + 0.5	1	0	577.5	0
			∑33104.5	∑36465.0

Calibration 0.1 V = 55pC.

DISCHARGE MAGNITUDE AND AVERAGE INTEGRATED CHARGE/HALF CYCLE

TABLE 4.4.1

V + ΔV	Nc/100s	Average integrated discharge energy/cycle (μJ)
0.1 + 0.1	107	98.88
0.2 + 0.1	56	78.40
0.3 + 0.1	29	56.84
0.4 + 0.1	20	50.40
0.5 + 0.1	13	40.04
0.6 + 0.1	8	29.12
0.7 + 0.1	10	42.00
0.8 + 0.1	7	33.32
0.9 + 0.1	6	31.92
1.0 + 0.1	2	11.20
		$\sum$ 472.12

Calibration 01V = 5.6 μJ. Total average discharge energy/cycle = 472 μJ. Sample capacitance C_x = 280pF

Expressing in J/μF/cycle = $472 \times 10^{-6} \quad \frac{10^6}{280} =$

1.7J/μF/cycle

TOTAL AVERAGE DISCHARGE ENERGY LOSS/CYCLE

TABLE 4.4.3

R_{1-2}	9 MΩ ±10%, 20 kV (r.m.s)
R_3	1 MΩ ±2% ½ Watt
R_4	220 kΩ ±2% ½ Watt
R_{5-7}	3.3 kΩ ±2% ½ Watt
R_{8-13}	4.7 kΩ ±2% ½ Watt
R_{14-15}	1 kΩ ±2% ½ Watt
R_{16}	10 kΩ ±2% ½ Watt
R_{17-18}	3.3 kΩ ±2% ½ Watt
R_{19}	2.7 kΩ ±2% ½ Watt
R_{20-34}	1 kΩ ±2% ½ Watt
R_{35}	330 Ω ±5% 1 Watt
R_{36}	1 kΩ ±5% 1 Watt
R_{37}	150 Ω ±5% 1 Watt
R_{38}	3.3 kΩ ±5% 1 Watt
R_{39}	11 Ω ±5% 1 Watt
VR_X	100 kΩ ±20% 2 Watt
VR_{1-5}	10 kΩ ±20% 2 Watt
VR_6	50 kΩ ±20% 2 Watt
VR_7	100 kΩ ±20% 2 Watt
VR_{8-12}	1 kΩ ±20% 2 Watt
C_1	0.33μF ±20% 100 kV (r.m.s)
C_{2-3}	0.01μF ±20% 100 kV
C_4	0.005μF ±20% 100 kV
C_5	25μF ±20% 30 kV
C_6	200μF ±20% 30 kV

COMPONENTS LIST FOR INSTRUMENT TO MEASURE TOTAL De(0.1)

TABLE 4.5.1

C_7	100 µF ±20% 30 V
C_{8-17}	0.1 µF ±20% 160 V
C_{18}	1000 µF ±20% 160 V
C_{19}	100 µF ±20% 160 V
C_{20}	470 µF ±20% 160 V
C_{21}	1000 µF ±20% 160 V
C_{22}	470 µF ±20% 160 V
C_{23}	100 µF ±20% 160 V
C_{24}	3500 µF ±20% 160 V
D_{1-20}	DD006 diodes 400 p.i.v. 500 mA. (Lucas)
ZD_1	20 V 1 Watt Zener diode 1220 (International)
ZD_2	15 V 1 Watt Zener diode 1215 (International)
RG	15 V regulator. LM337 (Rastra)
A_{1-11}	741 operational amplifiers (SGS)
T_{1-8}	BFY 52 transistors (Mullard)
T_9	ACY 21 transistors (Mullard)
X_1	AD 530 Multiplier (Analog Devices)
B_{1-5}	SN 7473N dual binary dividers (Texas)
RL	12 V relay (Omron)
CR_{1-5}	Veeder root electro-mechanical counters type KE/1643 24 V
M_1	1 mA moving coil meter (Sifam)
TR_1	240/20 V transformer (radio-spares)
TR_2	240/6.3 V -0-6.3V transformer (radio-spares)
L	6.3 V/0.3 A pilot bulb
S	Counter reset switch

COMPONENTS LIST FOR INSTRUMENT TO MEASURE TOTAL De(0.1)

TABLE 4.5.2

SAMPLE RECORDING TABLE FOR THE CALCULATION OF TOTAL AVERAGE DISCHARGE ENERGY LOSS/CYCLE AT 0.1 Hz i.e. TOTAL De(0.1). SPECIMEN D, AGED FOR 219 HRS.

TABLE 4.5.3

Discriminator energy counts/10 cycles		Corrected Channel energy counts/10 cycles		Average energy loss/cycle	
Counter	No	Correction	No	Factor	μJ
1	45	8(1-2) = Ch 1	144	$0.15E_1N_1$	43.3
2	54	4(2-3) = Ch 2	98	$0.25E_1N_2$	49.0
3	59	2(3-4) = Ch 3	22	$0.35E_1N_5$	15.4
4	48	2(4-5) = Ch 4	18	$0.45E_1N_4$	16.2
5	39			$\sum$	123.8
Test Voltage $k\hat{V}$ = 12				Energy discriminator level (V) = 2	
Amplifier Attenuation γ = 260				Sample capacitance (C_x) = 134 pF	

Energy Calibration

$E_1 = \propto C_x V_s V_{dc}$ (For a given γ)

where $\propto$ = VLF supply attenuation = 10^4

V_{dc} = Direct voltage calibration to multiplier (Yin) = 1.5

V_s = Square wave calibration signal injected into C_x (X_{in})

$\therefore$ $E_1 = 1.5 \times 10^4 C_x V_s$

Here $E_1 = 1.5 \times 10^4 \times 1.34 \times 10^{-10} \times 1.0 = 2.0$ μJ

Total De(0.1) x 10^{-4}J	T=0	T=46	T=112	T=157	T=201	T=266	$(V-V_i)^2 \times 10^6 V$
	0.00	0.10	0.02	0.02	0.03	0.02	0
	0.02	0.50	0.75	1.10	1.20	1.50	4
	0.37	1.20	2.10	2.60	3.25	4.50	16
	0.80	1.80	3.70	4.30	5.30	6.60	36
	1.50	2.70	4.20	6.50	7.30	10.10	64
	2.10	3.80	7.10	9.20	10.40	12.70	100

Specimen C

Total De(0.1) x 10^{-4}J	T=0	T=69	T=111	T=172	T=219	T=262	$(V-V_i)^2 \times 10^6 V$
	0.00	0.10	0.03	0.02	0.18	0.01	0
	0.02	0.21	0.57	1.20	1.24	1.50	4
	0.58	0.78	1.64	2.00	2.82	3.50	16
	0.78	1.90	3.20	4.80	5.30	5.75	36
	1.20	3.10	5.30	6.10	8.20	8.90	64
	1.60	4.70	7.50	8.60	10.10	12.90	100

Specimen D

RECORDED VALUES OF THE VARIATION AND INCREASE OF De(0.1) WITH AGEING TIME OF THE SPECIMENS VERSUS $(V-V_i)^2$.

TABLE 5.2.1

$\delta_1 \times 10^{-3}$	$\delta_{2m} \times 10^{-3}$	T(hr)
7.6	0.74	0
17.1	2.58	69
22.0	4.41	111
28.2	5.22	172
33.0	6.13	219
36.0	7.87	262

Specimen D

$\delta_1 \times 10^{-3}$	$\delta_{2m} \times 10^{-3}$	T(hr)
8.1	1.20	0
15.2	2.00	46
22.0	3.50	112
26.1	5.10	157
33.0	6.10	201
37.0	7.00	266

Specimen C

RECORDED VALUES OF THE VARIATION AND INCREASE OF δ_1 and δ_{2m} WITH AGEING TIME OF THE SPECIMENS

TABLE 5.2.2

Test Volts kV̂	Average Channel Energy, (μJ)				Channel counts (average No/cycle)			
	1	2	3	4	1	2	3	4
10	0	0	0	0	0	0	0	0
12	0	2	0	0	0	1	0	0
14	0	37	0	0	0	14	0	0
16	0	79	2	0	0	31	1	0
18	4	62	11	3	3	23	3	1
20	77	92	29	9	50	36	8	2

Specimen C - before thermal ageing

Test Volts kV̂	Average Channel Energy, (μJ)				Channel counts (average No/cycle)			
	1	2	3	4	1	2	3	4
10	1	15	5	2	1	5	1	0
12	50	79	30	22	15	14	4	2
14	154	184	62	48	27	19	5	3
16	202	297	94	69	35	31	7	4
18	326	481	116	85	37	33	6	3
20	382	596	169	122	43	40	8	5

Specimen C - after thermal ageing

RECORDED VALUES OF CHANNEL ENERGY COUNTS PER CYCLE FOR THE AGED AND NON-AGED SPECIMENS

TABLE 5.7.1

Test Volts kV̂	Average Channel Energy, (μJ)				Channel counts (average No/cycle)			
	1	2	3	4	1	2	3	4
10	0	0	0	0	0	0	0	0
12	3	9	3	1	1	2	1	0
14	0	46	8	4	0	11	1	1
16	7	44	24	4	3	11	4	1
18	9	60	12	3	3	20	5	1
20	80	100	30	8	47	32	11	3

Specimen D - before thermal ageing

Test Volts kV̀	Average Channel Energy (μJ)				Channel counts (average No/cycle)			
	1	2	3	4	1	2	3	4
10	1	14	5	3	1	4	1	0
12	45	82	25	19	12	10	3	1
14	160	168	55	38	24	17	4	2
16	197	301	85	72	32	28	6	3
18	330	456	110	81	40	30	5	2
20	370	580	170	110	45	41	9	4

Specimen D - after thermal ageing

RECORDED VALUES OF CHANNEL ENERGY/COUNTS PER CYCLE

THE AGED AND NON-AGED SPECIMENS

TABLE 5.7.2

Test Volts ($k\hat{V}$)	R_1 (Ω)	C (μF)	$C_x = C_s \frac{R_2}{R_1}$ (pF)	TAN δ ($\omega R_2 C$)
8	2450.0	0.443	129.8	0.0443
10	2450.0	0.443	129.8	0.0443
12	2447.1	0.451	130.0	0.0451
14	2440.0	0.471	130.3	0.0476
16	2410.0	0.580	132.0	0.0580
18	2364.0	0.700	134.5	0.0700
20	2324.3	0.790	136.8	0.0790

Specimen C

Test Volts ($k\hat{V}$)	R_1 (Ω)	C (μF)	$C_x = C_s \cdot \frac{R_2}{R_1}$ (pF)	TAN δ ($\omega R_2 C$)
8	2666.0	0.120	119.3	0.0120
10	2665.0	0.130	119.3	0.0130
12	2658.0	0.150	119.6	0.0150
14	2636.0	0.220	120.6	0.0220
16	2585.0	0.369	123.0	0.0369
18	2517.2	0.520	126.3	0.0520
20	2462.1	0.610	129.2	0.0610

Specimen D

N.B. $C_s = 10^{-9}F$, $R_2 = 318.5\,\Omega$, $\omega R_2 \left[C\ (\mu F)\right] = 0.1$

$\Delta C_x = (C_x^1 - C_x)$ - over the range 10 - 20 $k\hat{V}$.

$\therefore \Delta C_x(C) \doteq 7pF$, $\Delta C_x(D) \doteq 10pF$.

SAMPLE TAN δ (50 Hz) TABLES FOR THERMALLY AGED SPECIMENS C AND D AFTER 260 HOURS OF AGEING AT 180°C

TABLE 5.8.1

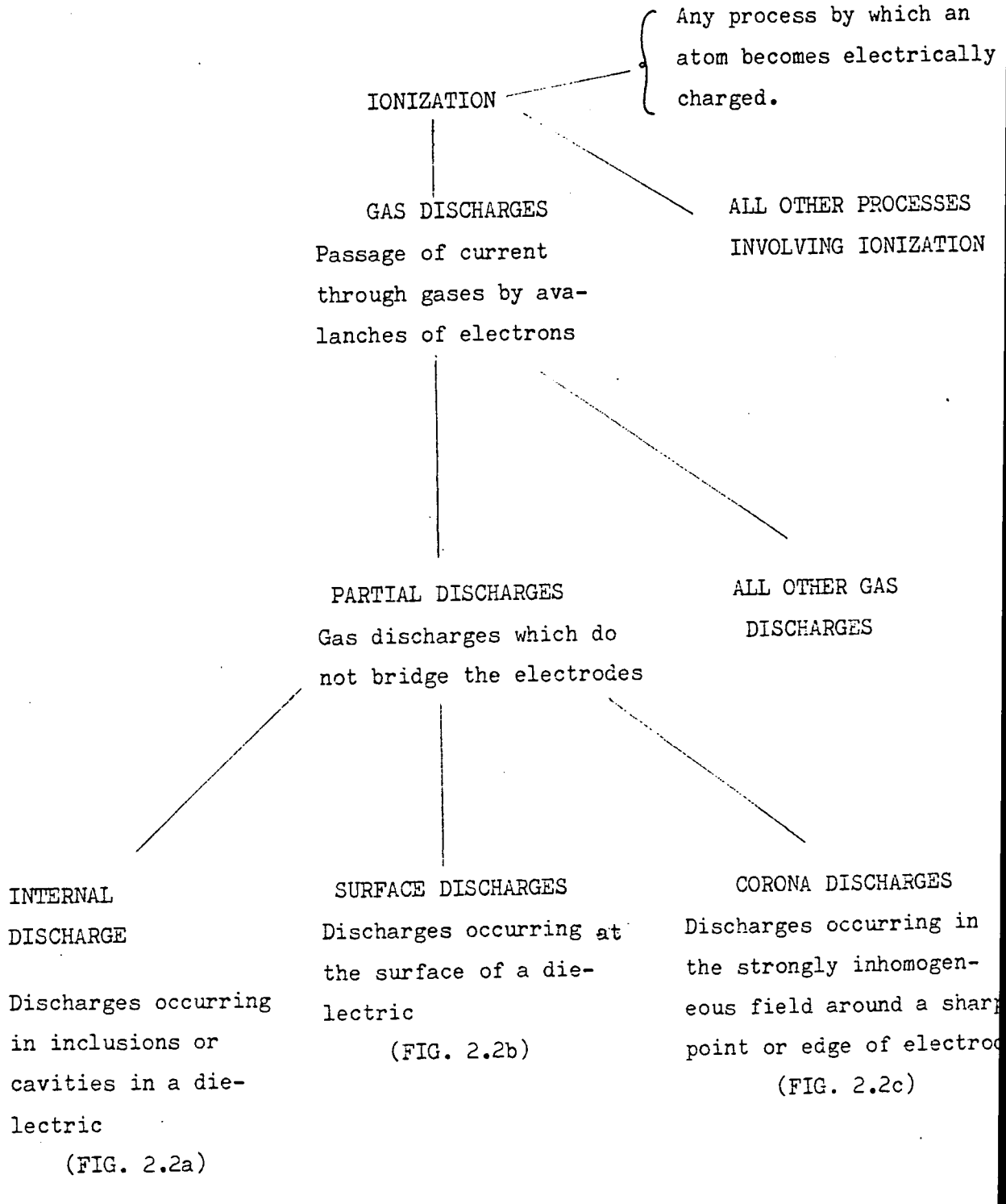

CLASSIFICATION OF DISCHARGES
(AFTER KREUGER[13])

FIG. 2.1

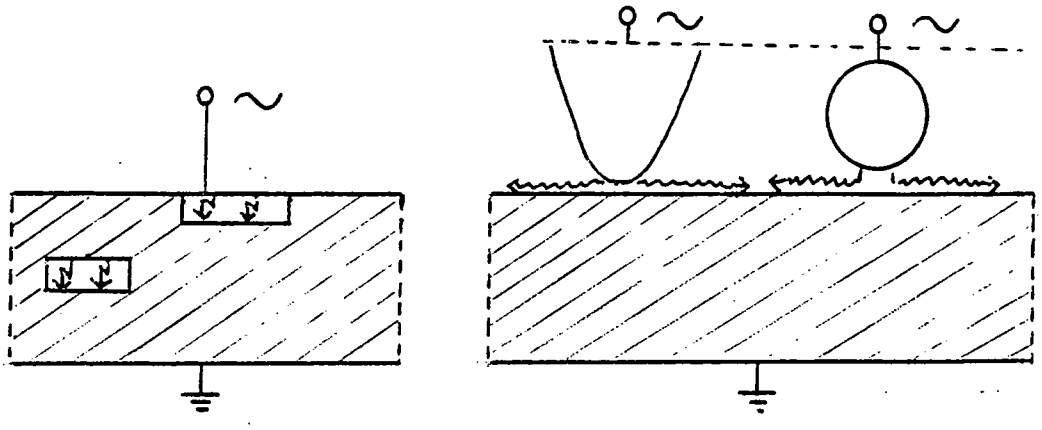

a b

c d

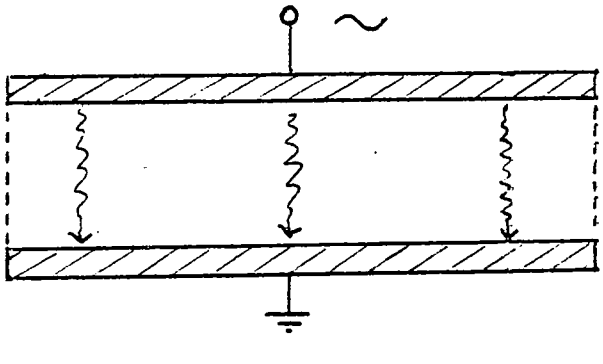

e

REALISATION OF THE DISCHARGES

(AFTER KREUGER[13])

FIG. 2.2

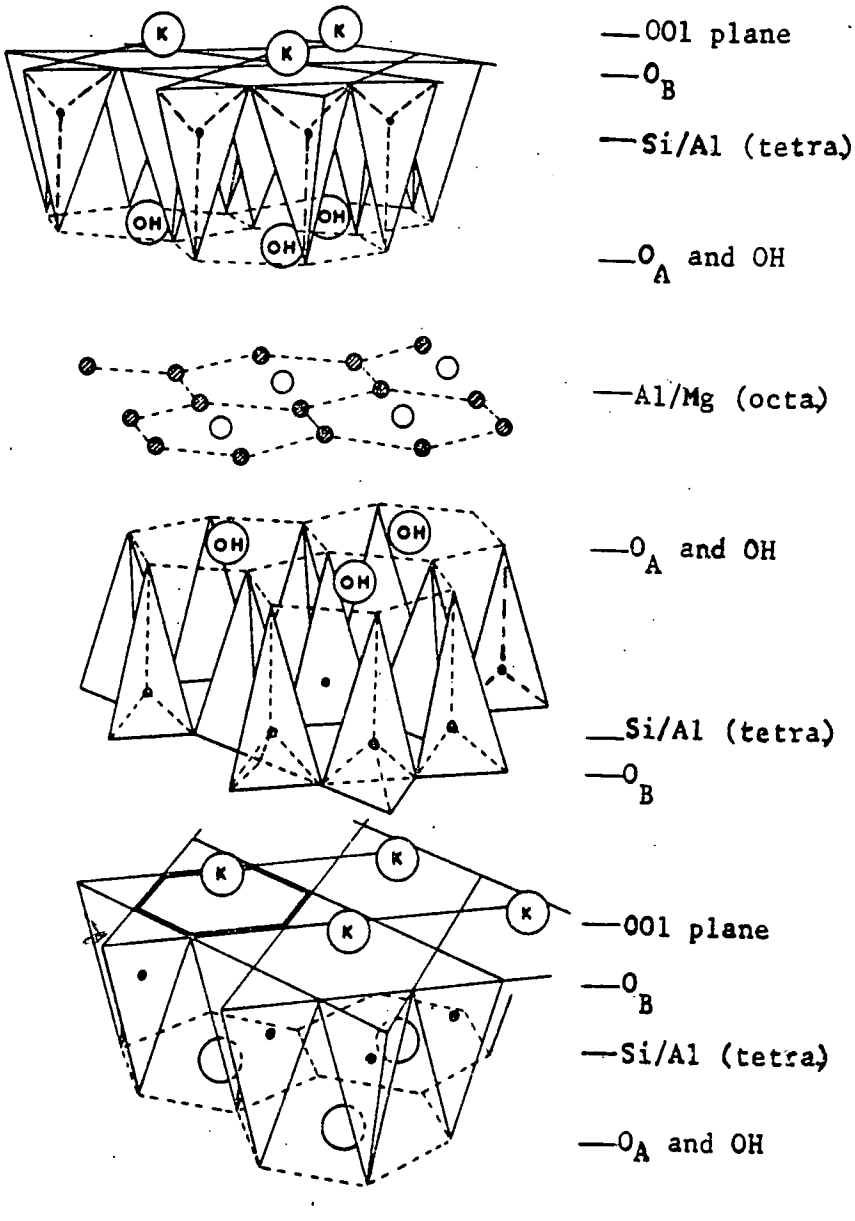

a) muscovite - $\frac{2}{3}$ octahedral sites filled with Al^{+++} ⊕

phlogopite- all octahedral sites filled with Mg^{++} ⊕○

EXPLODED VIEW OF THE IDEAL STRUCTURE OF MUSCOVITE AND PHLOGOPITE MICA
(AFTER RYDER [17])

FIG. 2.3

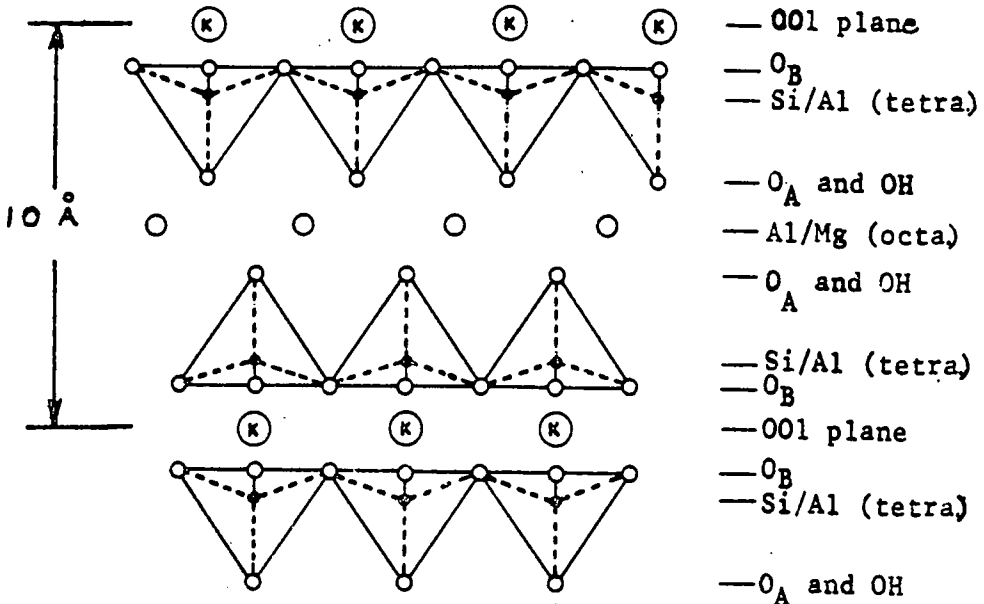

SIDE ELEVATION OF THE MICA LAYER CONSTRUCTION
(AFTER RYDER[17])

FIG. 2.4

(a)

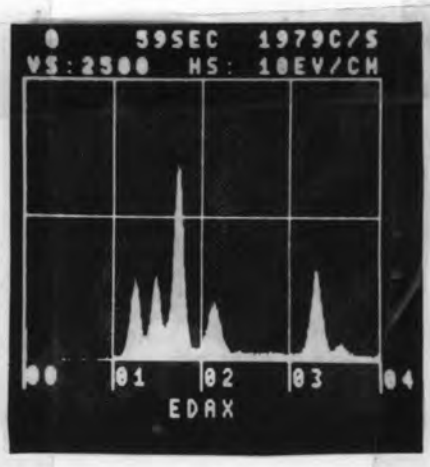

(b)

Fig. 2.5

S.E.M. AND EDAX ANALYSES OF A PLANE PHLOGOPITE SURFACE

EDAX INDICATES PEAKS OF Mg, Al, Si, Au and K RESPECTIVELY - Au IS USED TO COAT THE SPECIMEN FOR ANALYSIS (AFTER RYDER)[17]

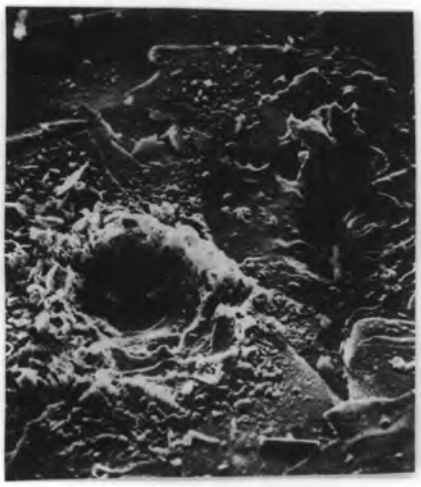

(a)

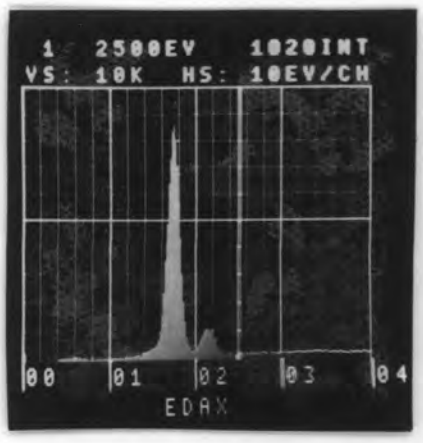

(b)

Fig. 2.6

S.E.M. AND EDAX ANALYSES OF A DETERIORATED PHLOGOPITE SURFACE

EDAX INDICATES PEAKS OF Si and Au RESPECTIVELY, THE PRINCIPAL PEAK BEING Si - THIS INDICATES THE TOTAL LOSS OF METALLIC CATIONS. (S.E.M. MAGNIFICATION IS SIMILAR FOR THE PLANE AND DETERIORATED SURFACES) (AFTER RYDER)[17]

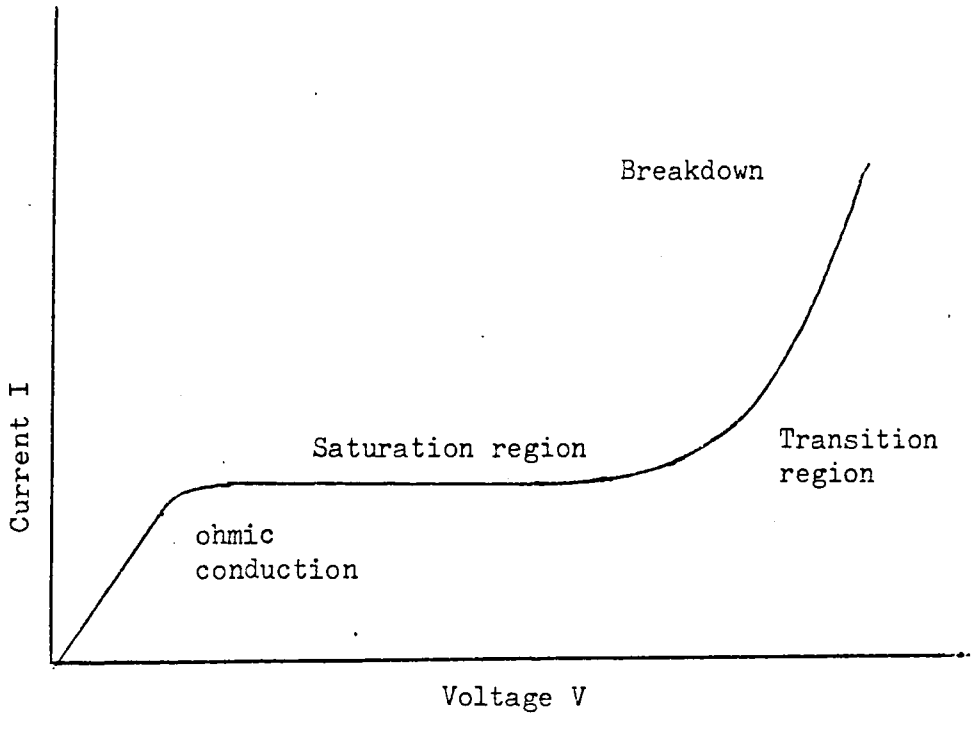

(a) Typical V/I plot for a gas subjected to a d.c. potential. Breakdown is usually by the Townsend mechanism

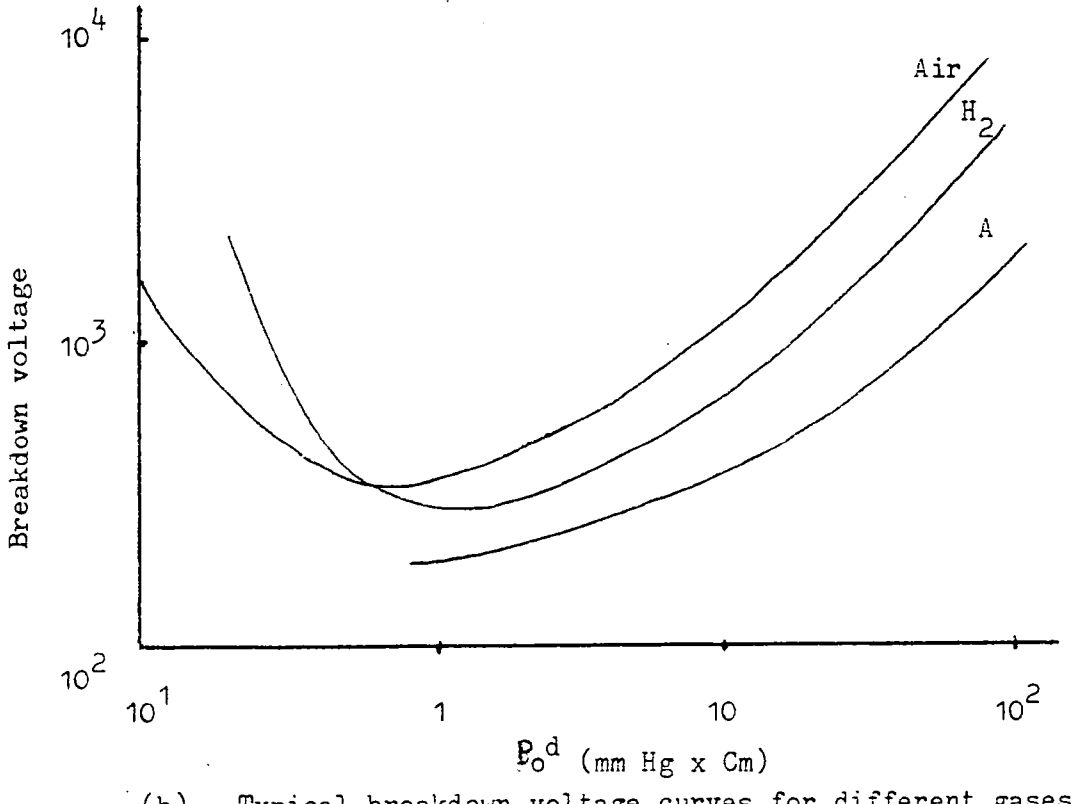

(b) Typical breakdown voltage curves for different gases between parallel plate electrodes. P_o is the gas pressure in m.m. Hg corrected to 0^oC. (After Meek, J.M. and Craggs, J.D.[22])

PASCHEN CURVES AND V/I CHARACTERISTICS FOR TYPICAL GASES

FIG. 2.7

CIRCUIT OF THE SIMPLE DISCHARGE MODEL

FIG. 2.8

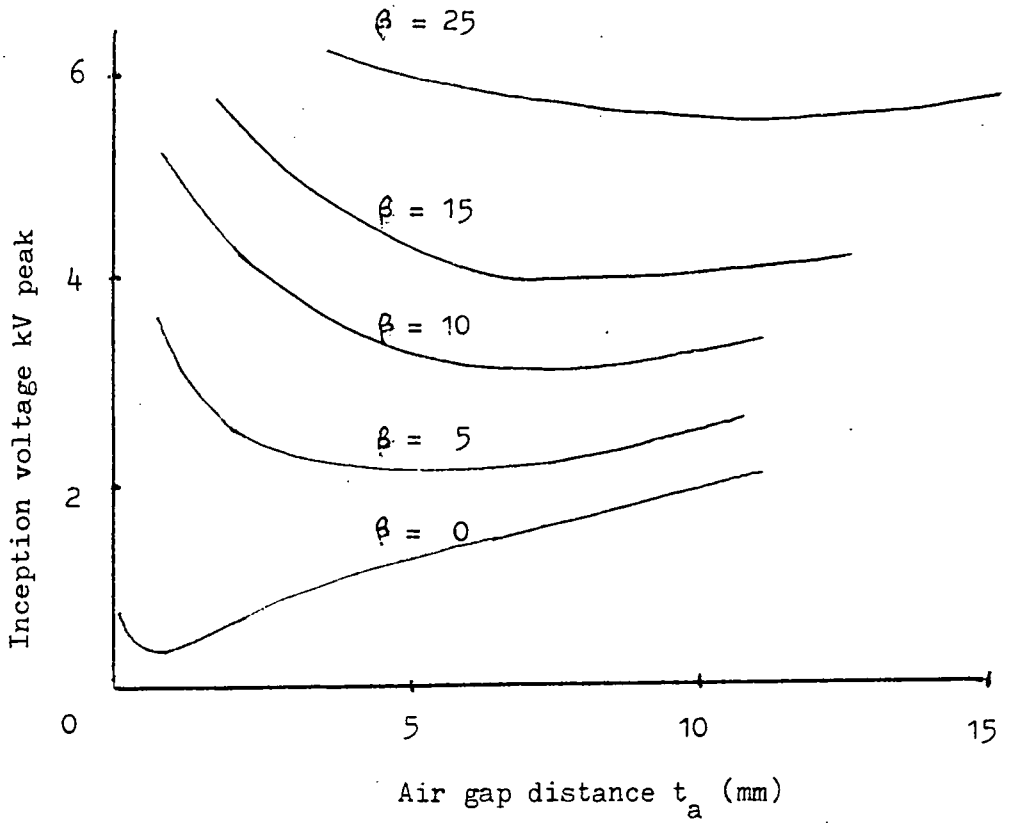

(a) Inception voltage as a function of air-gap distance at atmospheric pressure for various values of β. (After Halleck[23]). $\beta = t_d(\text{mm})/\varepsilon_d$.

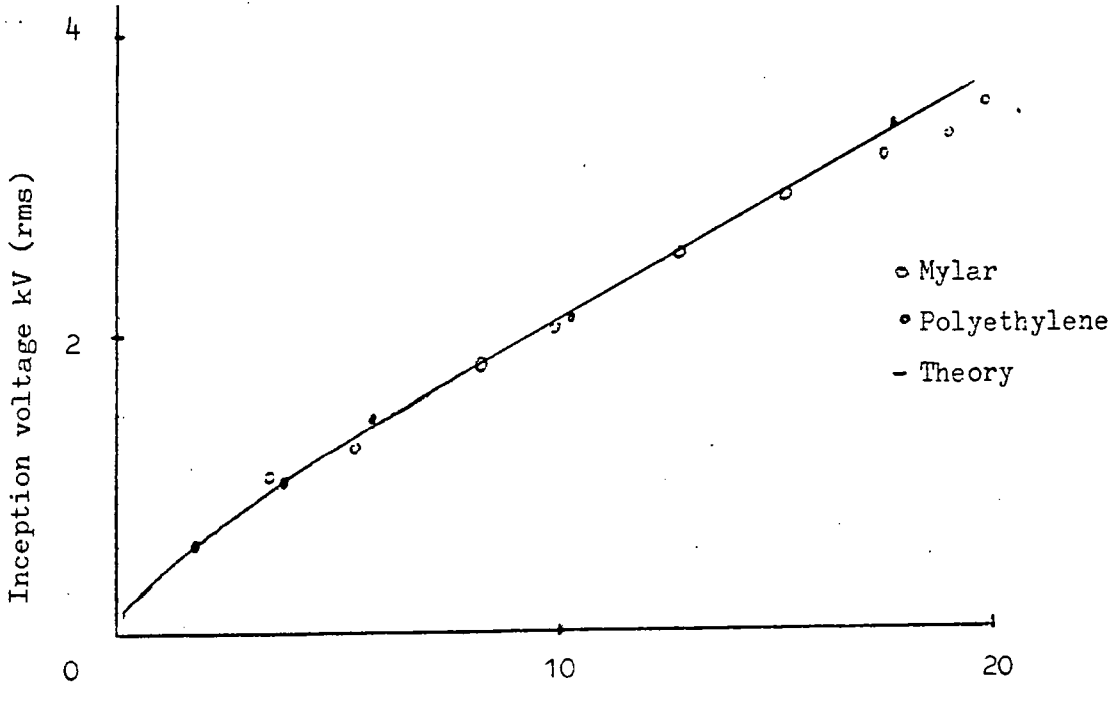

(b) Minimum incpetion voltage as a function of β. (After Halleck[23]).

CURVES OF INCEPTION VOLTAGE VERSUS t_a AND β.

FIG. 2.9

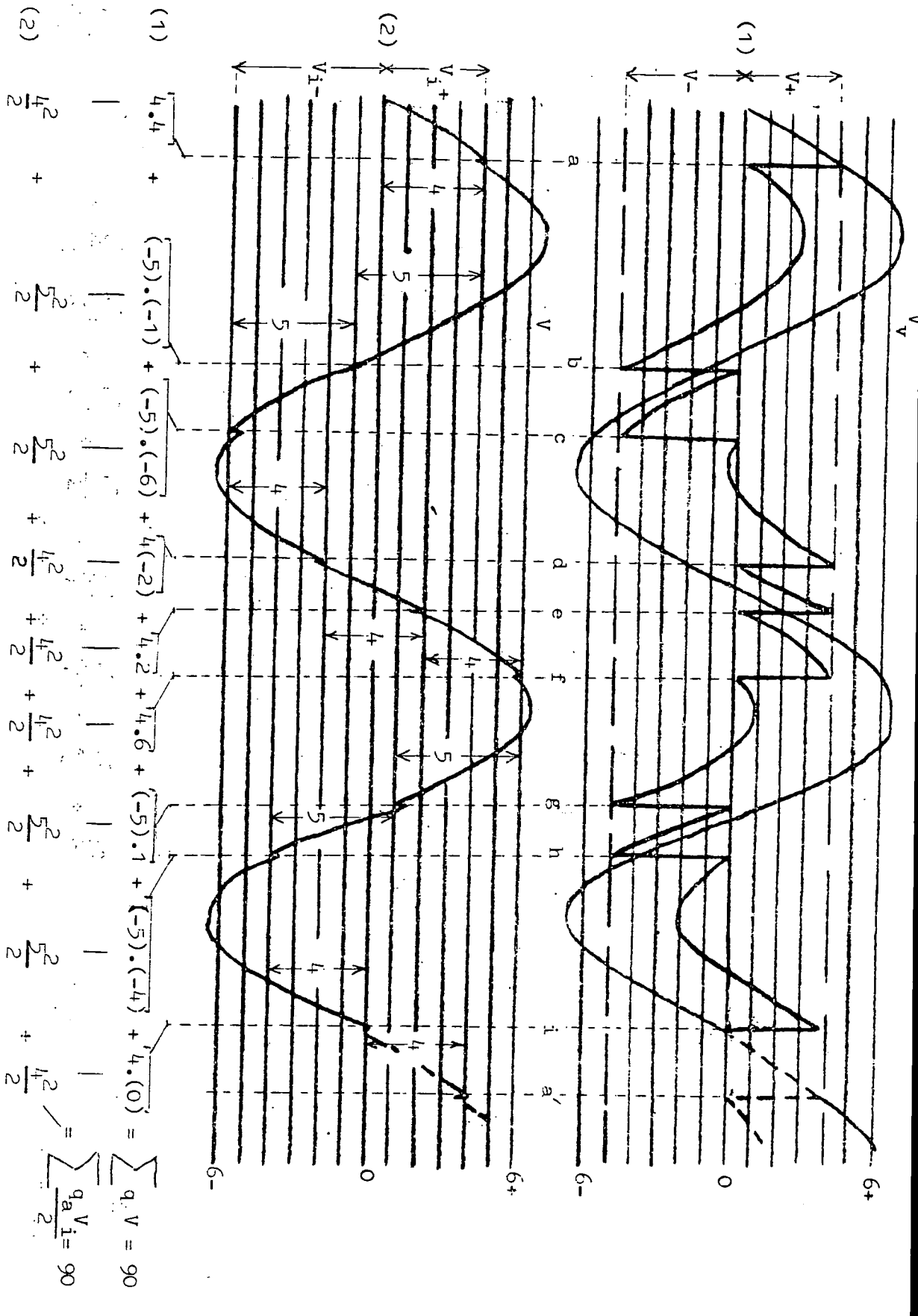

DIAGRAMS AND CALCULATION SHOWING THE EQUIVALENCE OF THE MEASUREMENT $\sum q_a V$ AND $\sum \frac{1}{2} q_a V_i$ (AFTER PELZER)[29]

FIG. 2.10

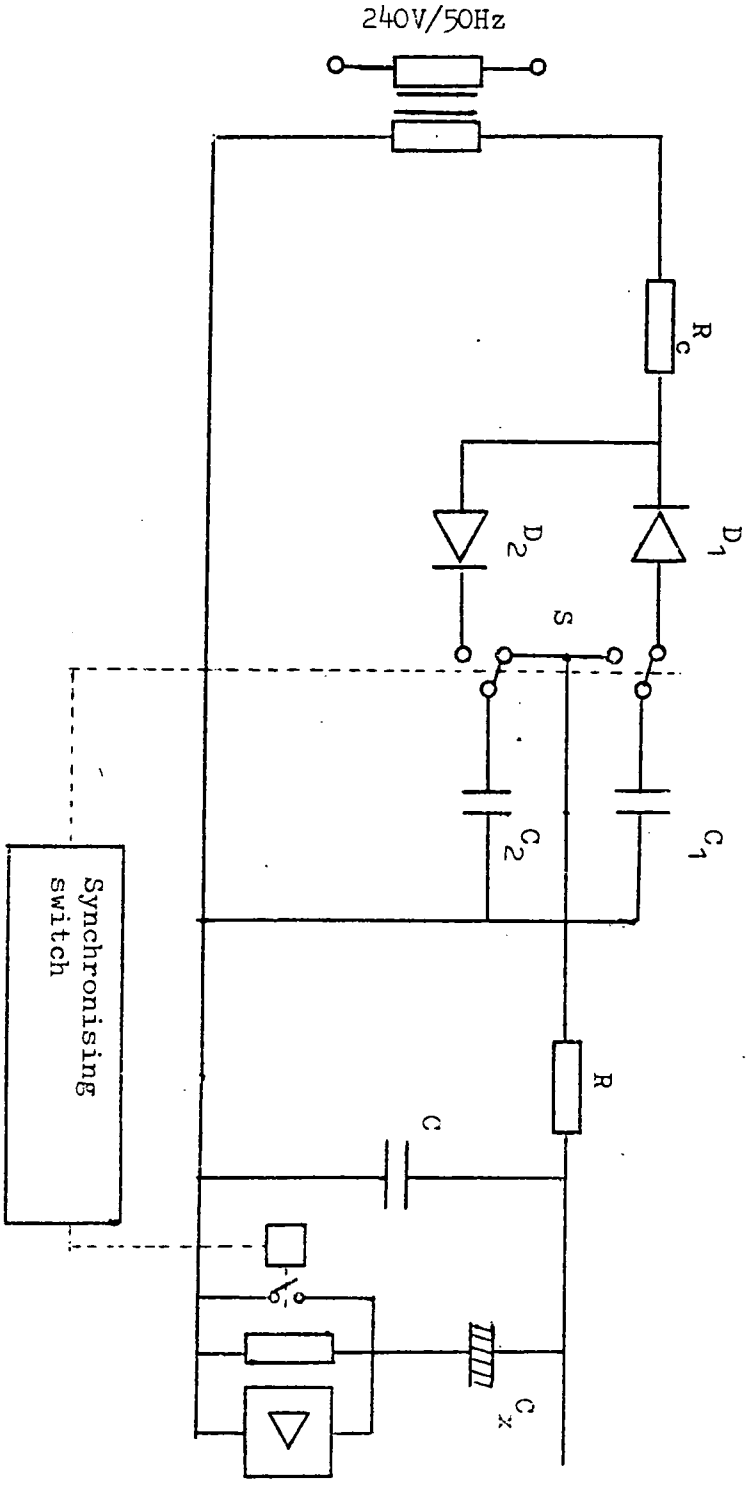

NON-SINUSOIDAL VARIABLE VLF WAVEFORM GENERATOR
(AFTER BOSSI, et al[30])

FIG. 3.1

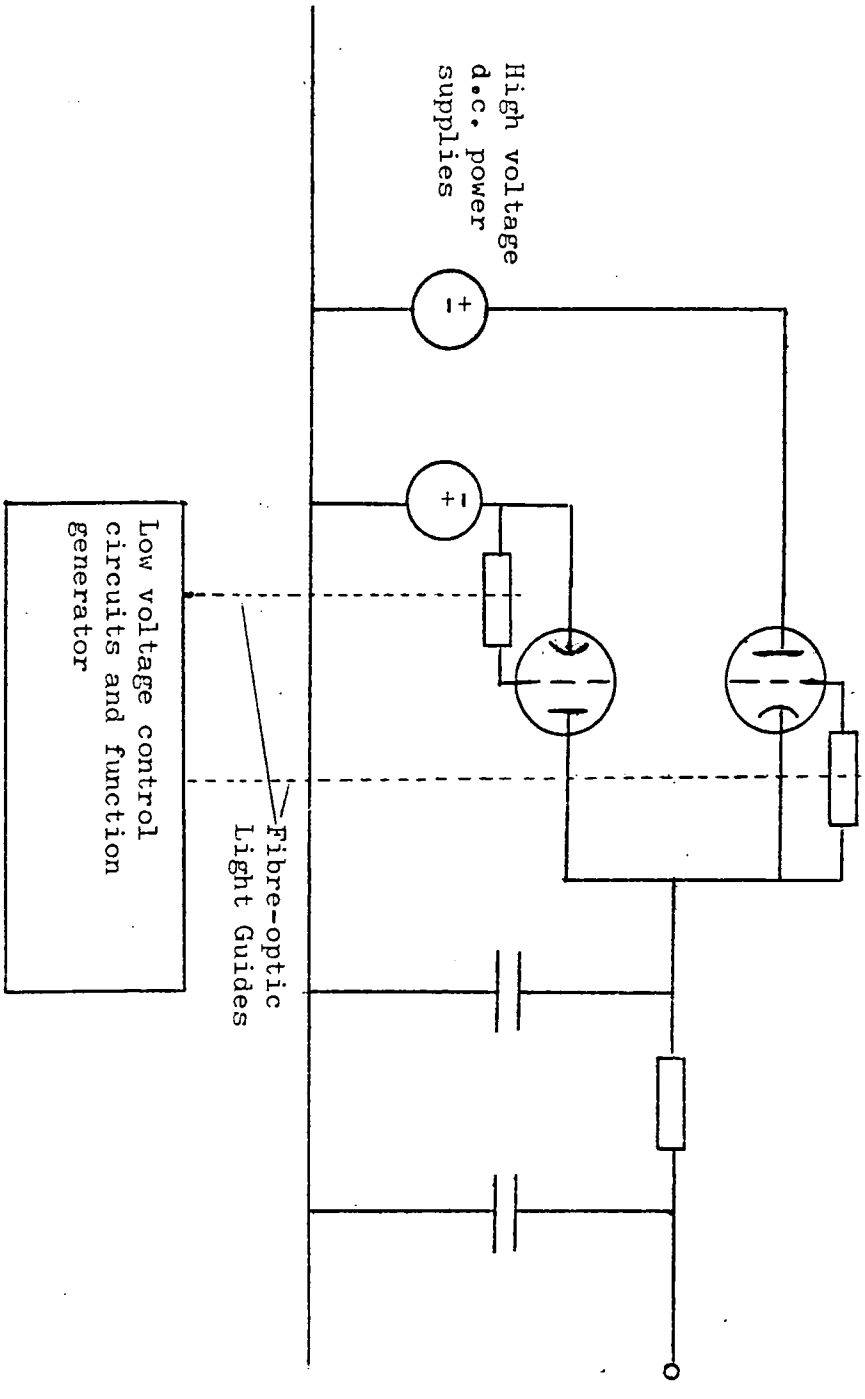

HIGH QUALITY VARIABLE SINUSOIDAL VLF GENERATOR
(AFTER MILLER[32], et al).

FIG. 3.2

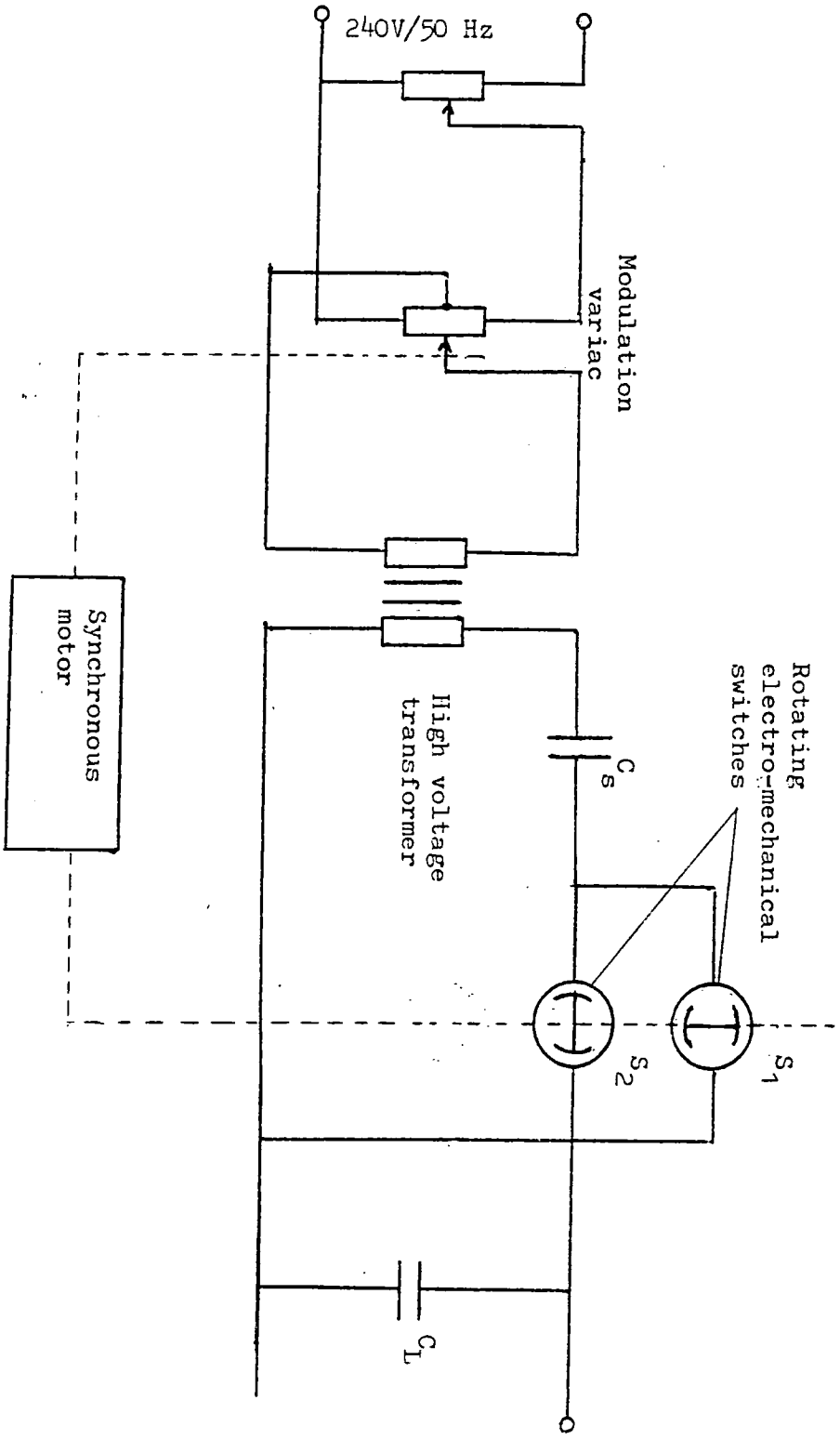

VLF GENERATOR USED IN THE PRESENT INVESTIGATION (AFTER ASEA[33])

FIG. 3.3

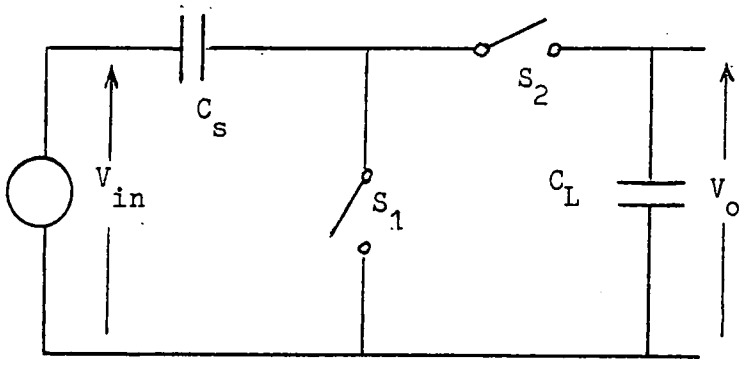

(a) The voltage multiplier

(Basic circuit of the VLF generator)

$S_{1,2}$ - Electro-mechanical rotating switches

C_s - Supply capacitor

C_L - Load capacitor

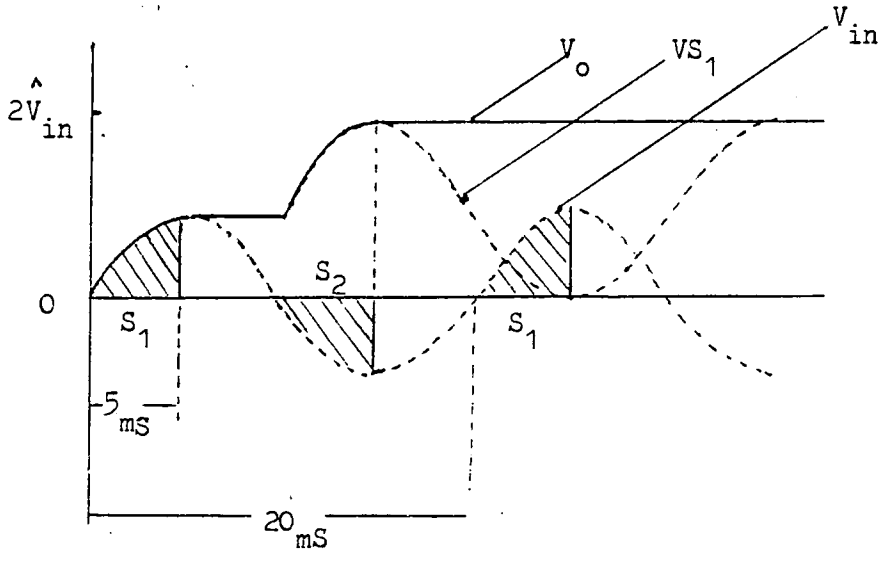

(b) Voltage waveforms and switching sequences of the VLF generator

BASIC CIRCUIT AND WAVEFORMS OF THE VLF GENERATOR.

FIG. 3.4

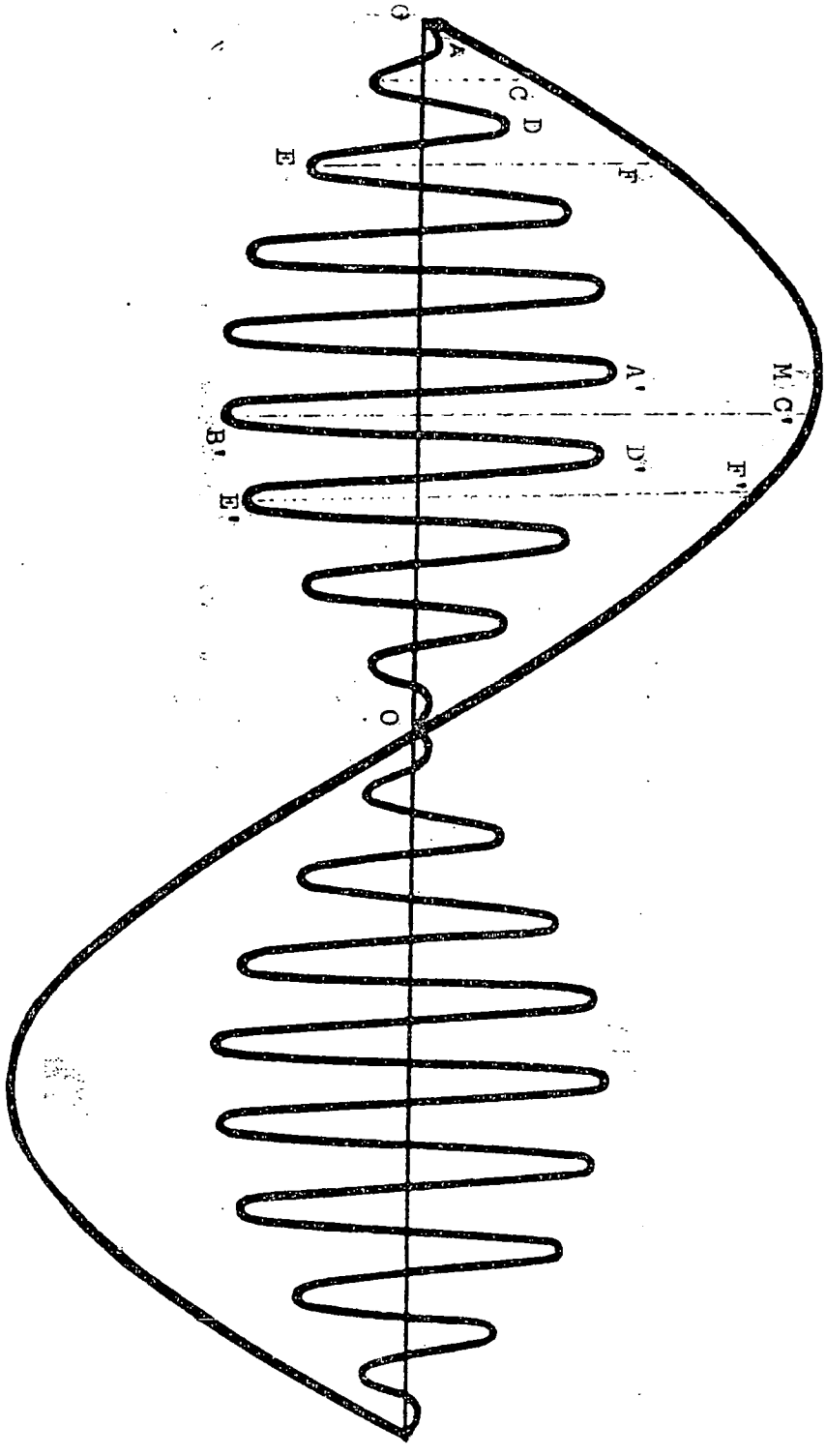

DEVELOPMENT OF THE VLF WAVEFORM (AFTER ASEA[33])

FIG. 3.5

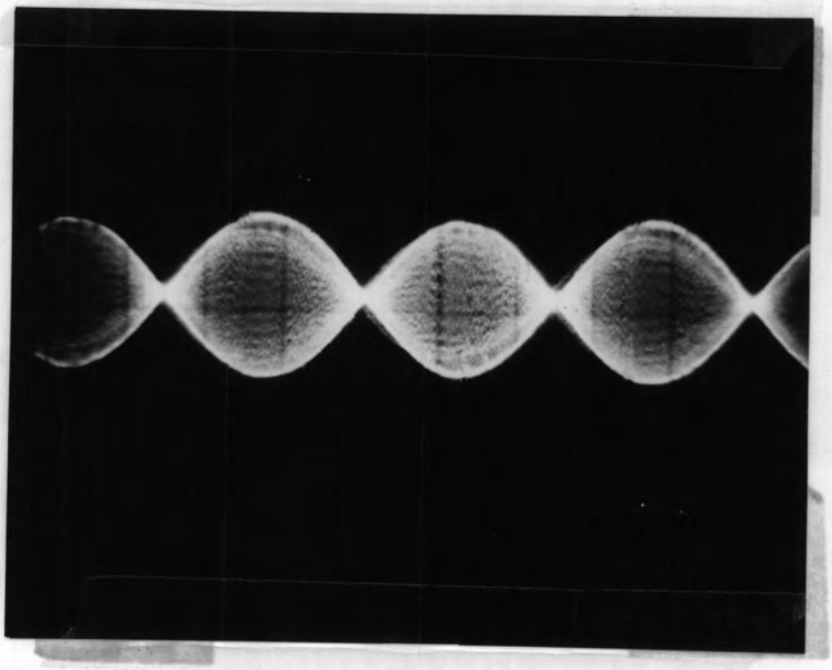

(a) 50 Hz Modulated input wave to h.v. transformer

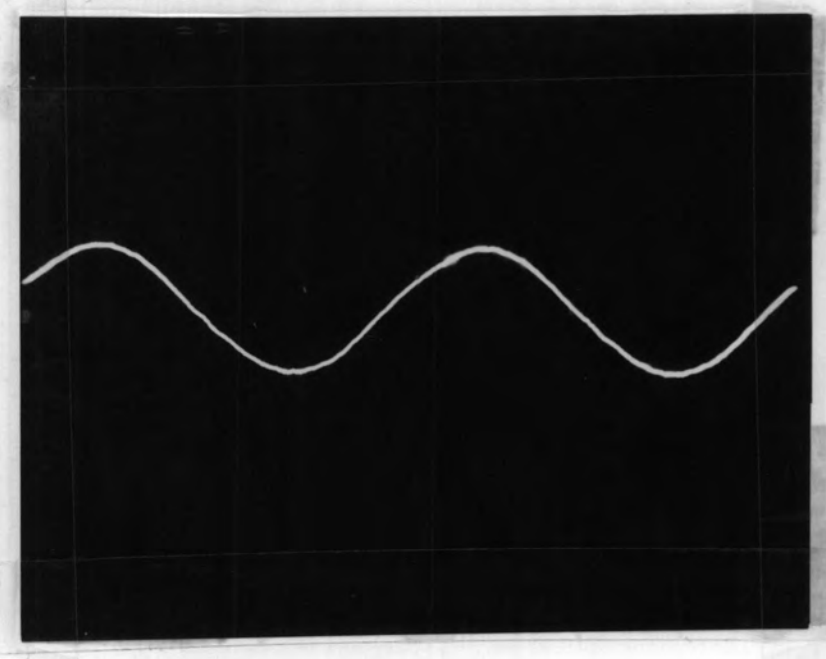

(b) 0.1 Hz demodulated output wave

VLF GENERATOR INPUT AND OUTPUT WAVEFORMS

FIG. 3.6

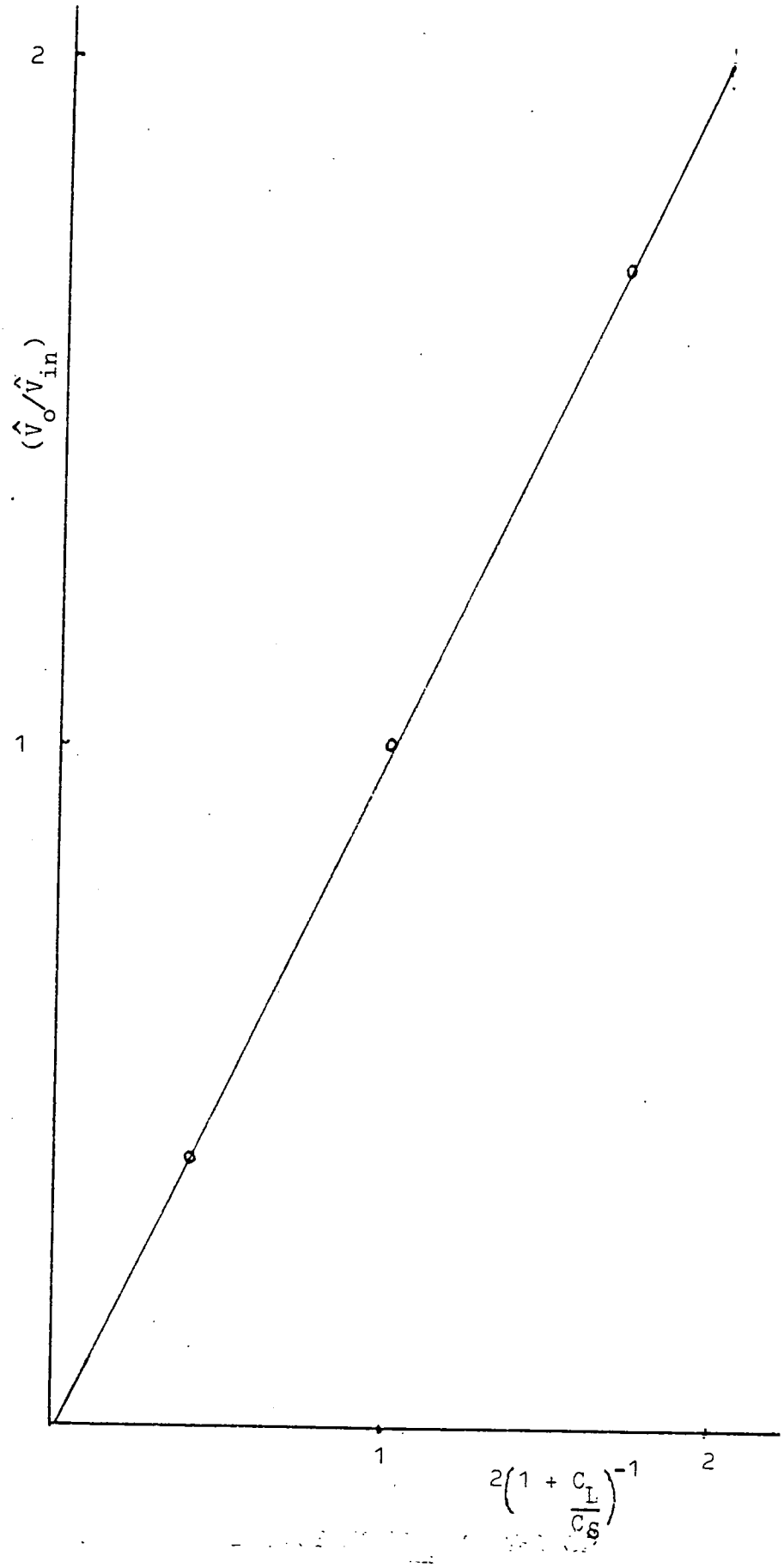

VOLTAGE EFFICIENCY $(\hat{V}_o/\hat{V}_{in})$ OF THE VLF GENERATOR DEPENDING UPON THE RATIO (C_L/C_S).

FIG. 3.7

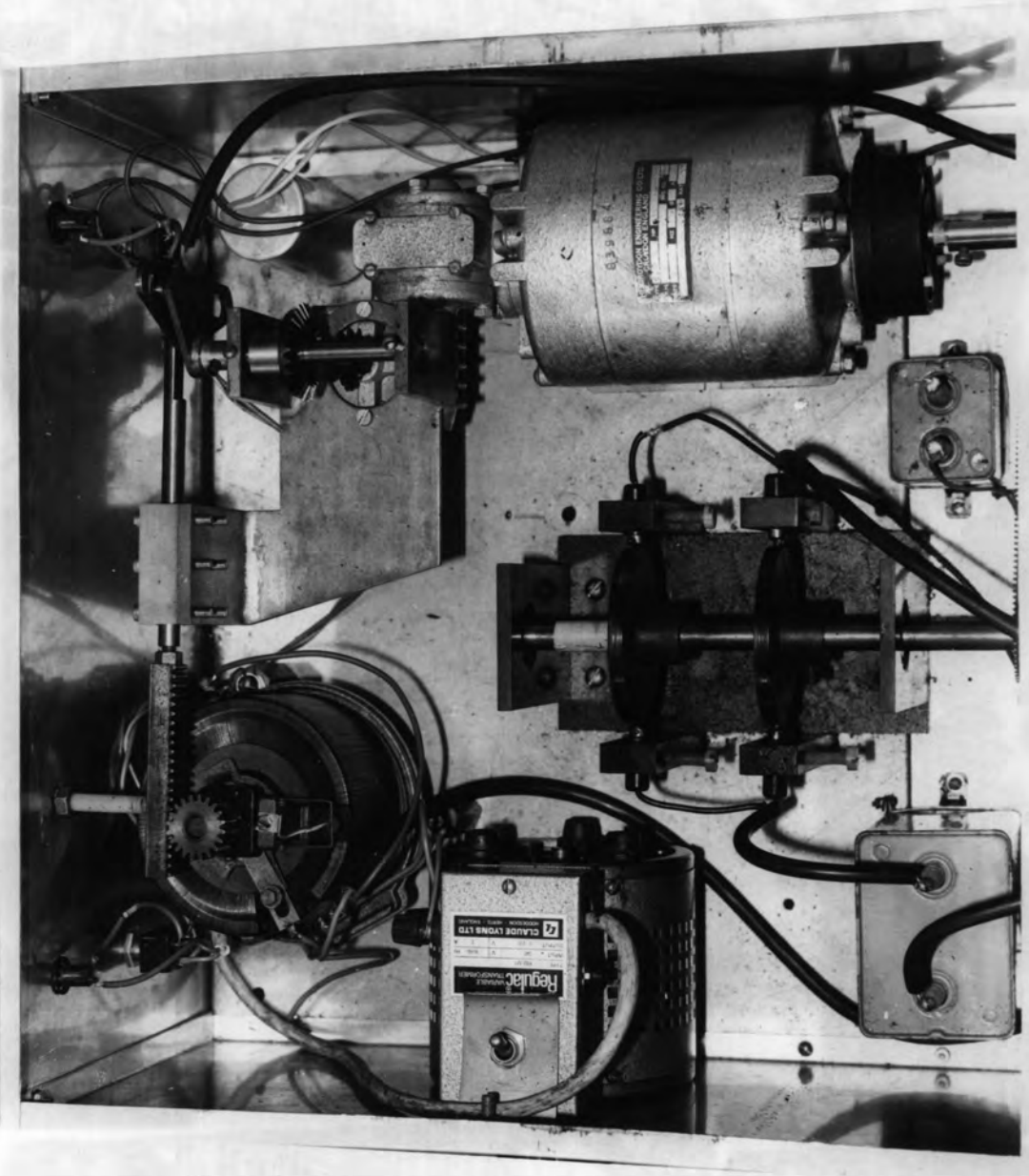

PRACTICAL LAYOUT OF THE VLF GENERATOR

FIG. 3.8

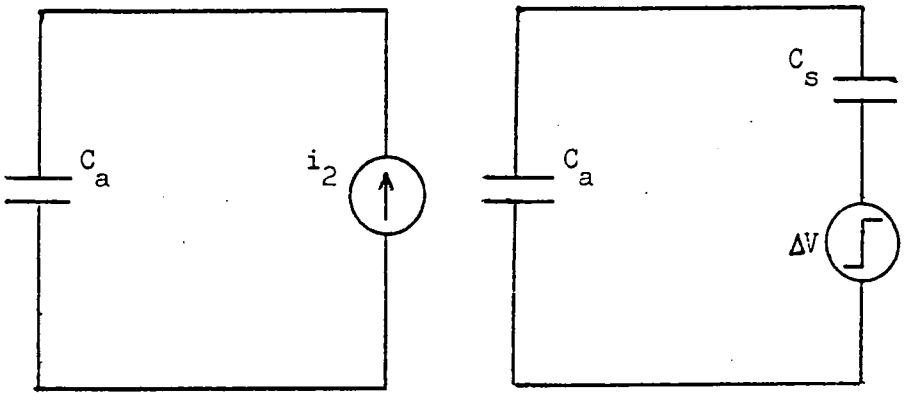

(a) Current generator (b) Voltage generator

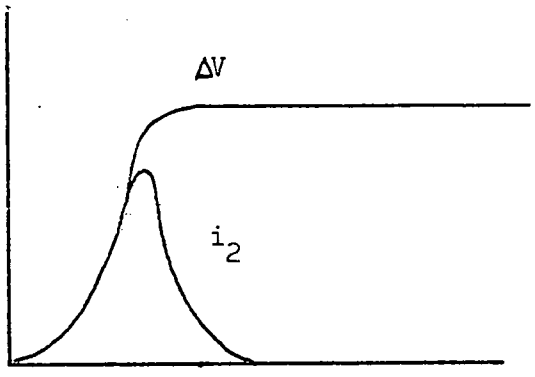

(c) Discharge current and voltage waveforms

EQUIVALENT CIRCUITS AND WAVEFORMS FOR A DISCHARGE

FIG. 4.1

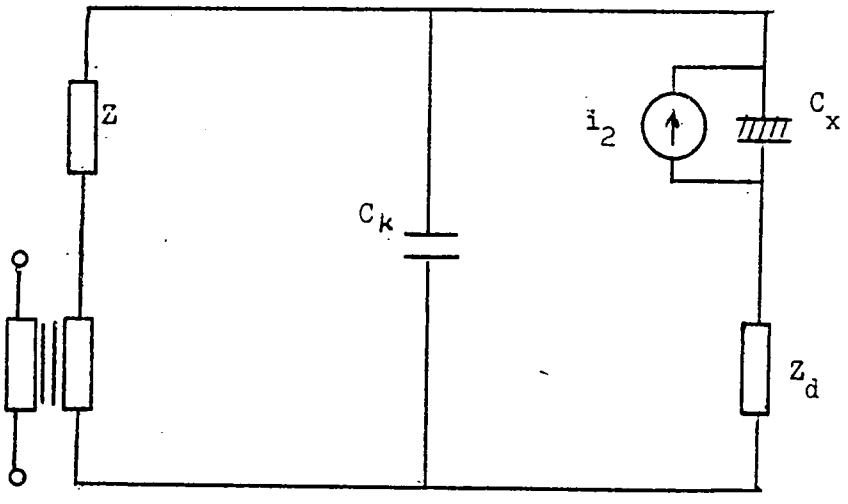

(a) Circuit B

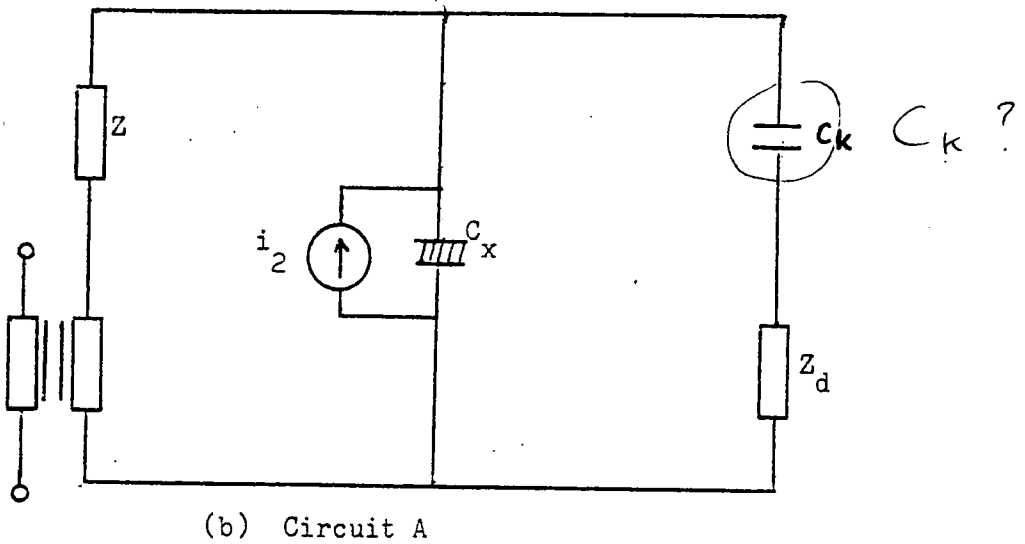

(b) Circuit A

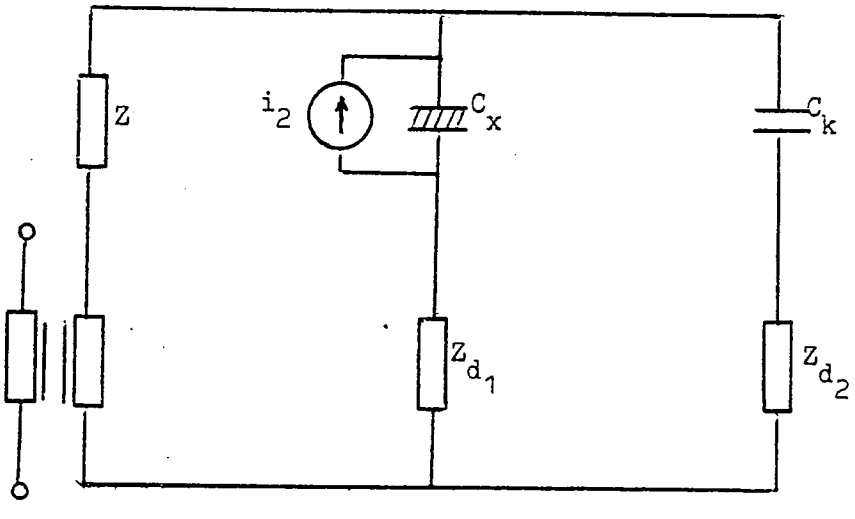

(c) Bridge Circuit C

BASIC DETECTION CIRCUITS

FIG. 4.2

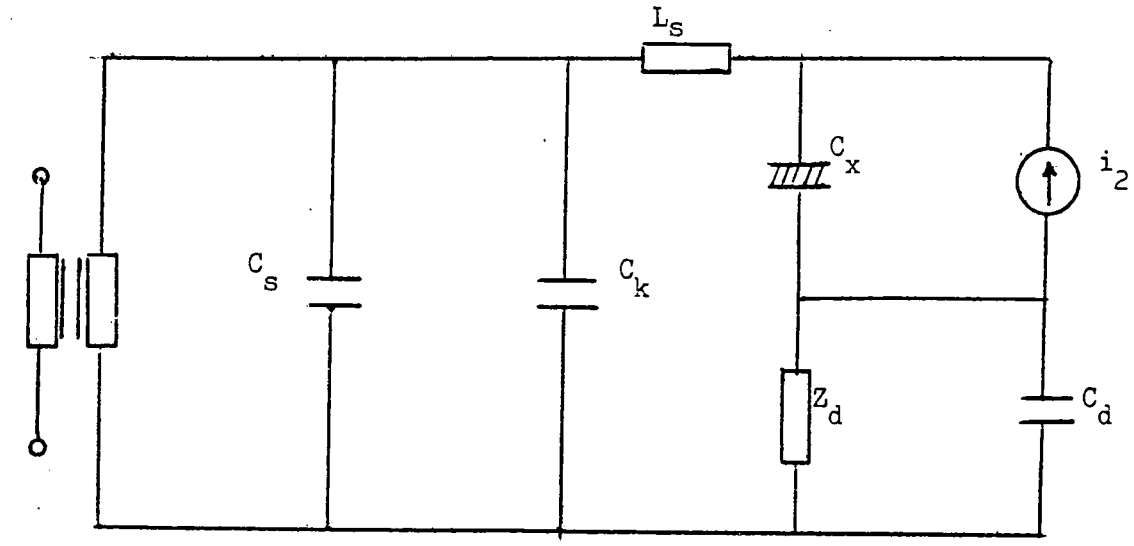

(b)

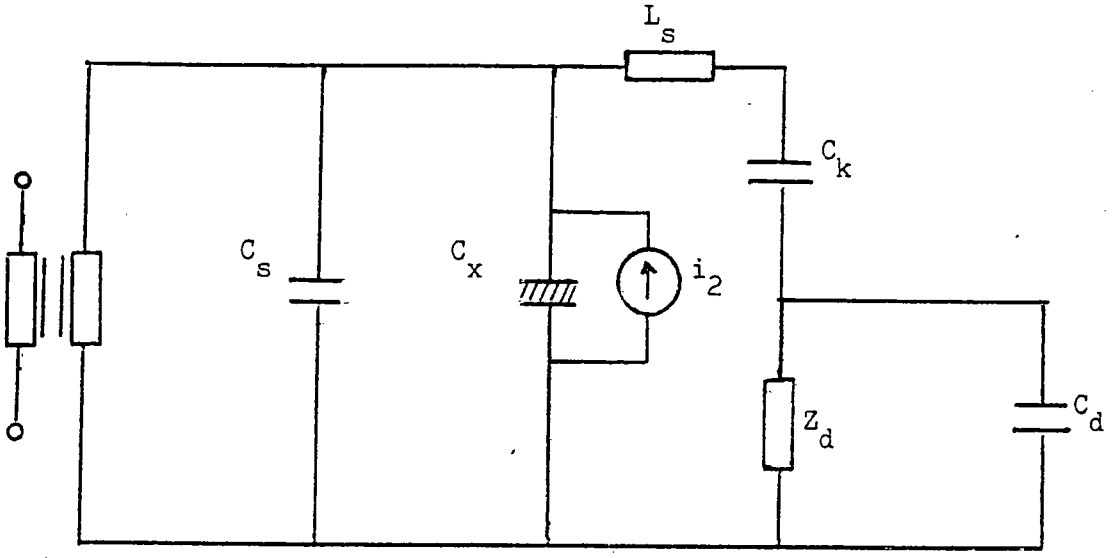

(a)

(d) Detector circuit with strays

Fig. 4.3

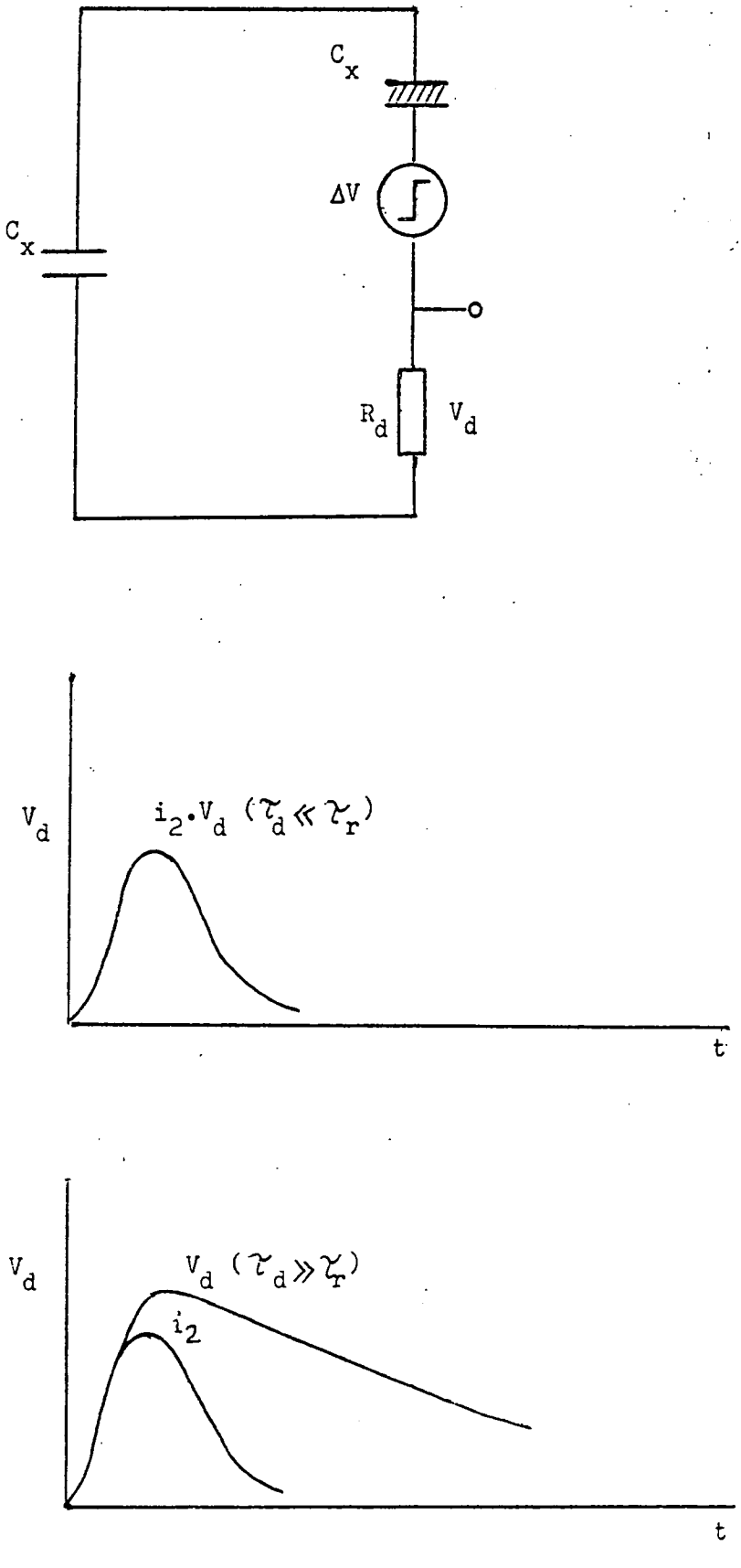

(a) Resitive detection circuit

Fig. 4.4

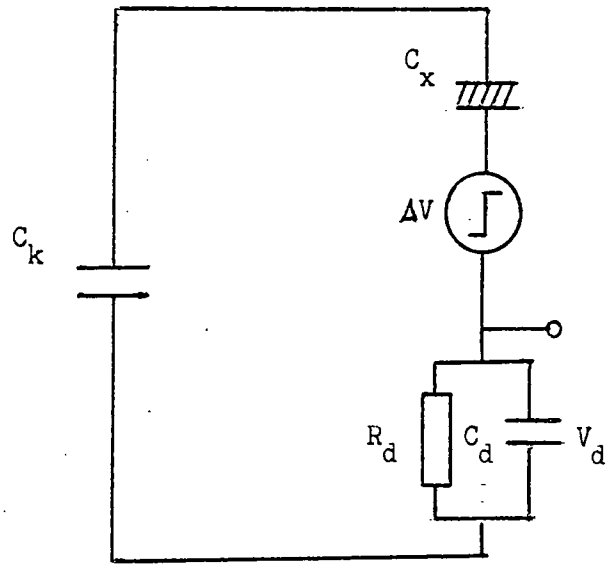

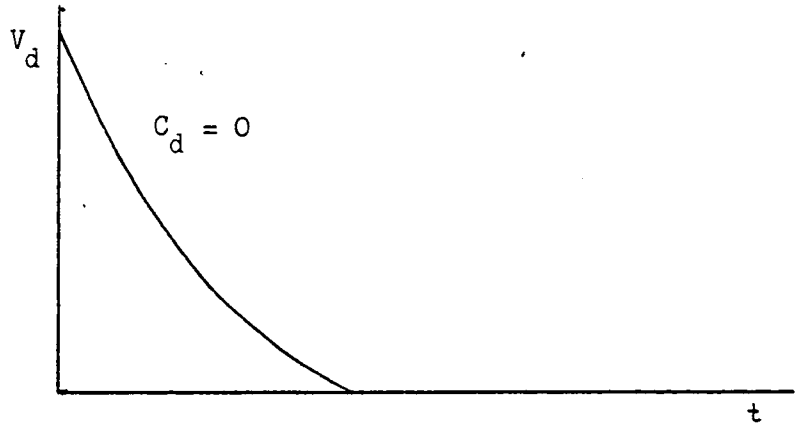

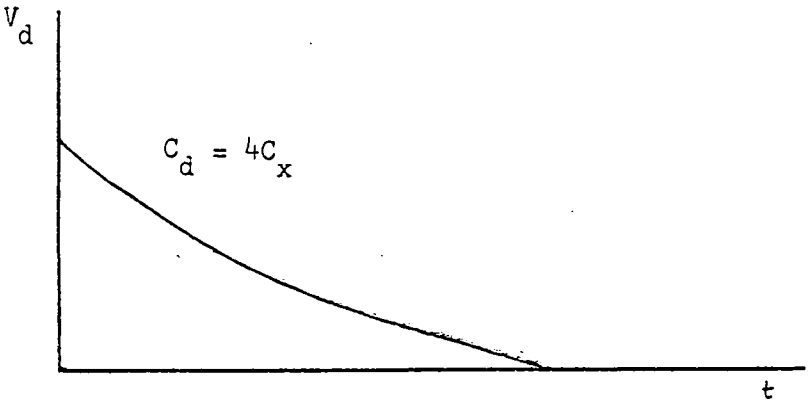

(b) Resistance and capacitance in parallel

FIG. 4.5

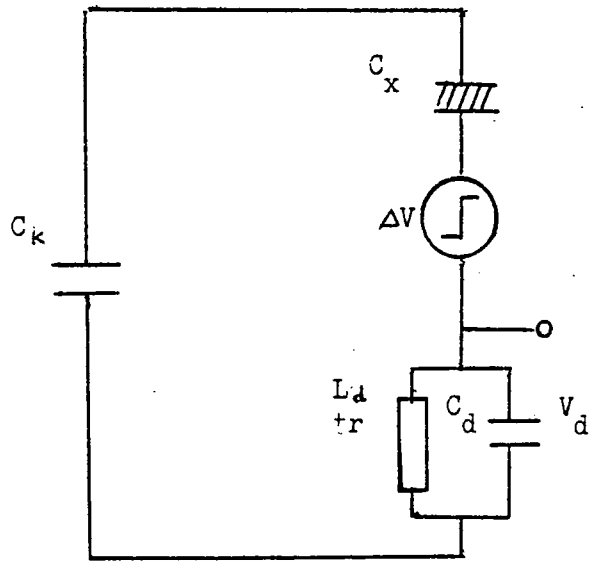

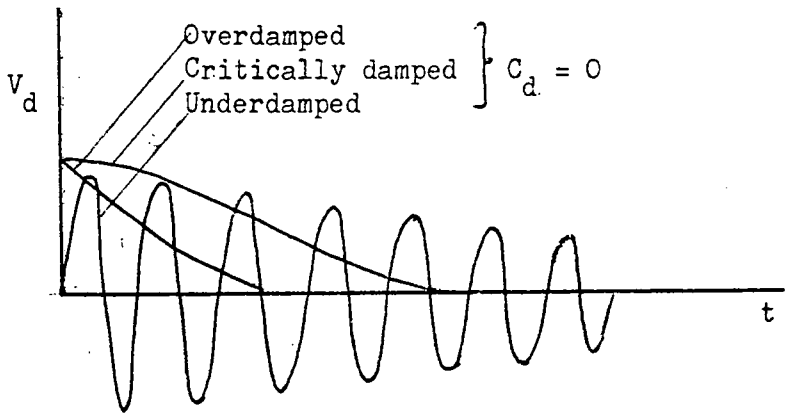

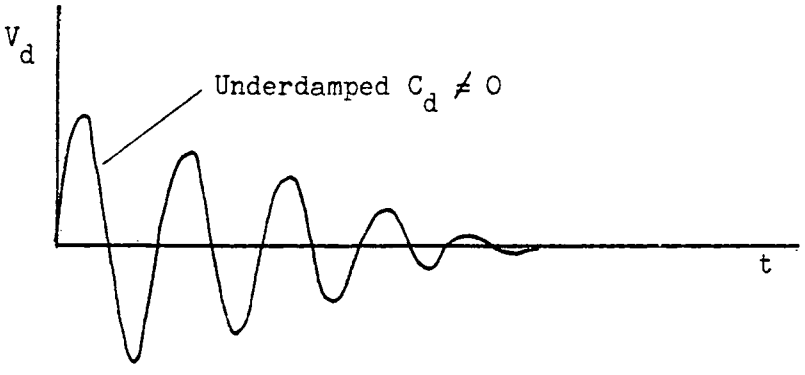

(c) Inductive detection shunts

FIG. 4.6

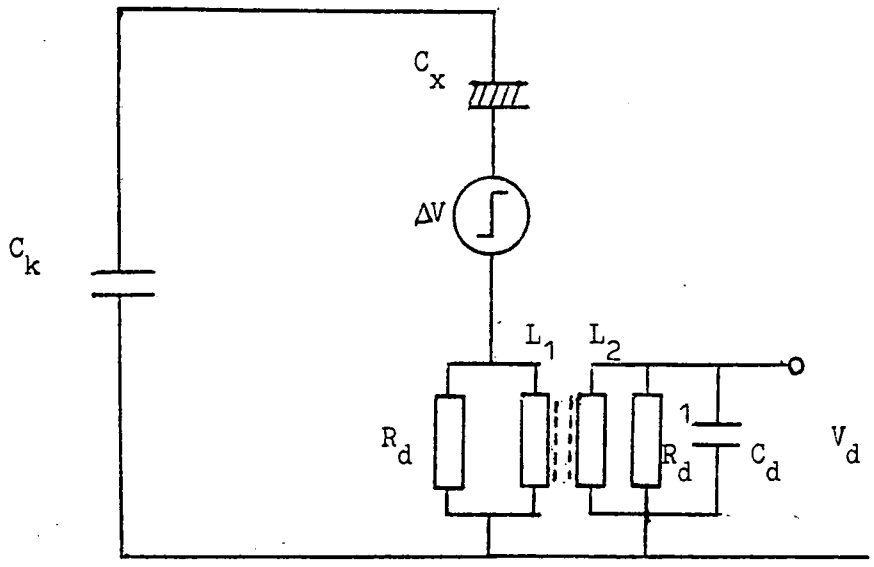

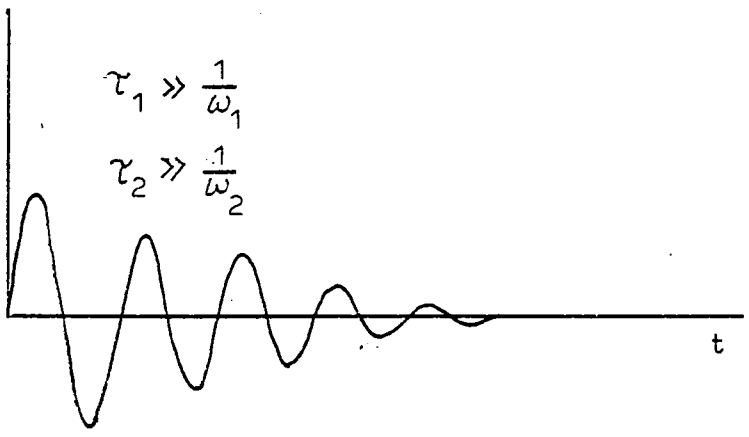

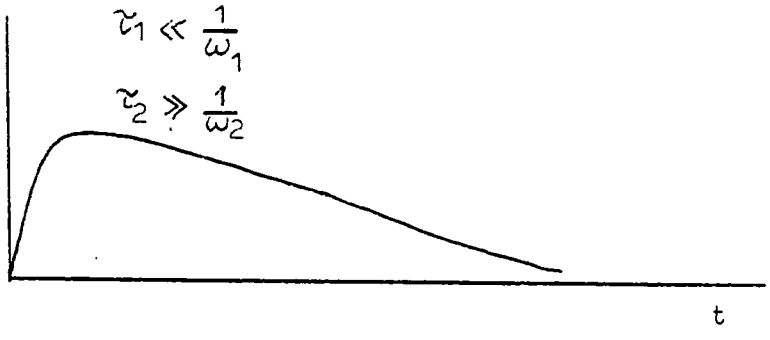

(d) Transformer coupled detection shunt

Fig. 4.7

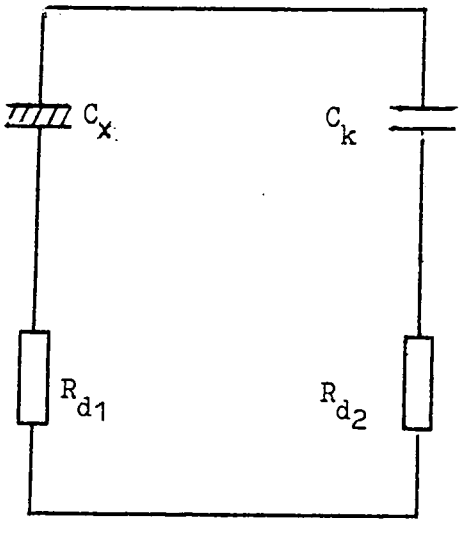

(a) Simple bridge circuit with resistive detection shunts.

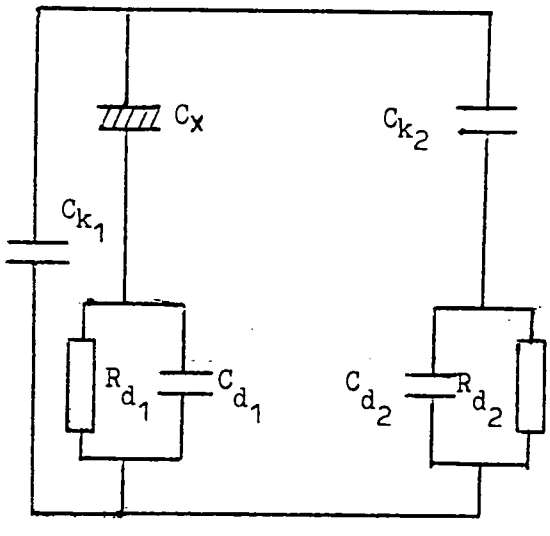

(b) Bridge circuit: capacitance in parallel with resistive detection shunt.

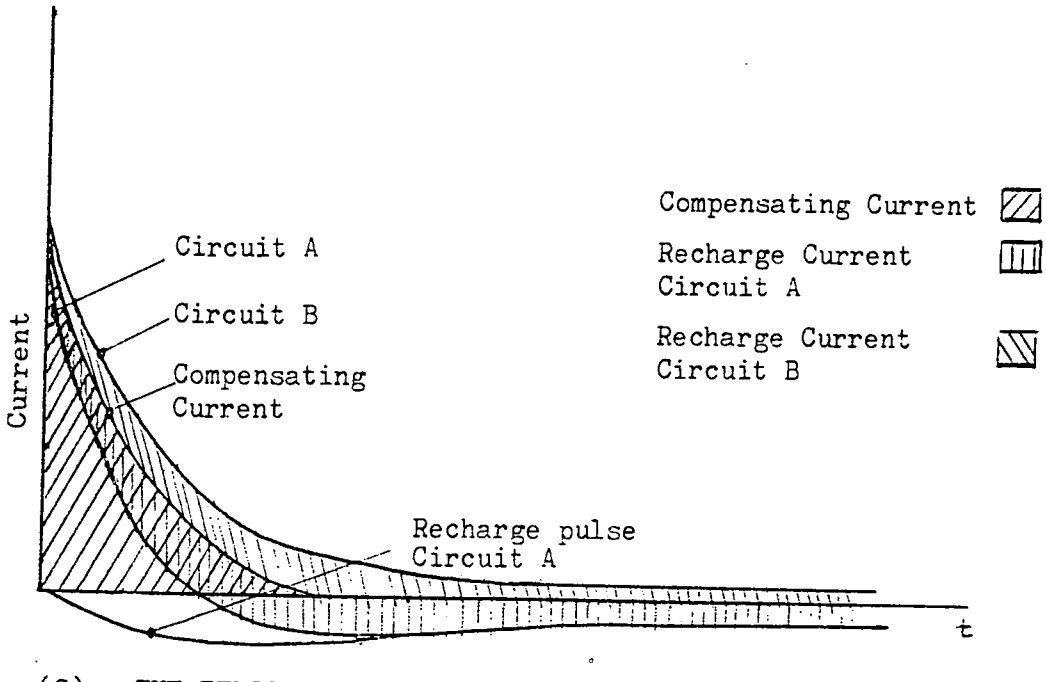

(C) THE EFFECT OF RECHARGE PULSE IN DETECTION CIRCUITS A AND B (AFTER HICKLING)

FIG. 4.8

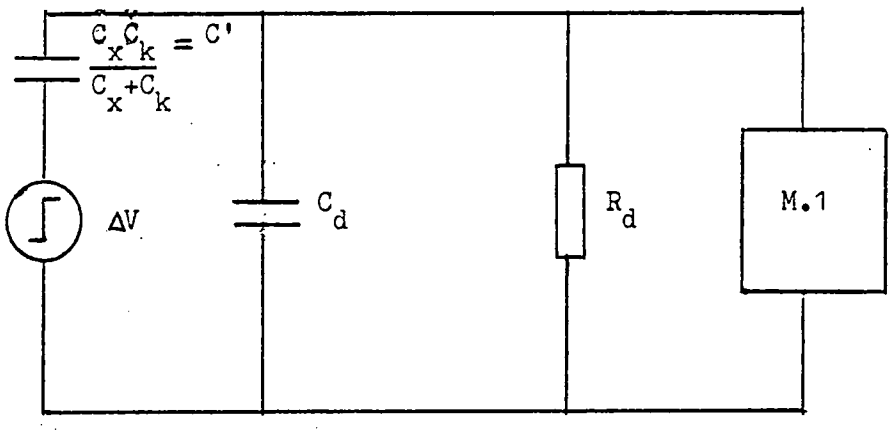

(a) Capacitively coupled

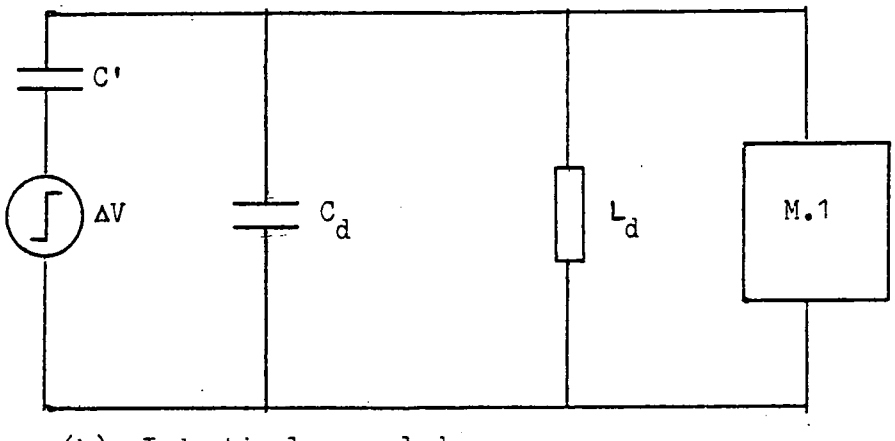

(b) Inductively coupled

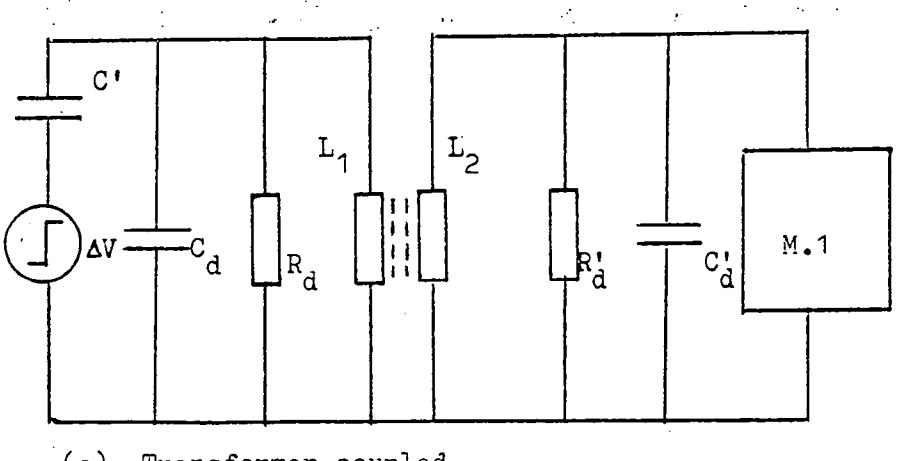

(c) Transformer coupled

CONNECTION OF MEASURING INSTRUMENTS (M.1)

FIG. 4.9

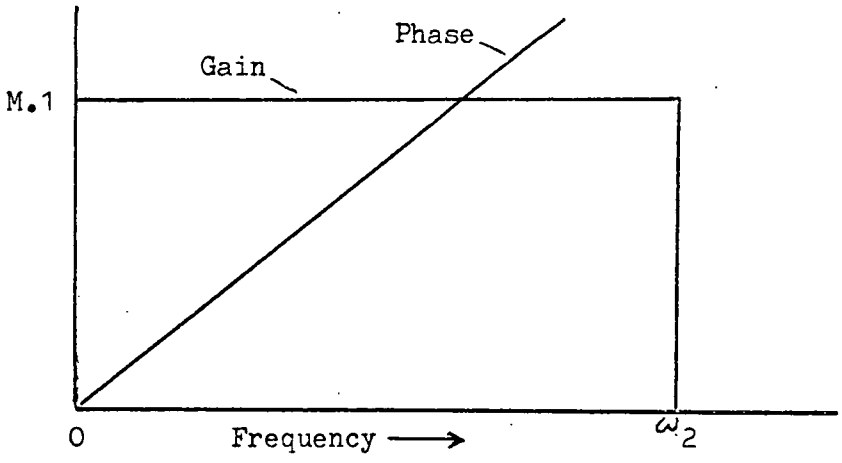

(a) Characteristic gain and phase relationship

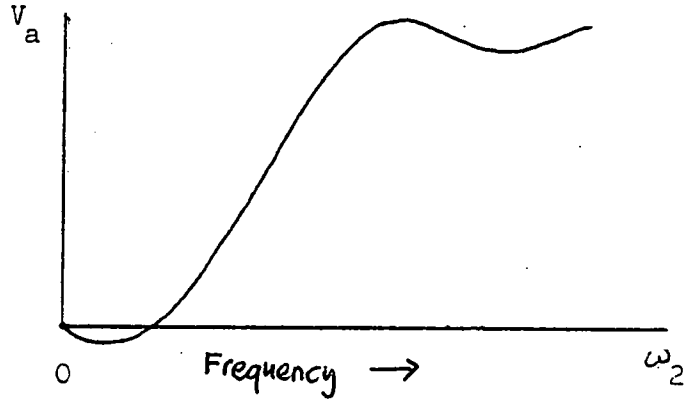

(b) Response to unit step wave

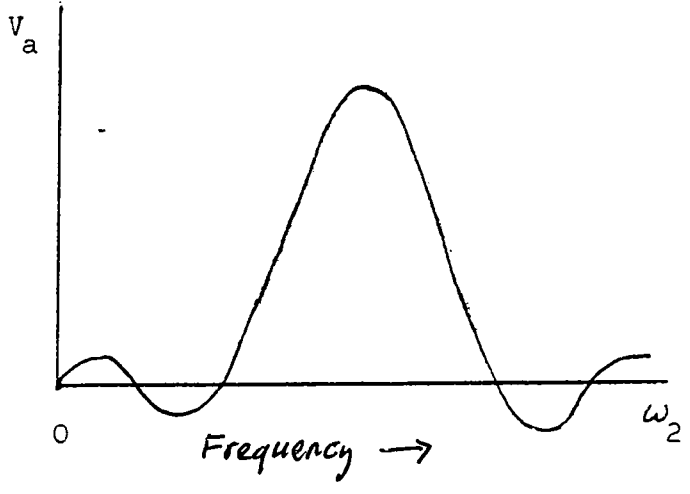

(c) Response to pulse (response to unit impulse has the same form)

LOW PASS AMPLIFIER: IDEAL CHARACTERISTICS AND RESPONSE

FIG. 4.10

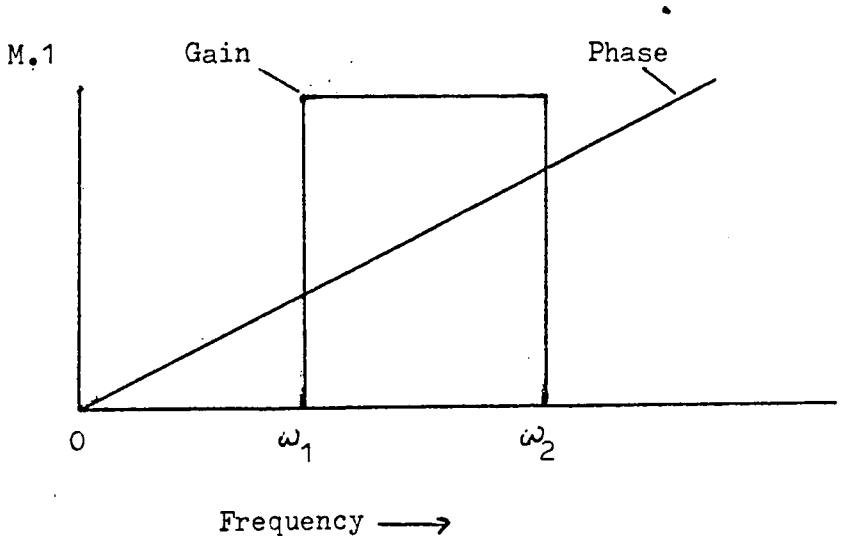

(a) Characteristic gain and phase relationship

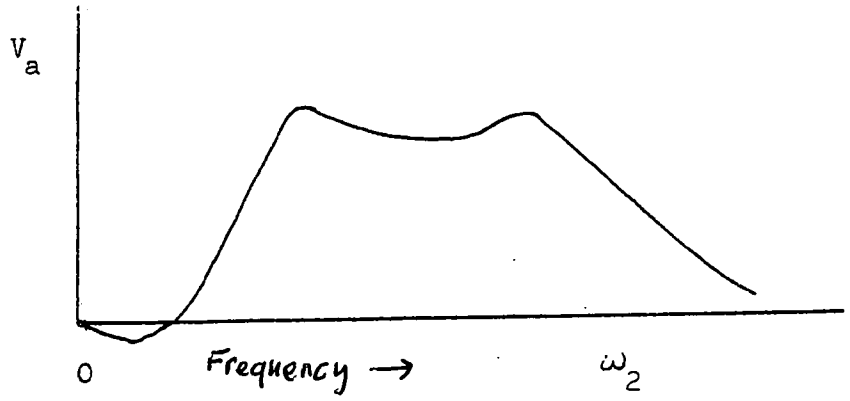

(b) Wide band amplifier response to step pulse

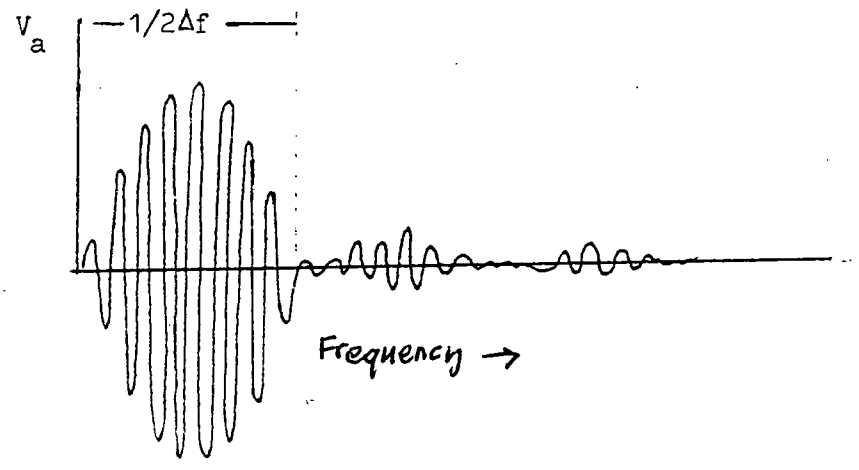

(c) Narrowband amplifier response to step pulse (also wide and narrowband response to unit impulse).

BANDPASS AMPLIFIER: IDEALIZED CHARACTERISTICS AND RESPONSES.

FIG. 4.11

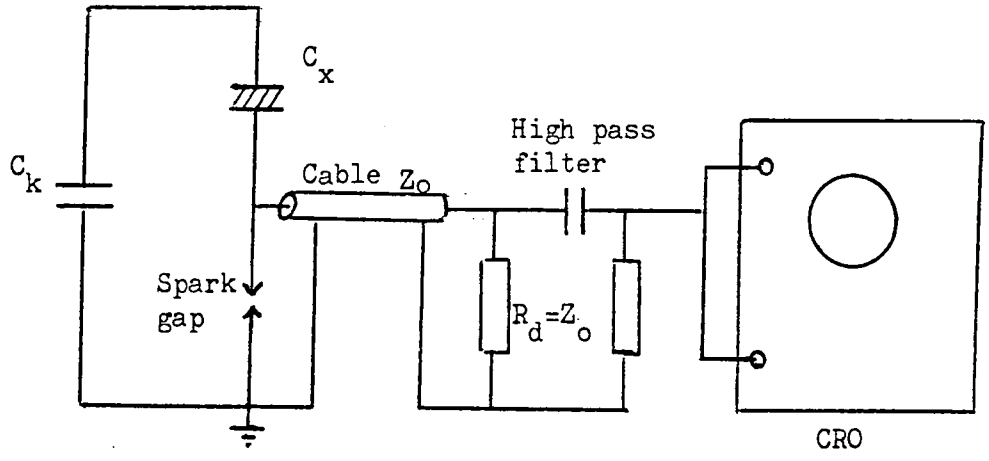

(a) Measuring arrangement for use with oscilloscope

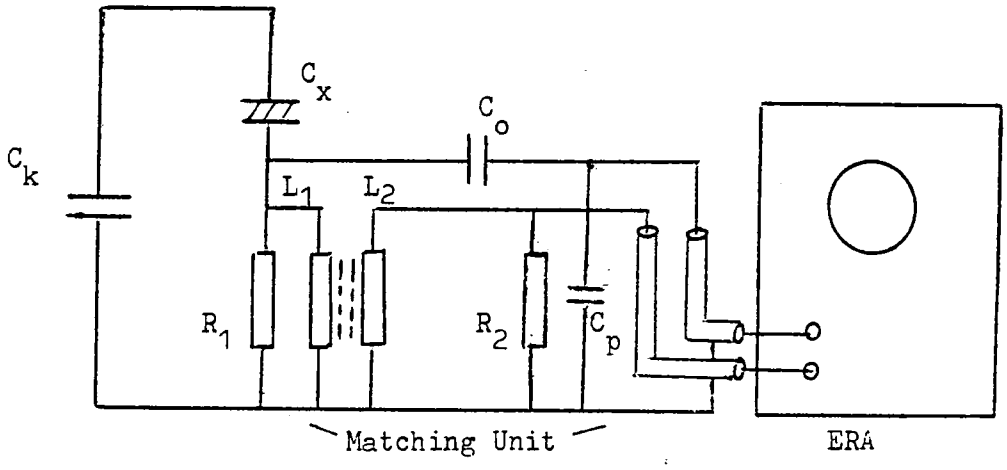

R_1, R_2, L_1, L_2, have values depending upon unit.

(b) Measuring arrangement with the ERA display

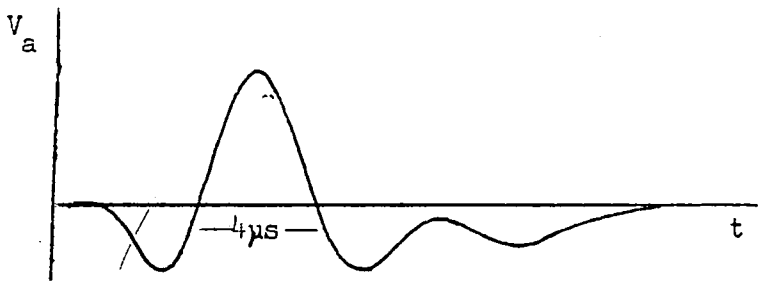

(c) Output voltage waveform from the ERA display

CRO AND ERA MEASURING CIRCUITS AND DISPLAY

FIG. 4.12

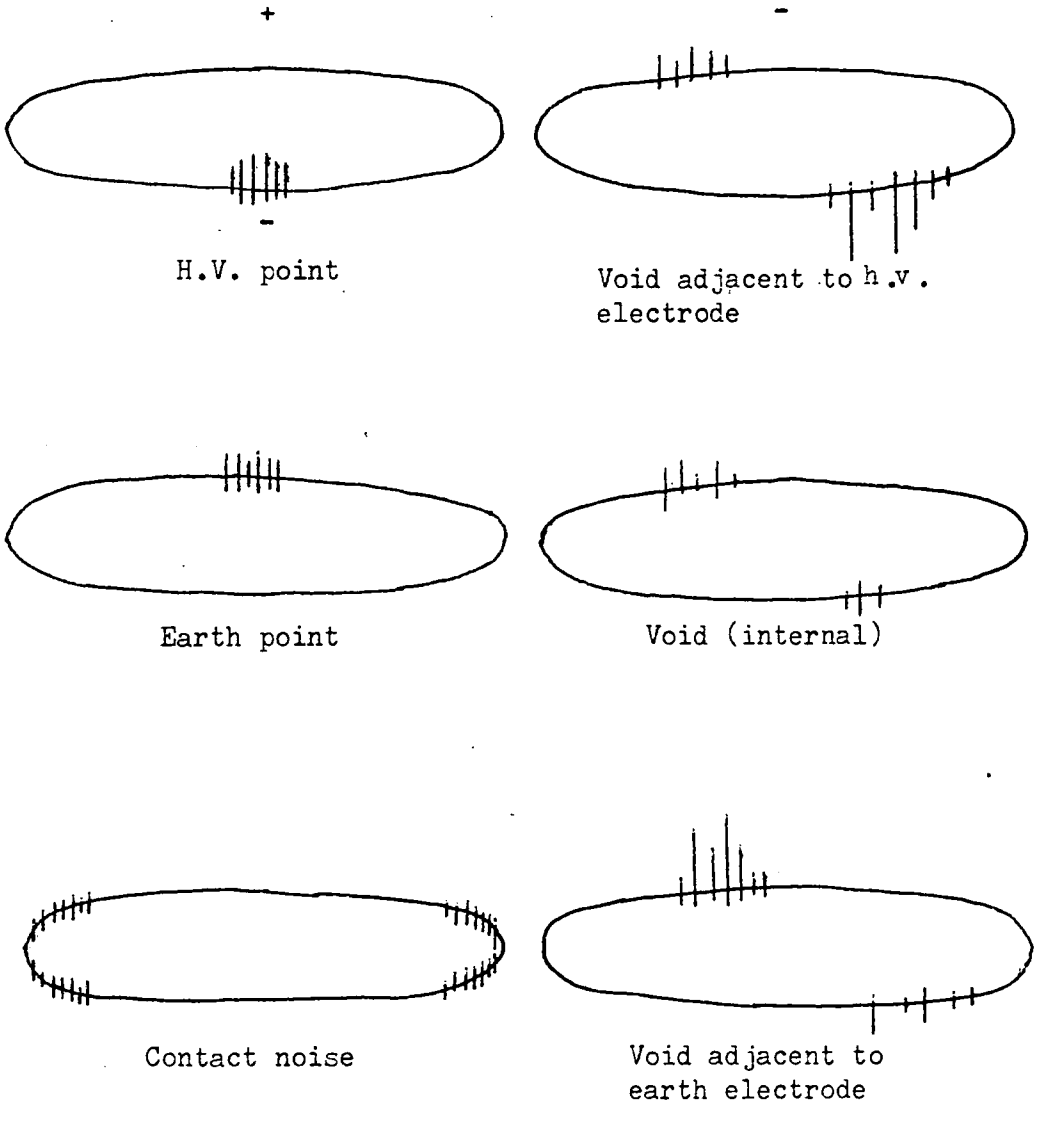

TYPICAL EXAMPLES OF DISCHARGE PATTERN OBTAINED WITH ERA MODEL III (MATCHING UNIT IN SERIES WITH SAMPLE)

FIG. 4.13

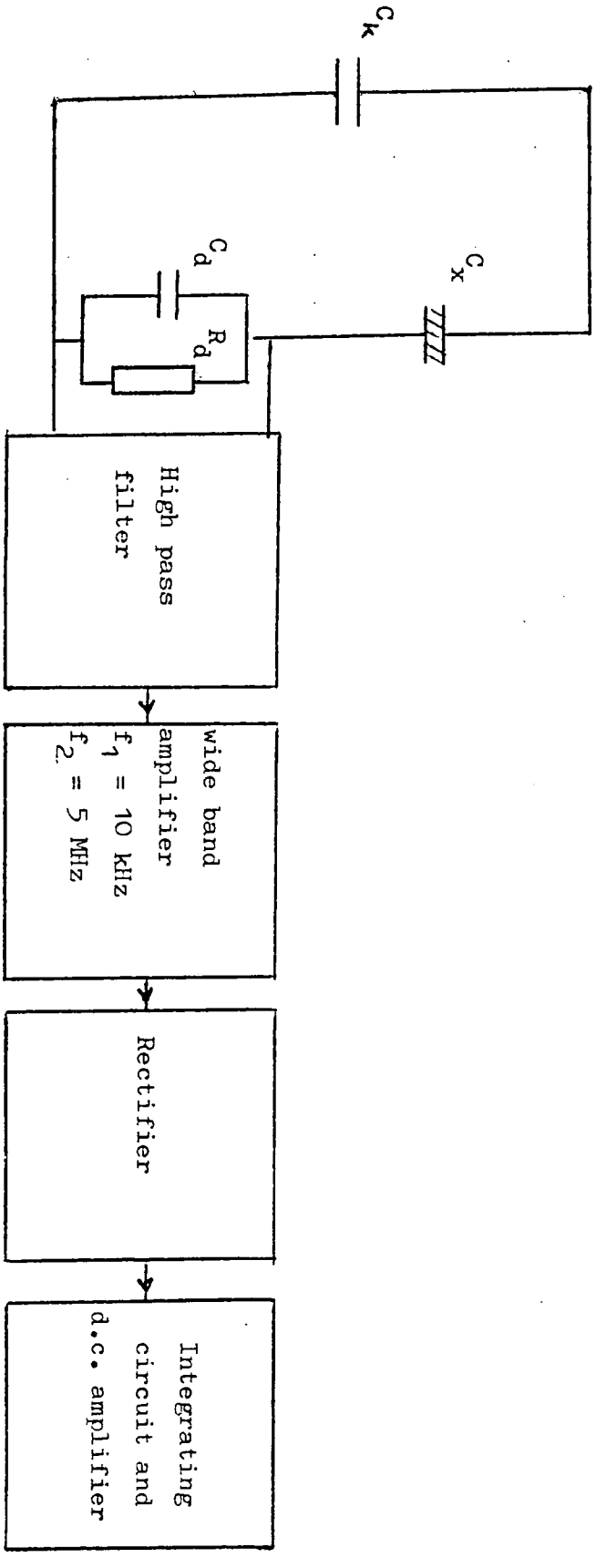

SCHEMATIC DIAGRAM OF A MEAN CURRENT METER

FIG. 4.14

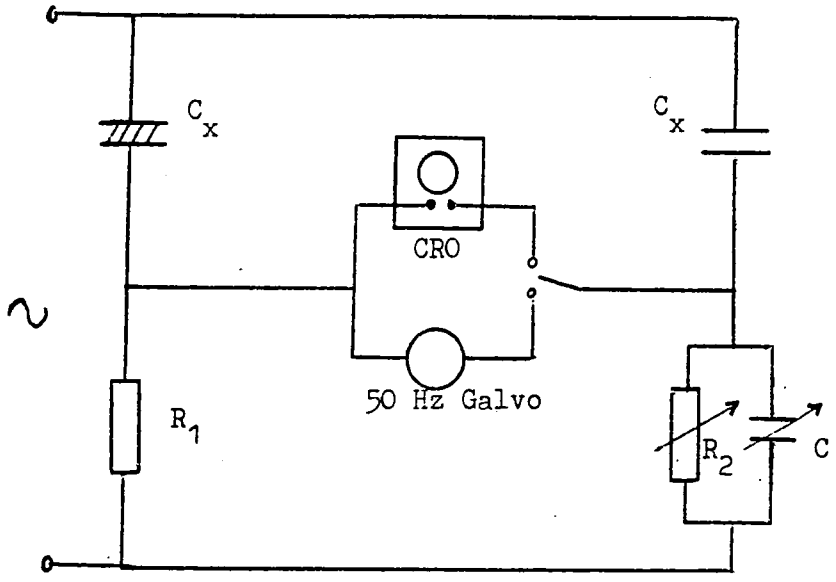

(a) Double balancing Schering bridge

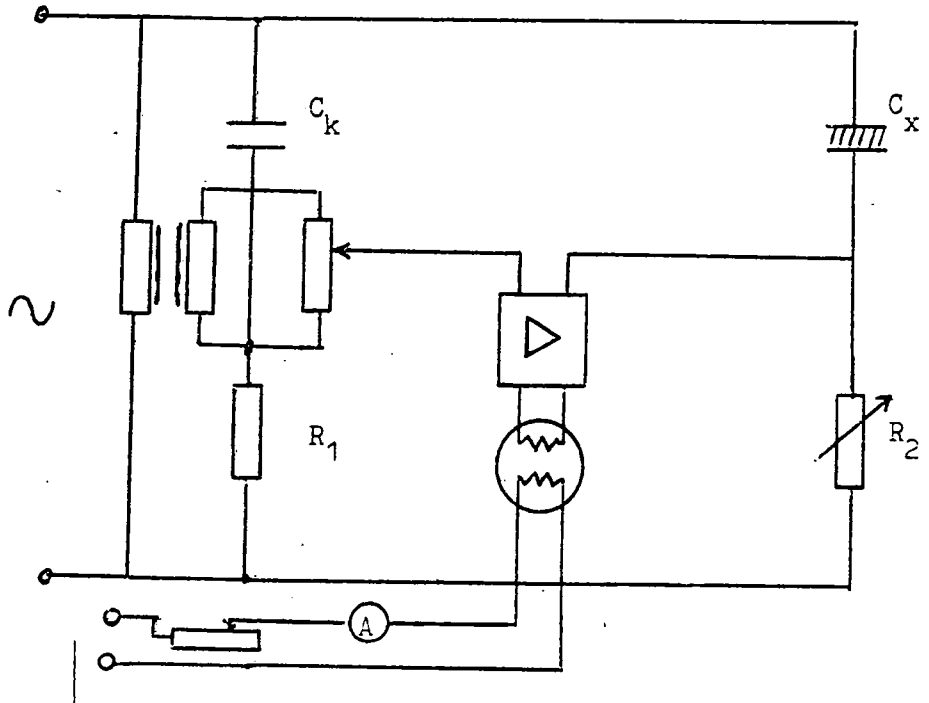

Supply from the l.v. side of testing transformer.

(b) Discharge power wattmeter circuit (after Veverka)

SCHERING AND WATTMETER BRIDGES

FIG. 4.15

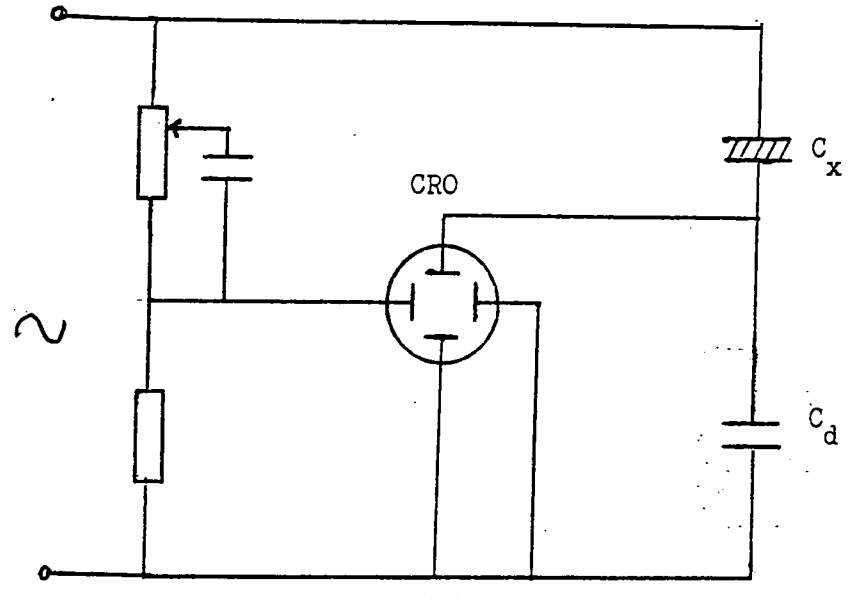

(a)

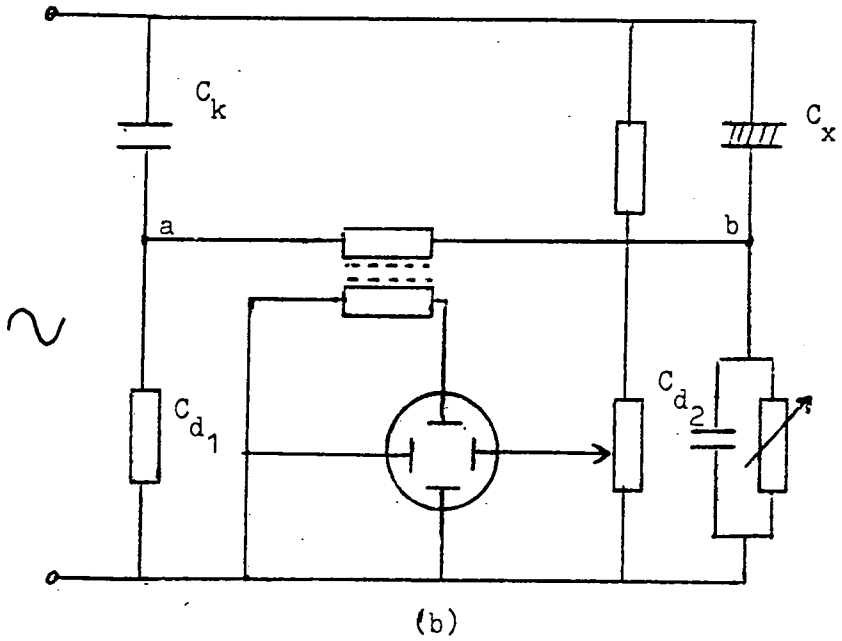

(b)

'LOOP TRACE' CIRCUITS (AFTER DAKIN)

FIG. 4.16

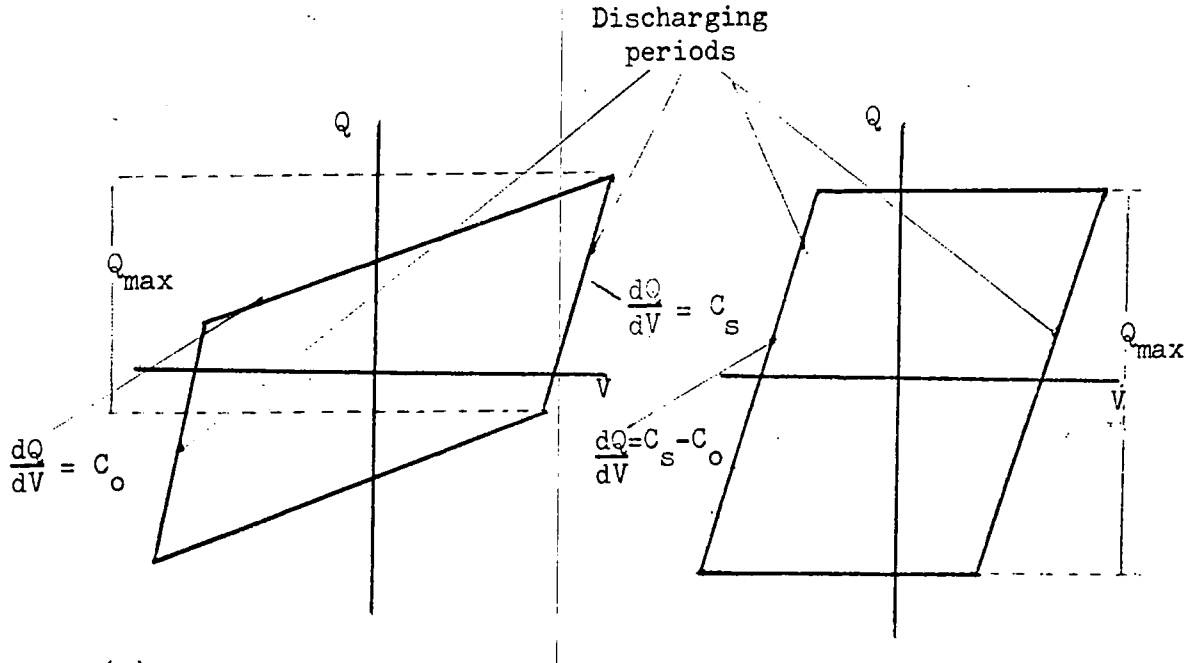

(a) Simple method for displaying charge transfer due to discharge

(b) Capacitance bridge method for displaying charge transfer due to discharge

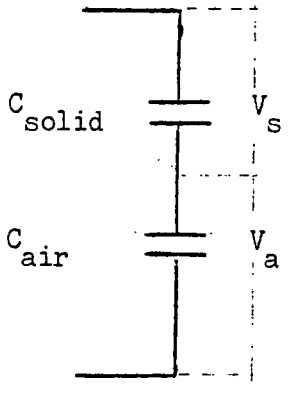

(c)

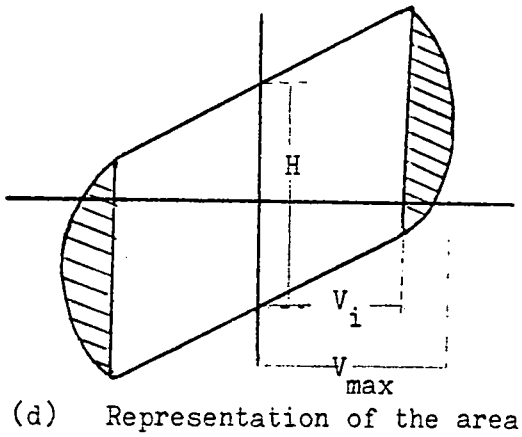

(d) Representation of the area of the charge diagram

'LOOP TRACE' DIAGRAMS

FIG. 4.17

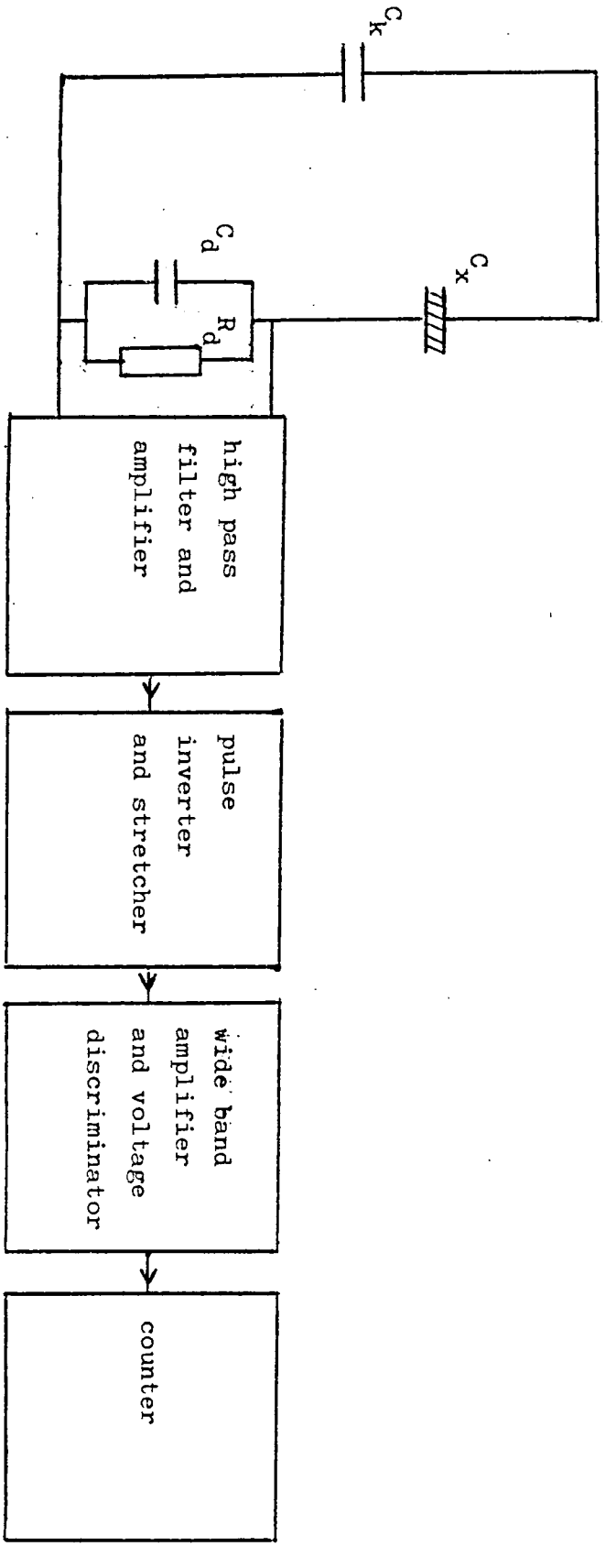

SCHEMATIC DIAGRAM OF SINGLE CHANNEL PULSE HEIGHT ANALYSER

FIG. 4.18

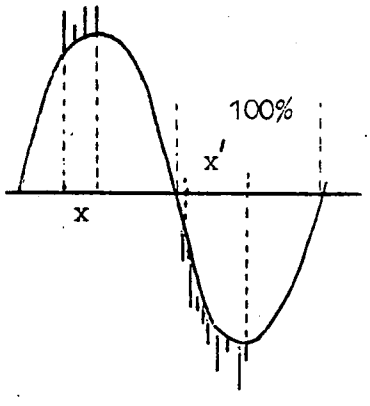

The graph shown below relates to errors in observed count for pulses occurring over x% or x'% of the half cycle of the applied-test voltage

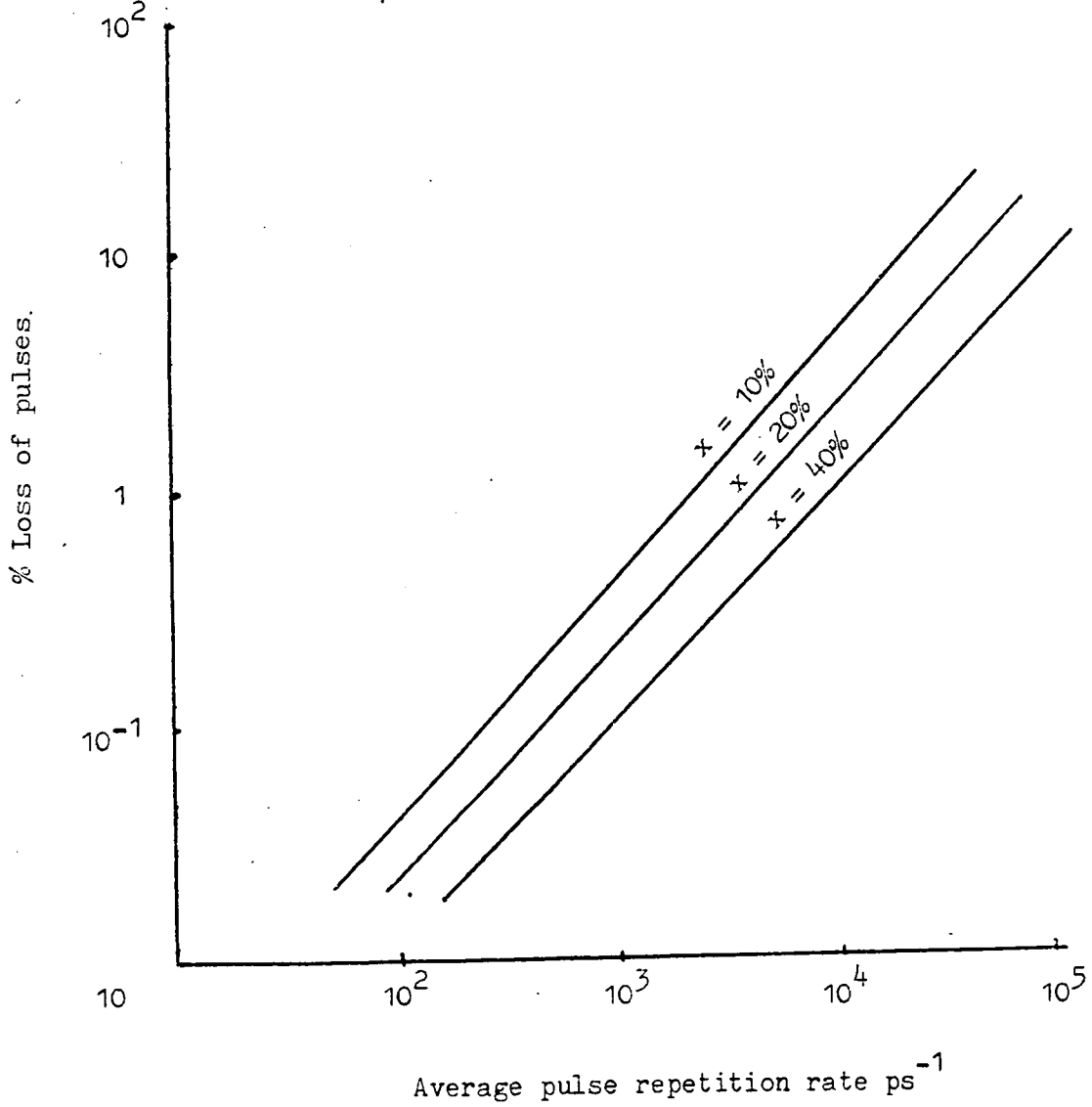

STATISTICAL LOSS OF PULSE COUNTS FOR A RANDOM TIME DISTRIBUTION. (ALLOWANCE IS MADE FOR BUNCHING OVER PART OF THE CYCLE).

FIG. 4.19

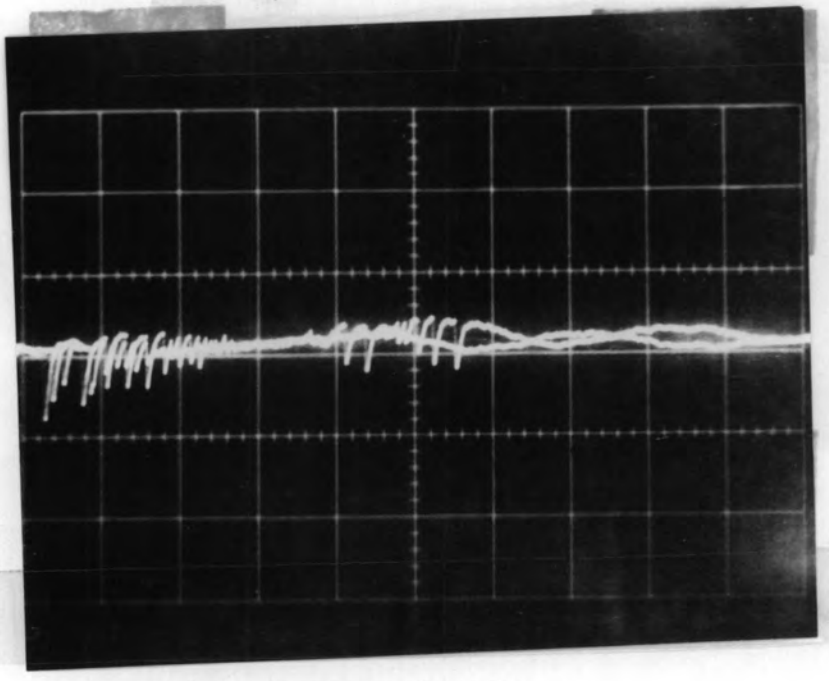

(a) Common mode voltage.
(0.5 V/div, 0.2 mS/div)

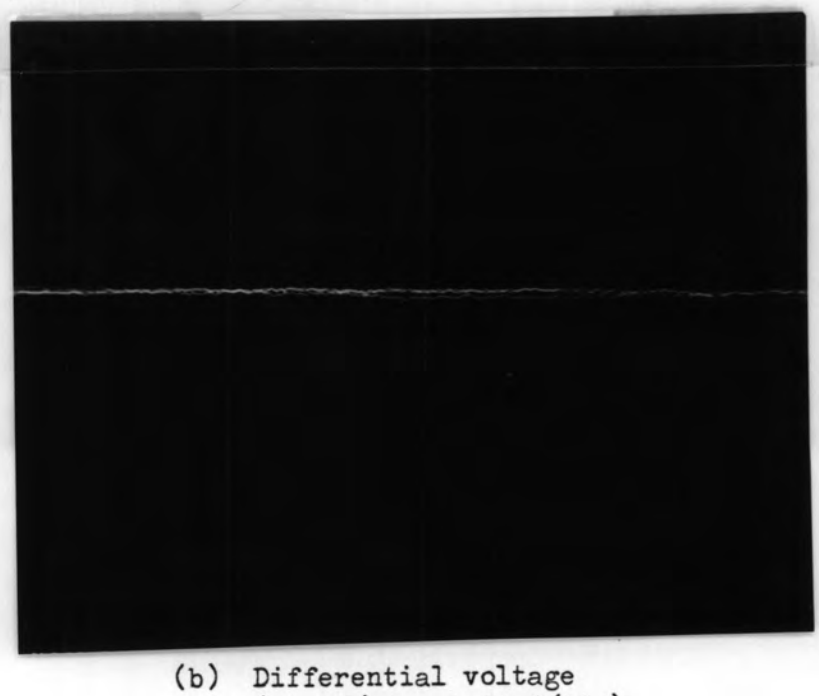

(b) Differential voltage
(0.1 V/div, 0.2 mS/div)

THE EFFECT OF DIFFERENTIAL MEASUREMENT ON COMMUTATION NOISE

(6 k$\hat{V}$/0.1 Hz applied to the bridge with discharge free specimen)

FIG. 4.20

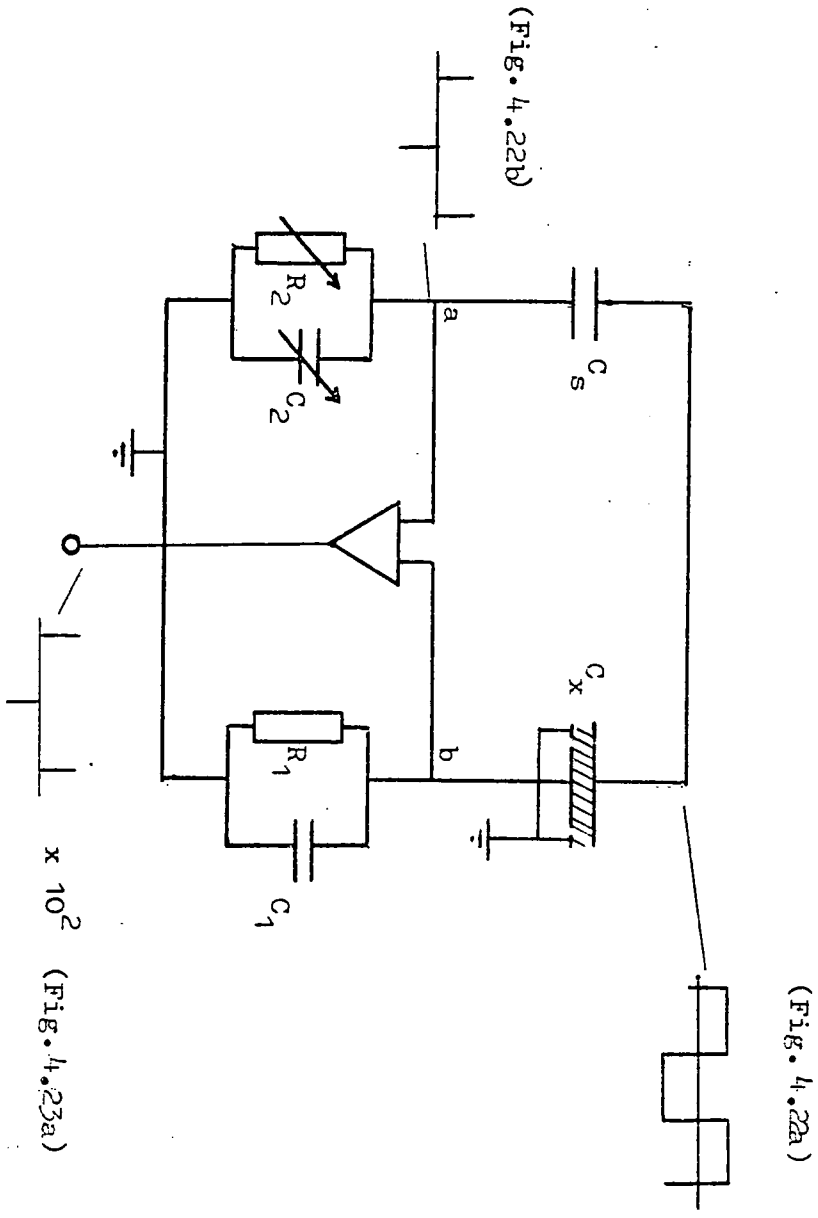

THE 0.1 Hz DIFFERENTIAL DISCHARGE BRIDGE AND ASSOCIATED BALANCING WAVEFORMS

FIG. 4.21

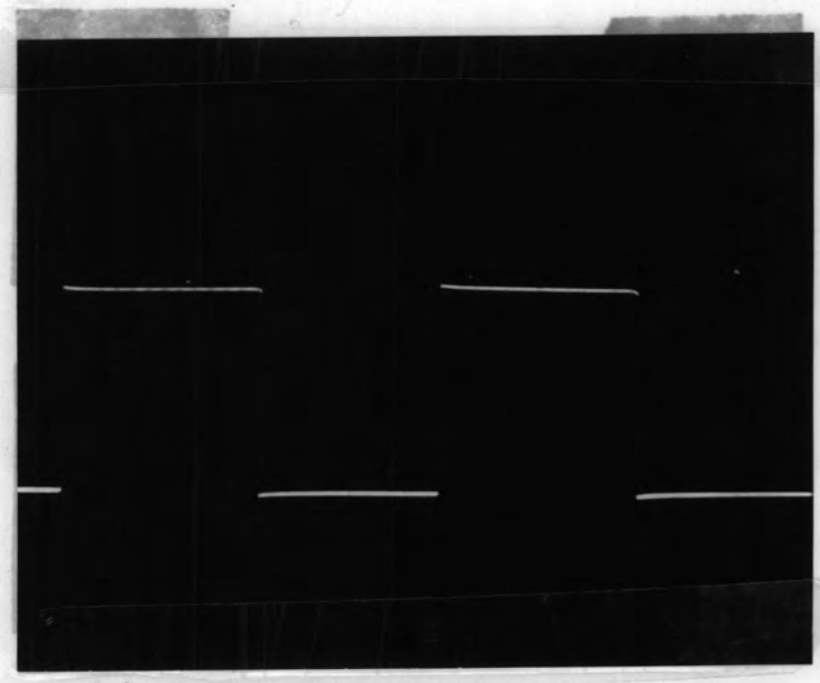

(a) Square wave injected at the top of the discharge bridge.
(2V/div, 0.2 mS/div)

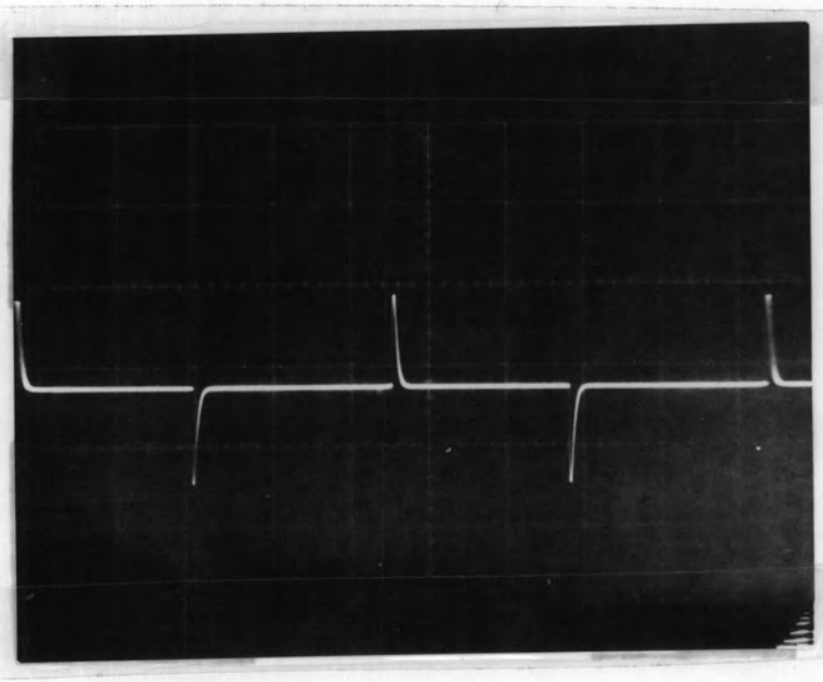

(b) Differentiated square wave at the bridge detector terminals, i.e., common mode voltage of the differential amplifier.
(2V/div, 0.2 mS/div).

DISCHARGE BRIDGE BALANCING WAVEFORMS

FIG. 4.22

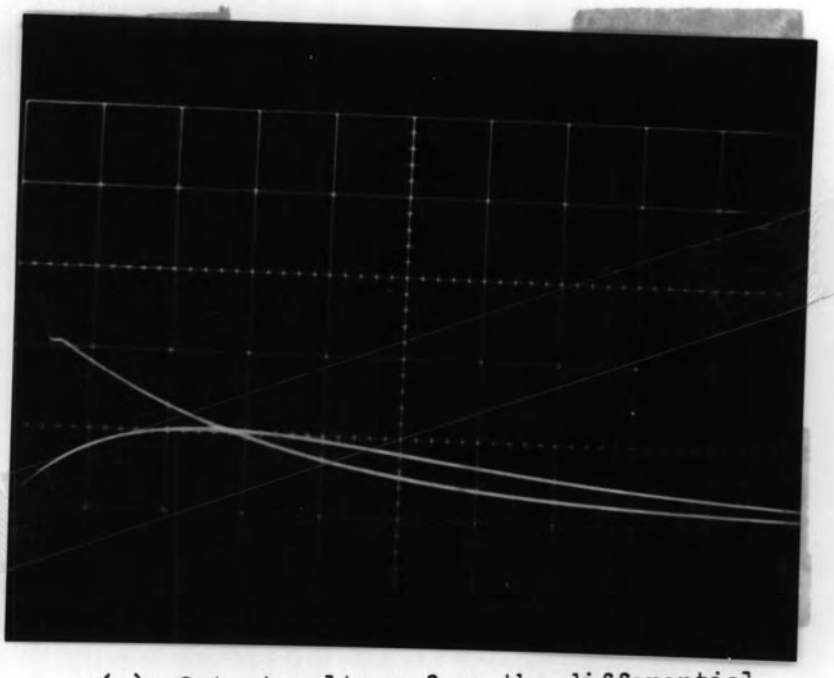

(a) Output voltage from the differential amplifier under bridge balanced conditions (0.02 V/div, 0.2 mS/div).

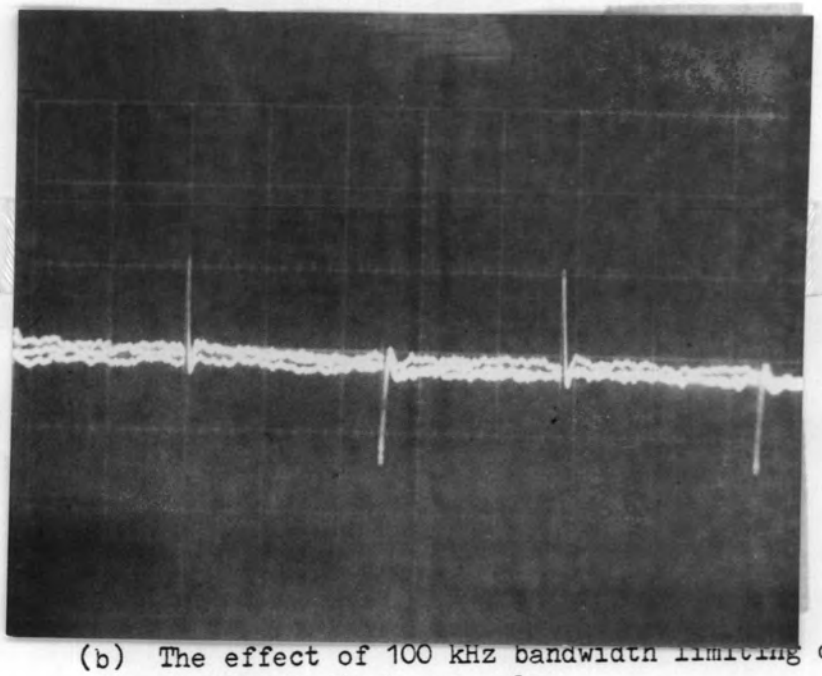

(b) The effect of 100 kHz bandwidth limiting on simulated discharge pulse.
(0.5 V/div, 2 μS/div).

DIFFERENTIAL AMPLIFIER OUTPUT WAVEFORMS

FIG. 4.23

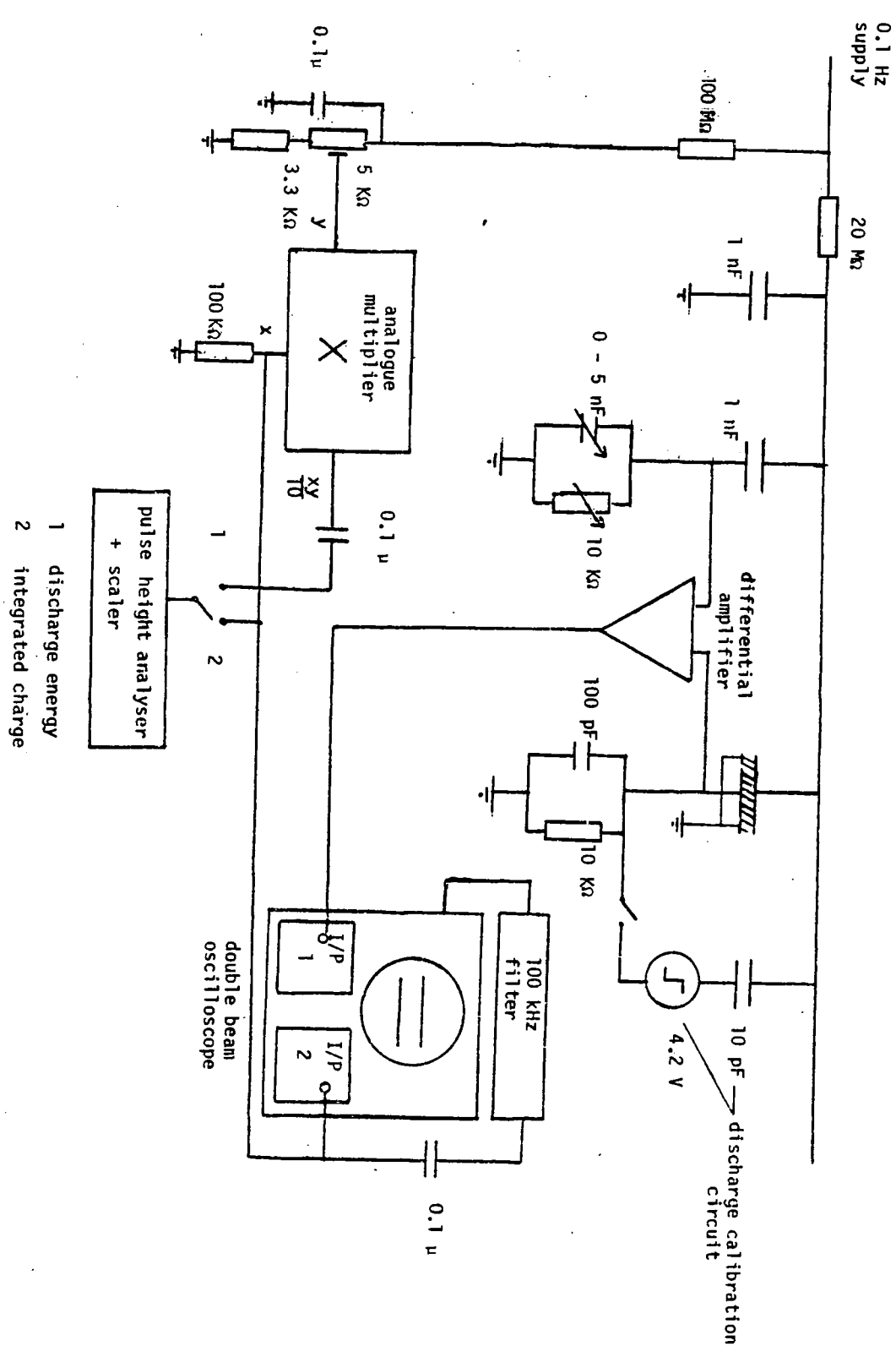

EXPERIMENTAL ARRANGEMENT FOR THE DETERMINATION OF CHARGE MAGNITUDE DISTRIBUTION/CYCLE AND TOTAL AVERAGE DISCHARGE ENERGY LOSS/CYCLE

FIG. 4.24

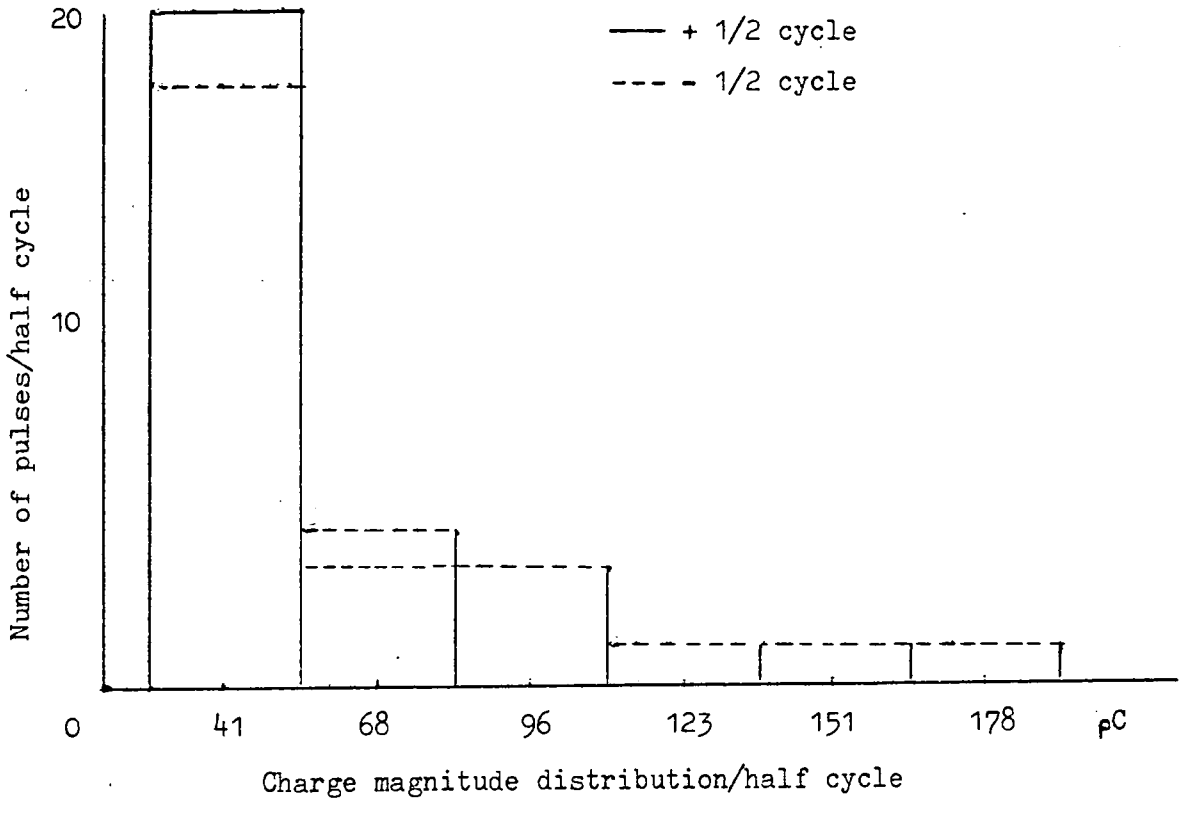

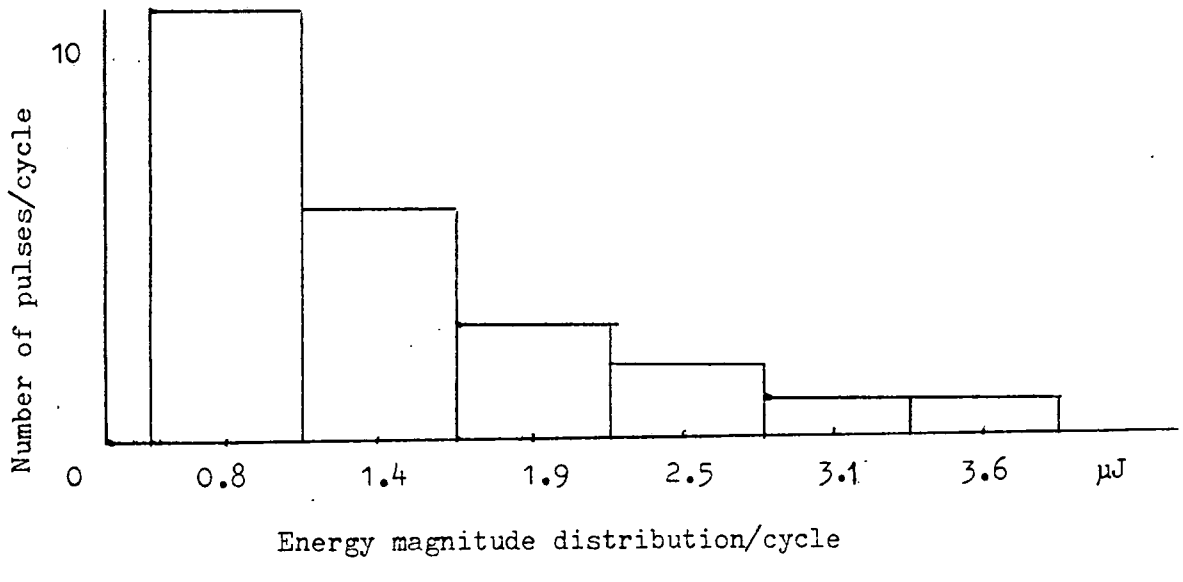

CHARGE AND ENERGY MAGNITUDE DISTRIBUTIONS

FIG. 4.25

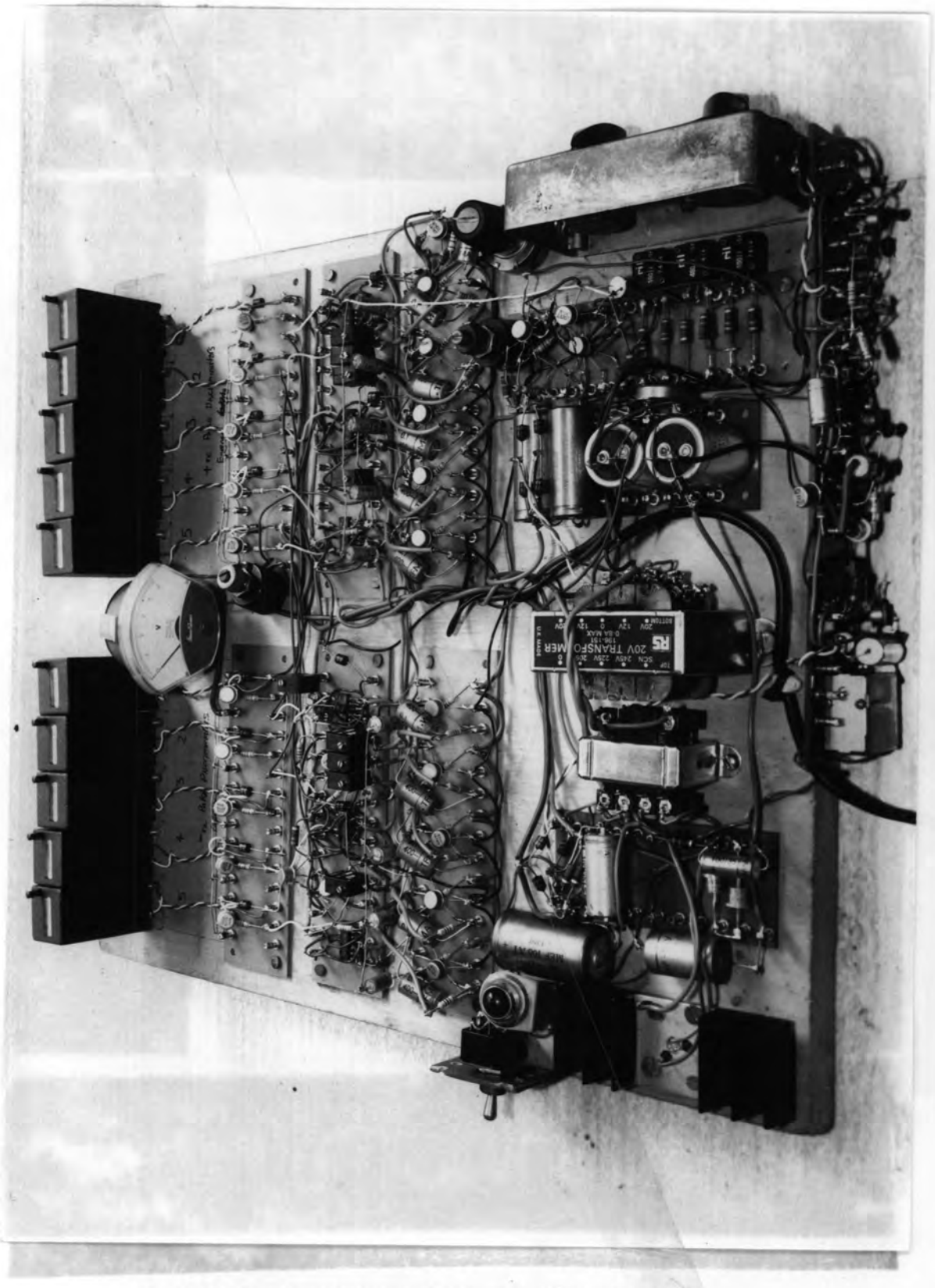

PRACTICAL LAYOUT OF THE INSTRUMENT USED TO MEASURE TOTAL AVERAGE DISCHARGE ENERGY LOSS/ CYCLE AT 0.1 Hz

FIG. 4.26

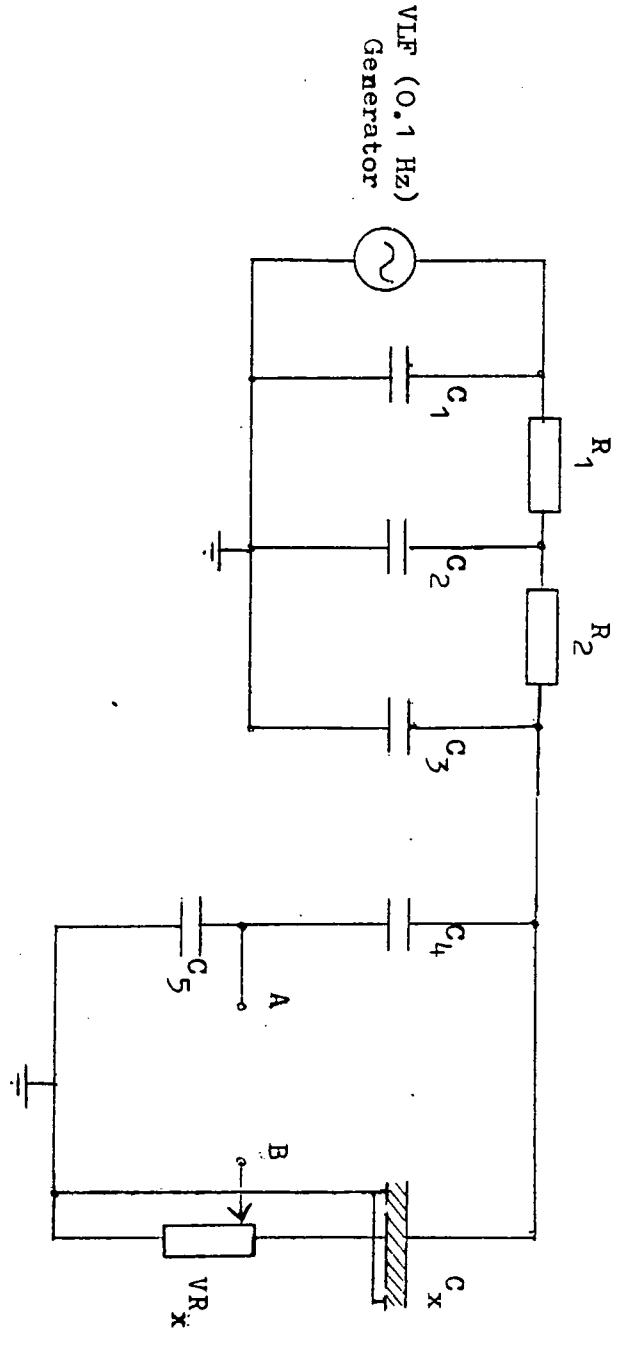

EXPERIMENTAL ARRANGEMENT FOR MEASURING THE INDIVIDUAL APPARENT DISCHARGES q_a AND TEST VOLTAGE V AT 0.1 Hz

FIG. 4.27

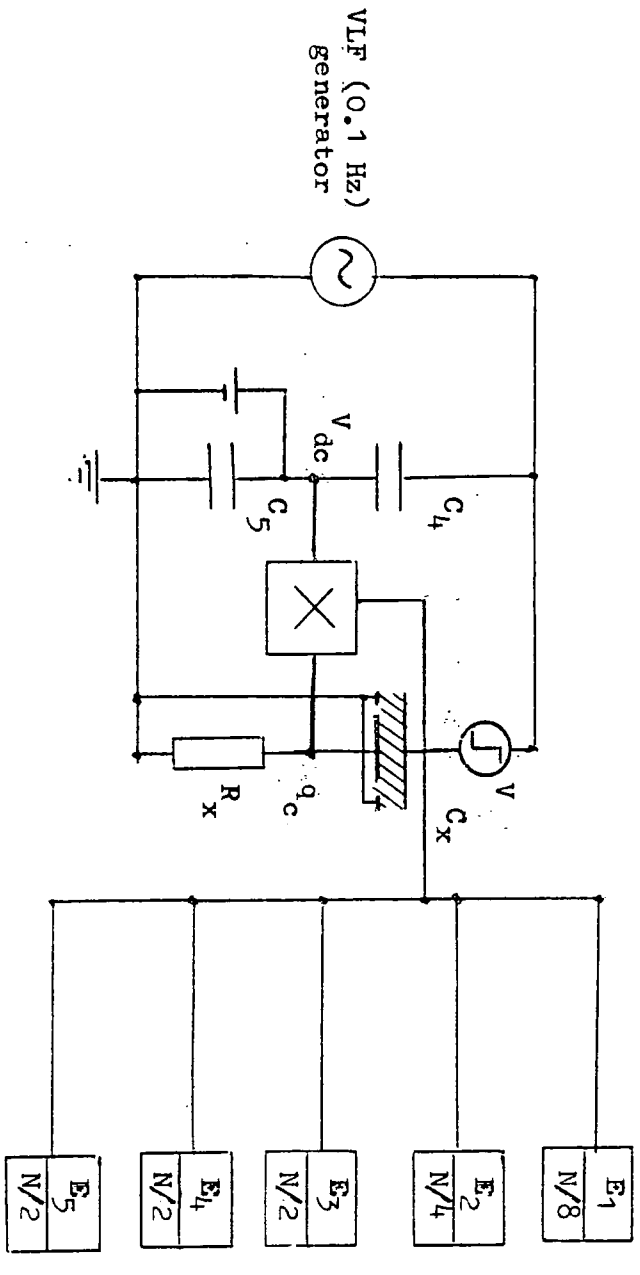

BLOCK DIAGRAM FOR THE MEASUREMENT AND CALIBRATION OF TOTAL AVERAGE DISCHARGE ENERGY LOSS/CYCLE AT 0.1 Hz

FIG. 4.28

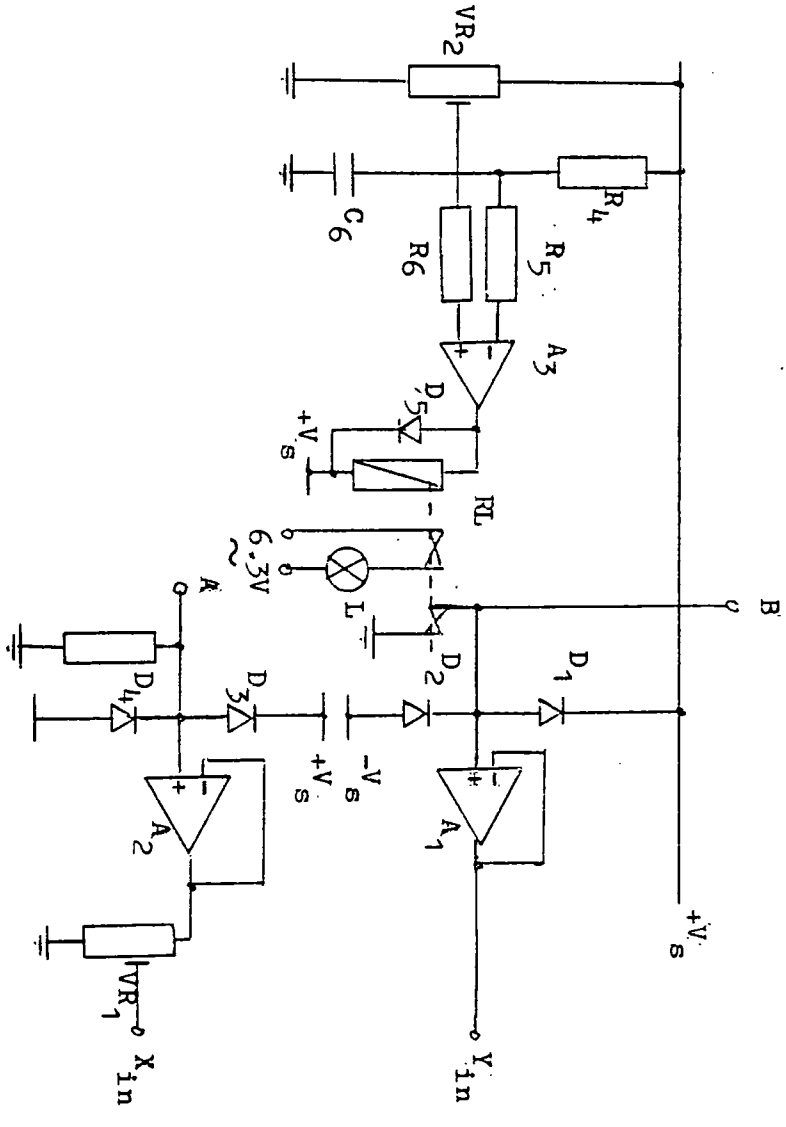

APPARENT DISCHARGE MAGNITUDE AND TEST VOLTAGE INPUT UNITS

FIG.4.29

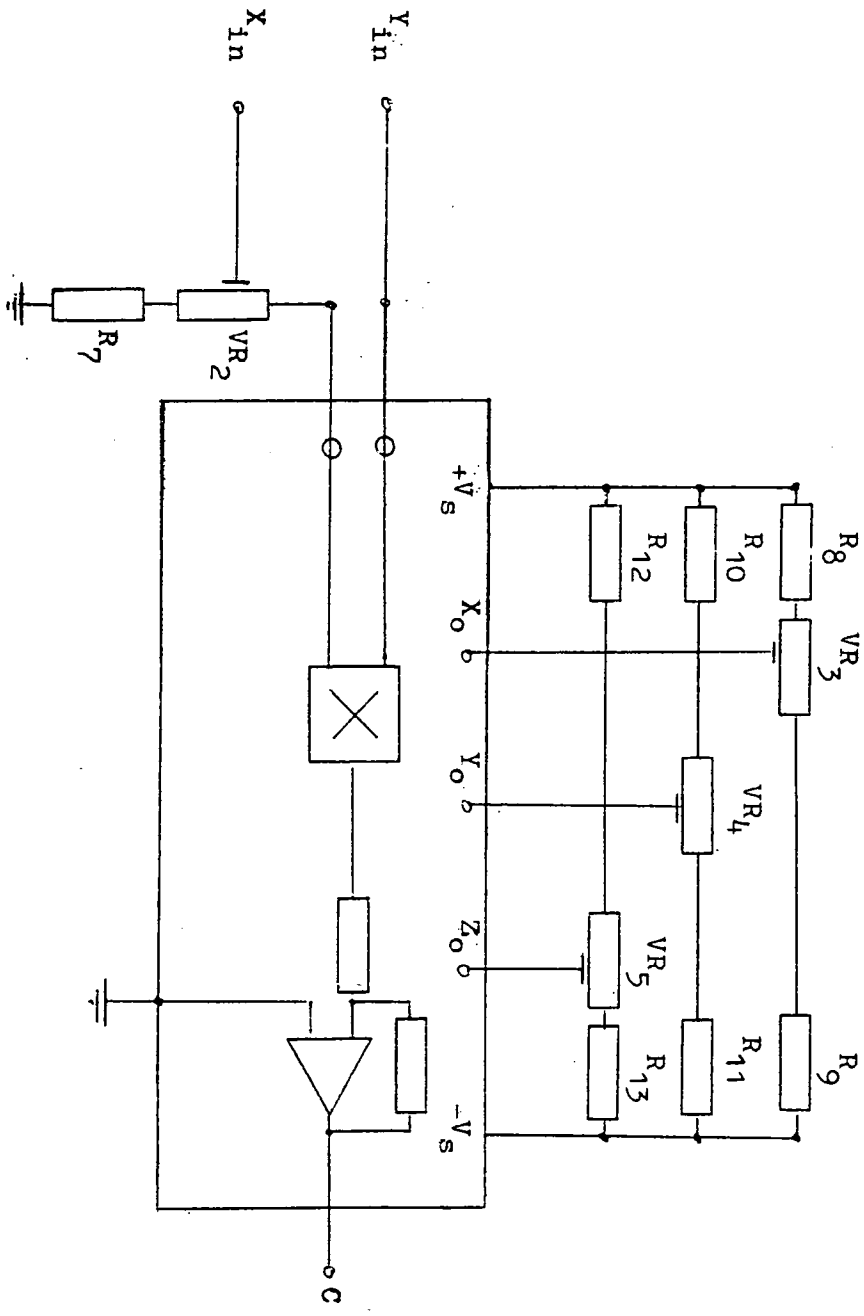

THE ANALOGUE MULTIPLIER CIRCUIT USED FOR OBTAINING THE PRODUCT $q_a V$

FIG. 4.30

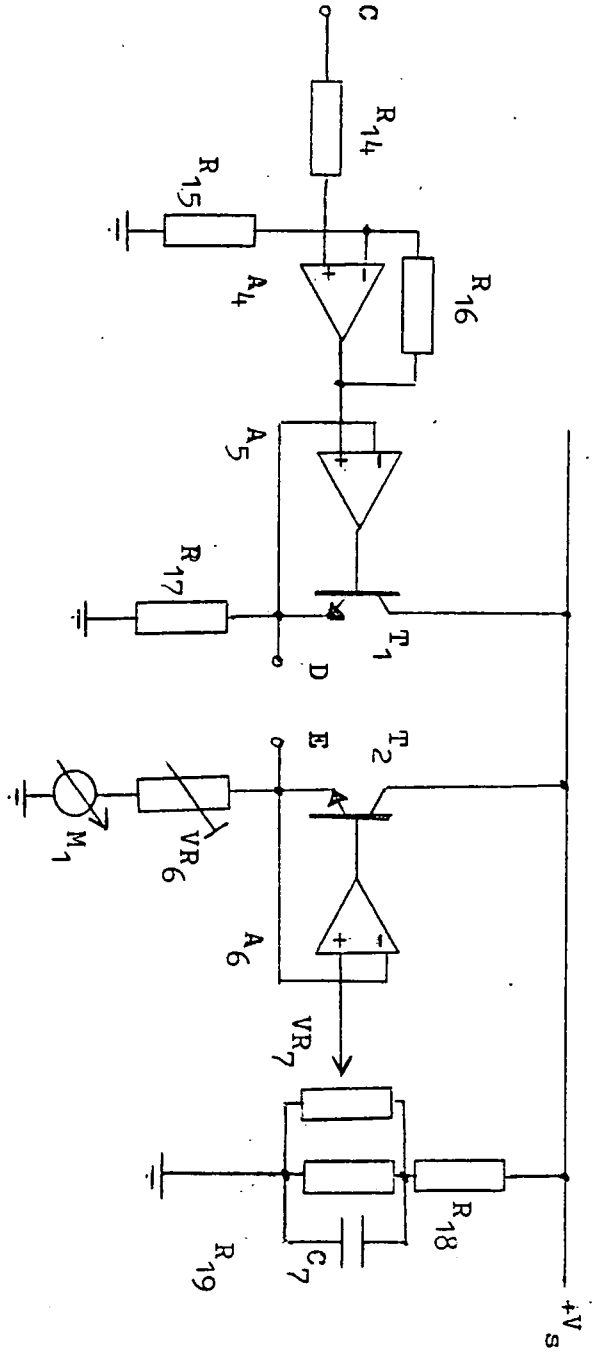

VOLTAGE DISCRIMINATOR LEVEL CONTROL AND PULSE DRIVER

FIG. 4.31

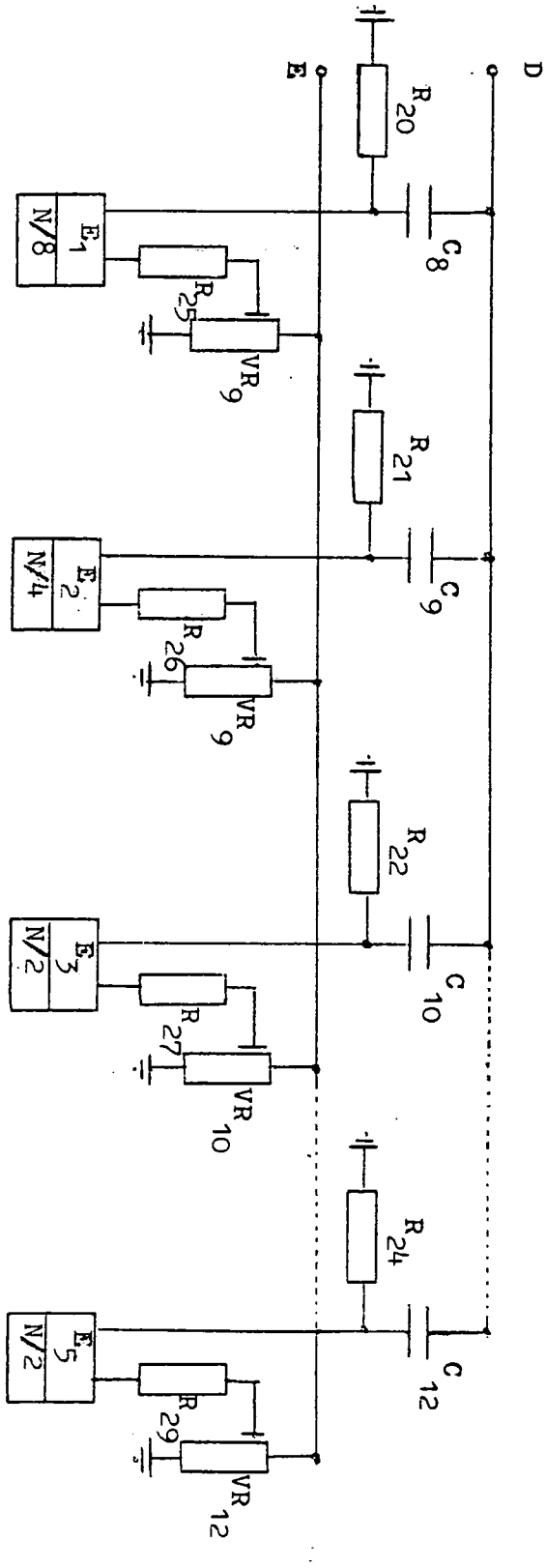

ARRANGEMENT OF THE PARALLEL CONNECTED ENERGY PULSE HEIGHT DISCRIMINATORS AND ELECTROMECHANICAL COUNTERS

FIG. 4.32

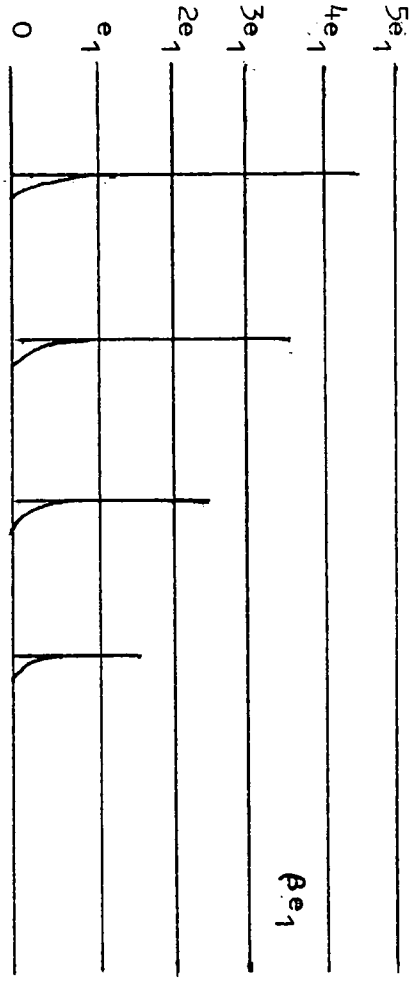

ARRANGEMENT OF ENERGY DISCRIMINATION LEVELS
(e_1-$5e_1$) AND CHANNEL ENERGY SEPARATION (βe_1)

FIG. 4.33

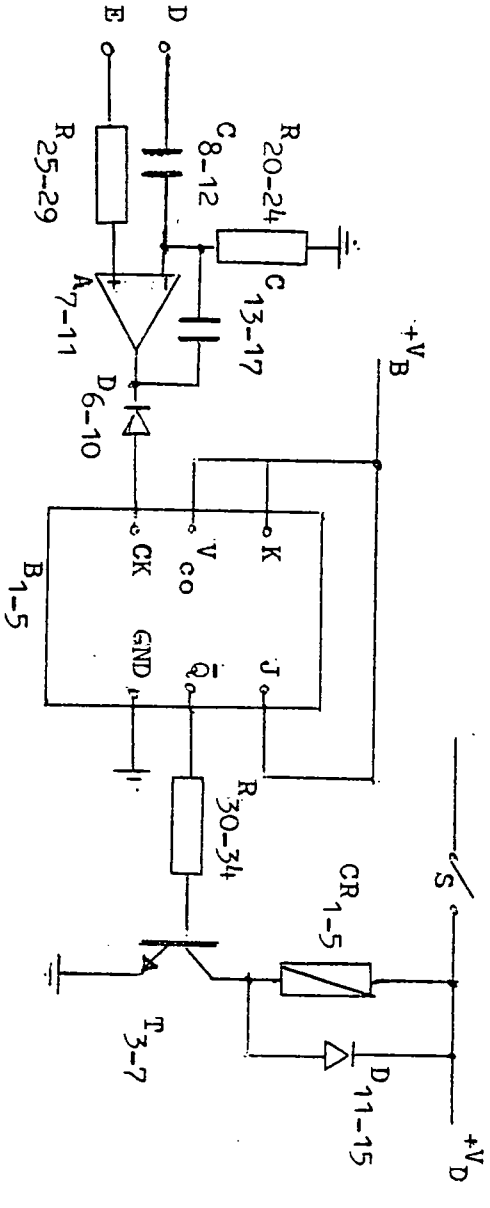

THE ENERGY PULSE DISCRIMINATOR AND ELECTRO-MECHANICAL COUNTER UNIT

FIG. 4.34

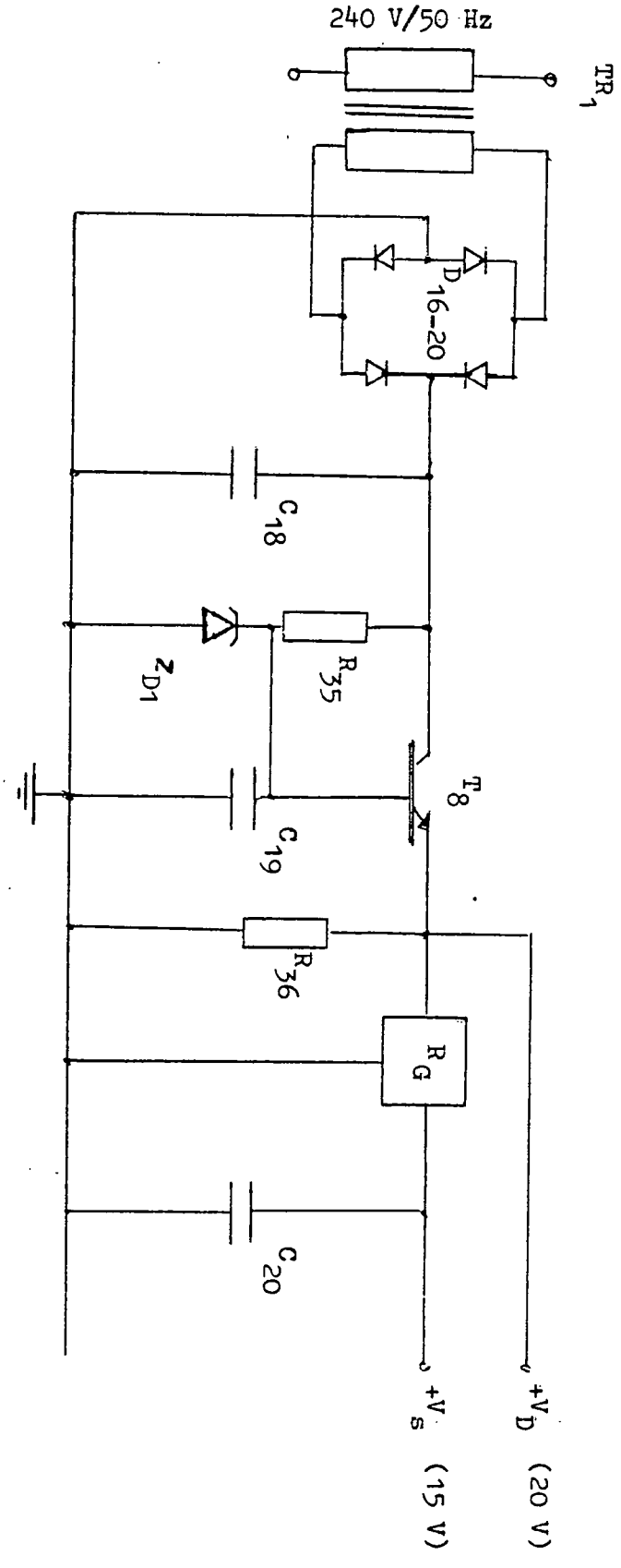

ELECTRO-MECHANICAL COUNTER AND POSITIVE RAIL/DISCRIMINATOR POWER SUPPLIES

FIG. 4.35

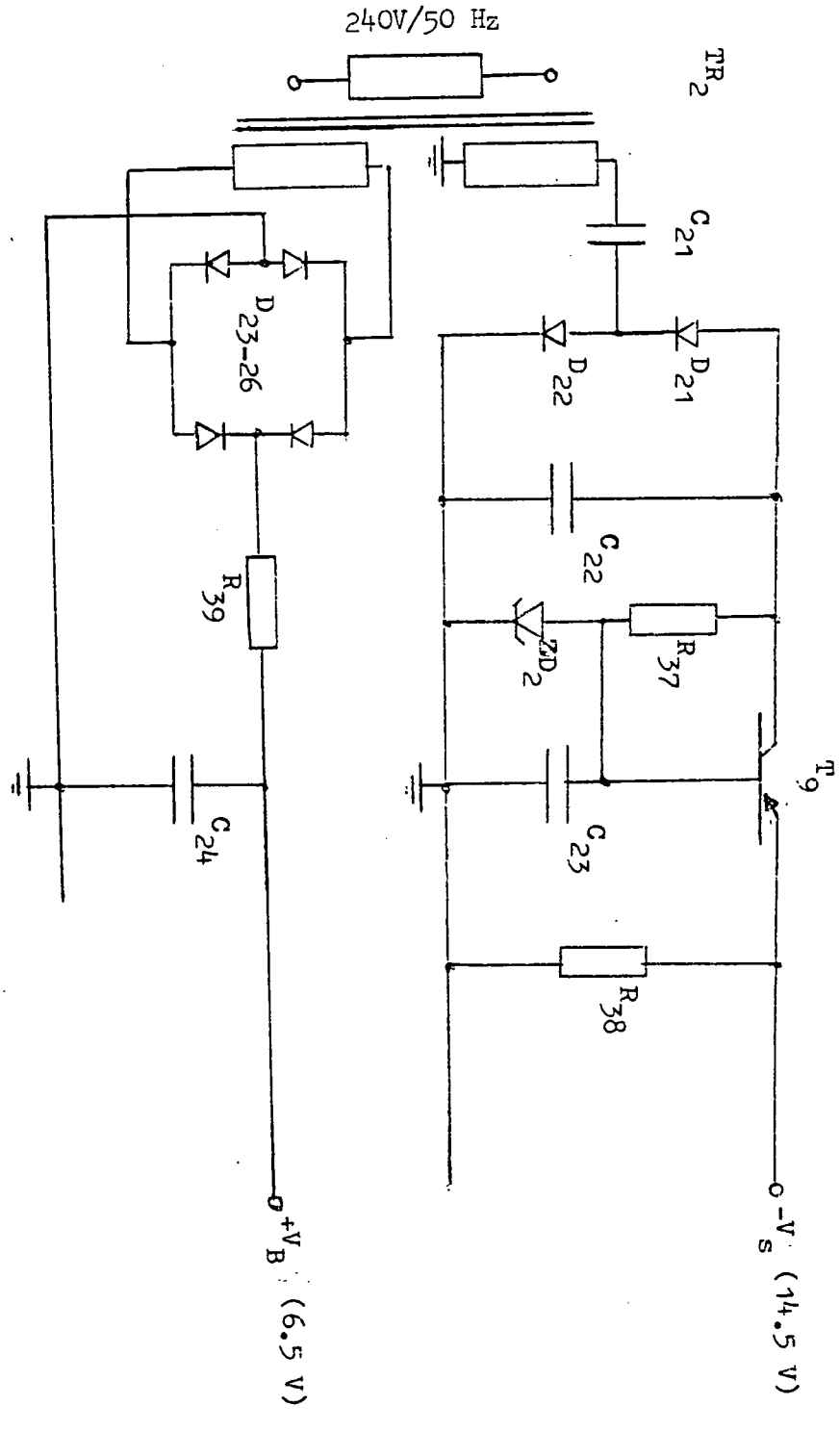

BINARY DIVIDER AND NEGATIVE RAIL POWER SUPPLIES

FIG. 4.36

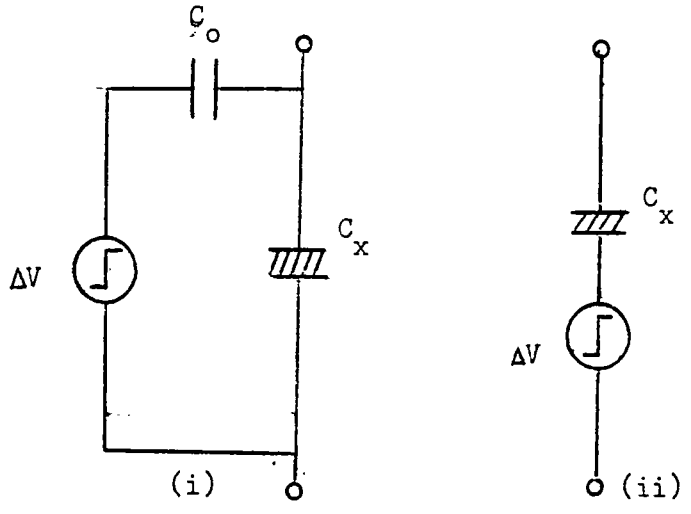

(a) Direct calibrators

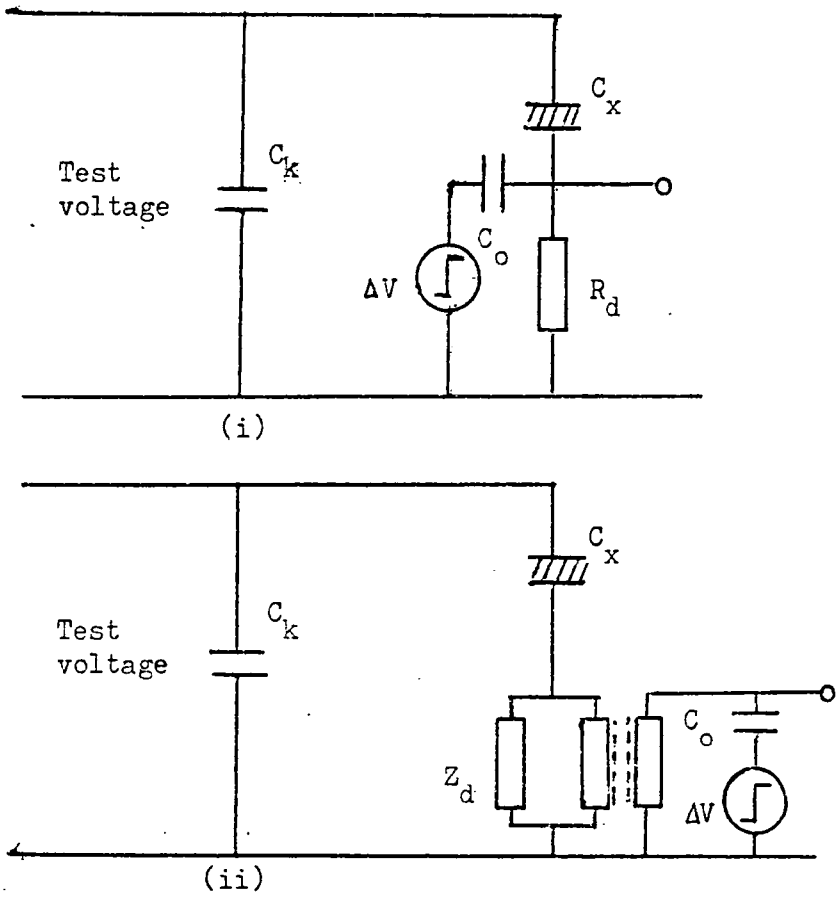

(b) Indirect calibrators

CONNECTION OF DIRECT OR INDIRECT CALIBRATORS

FIG. 4.37

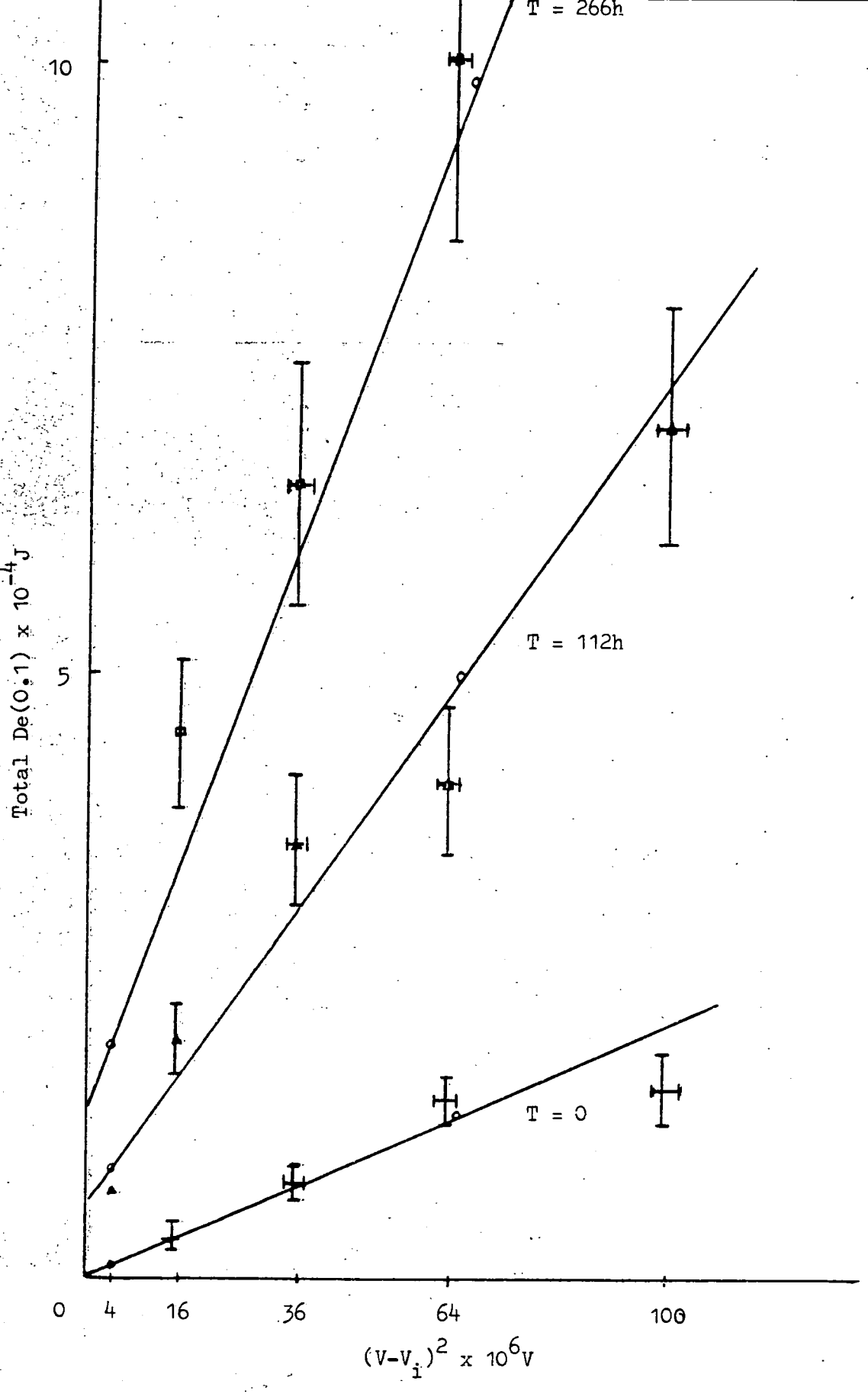

VARIATION OF De(0.1) WITH AGEING TIME (T) OF SPECIMEN C VERSUS $(V-V_i)^2$ - SEE TABLE 5.2.1

FIG. 5.1

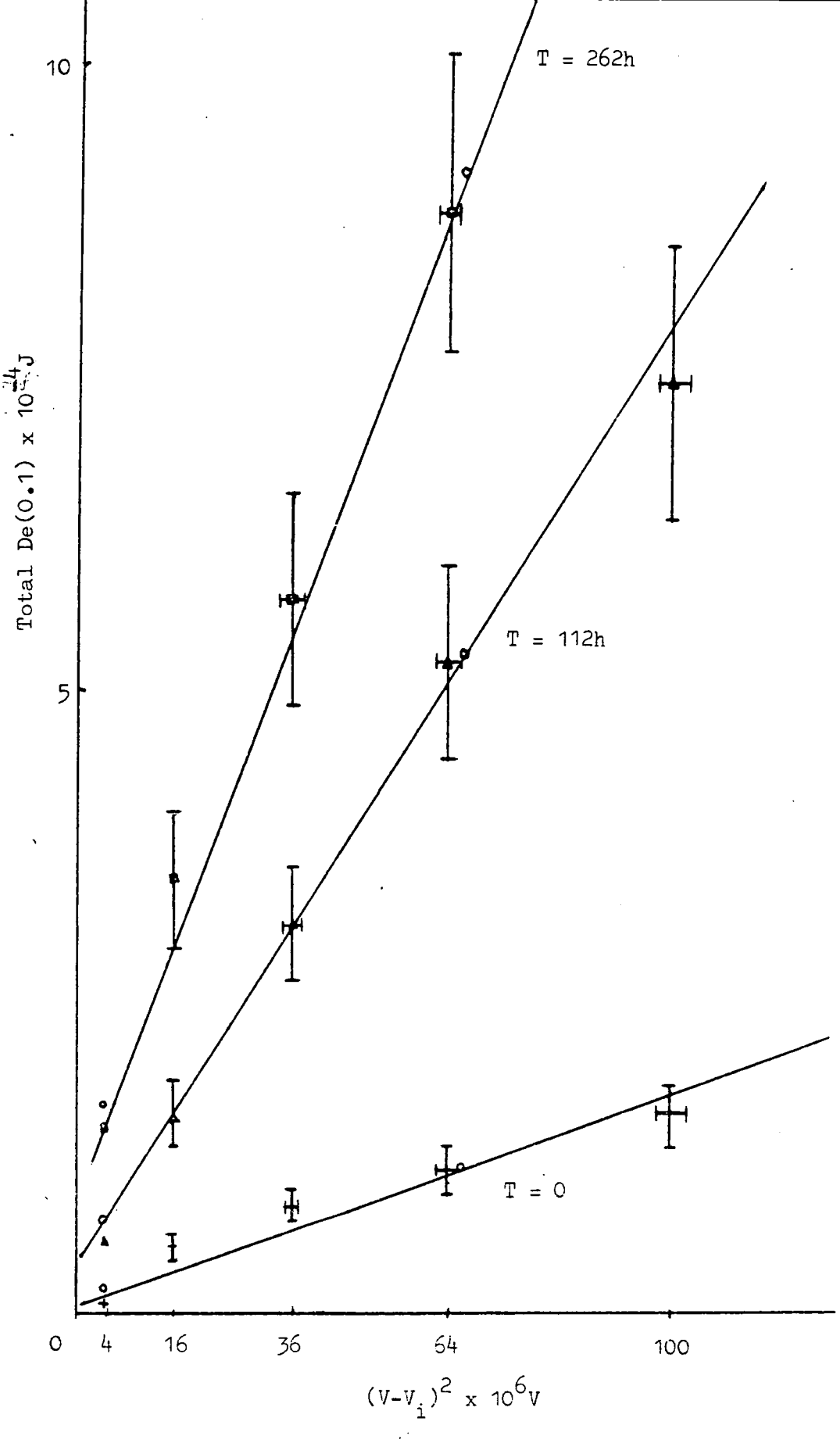

VARIATION OF De(0.1) WITH AGEING TIME (T)
OF SPECIMEN D VERSUS $(V-V_i)^2$ - SEE TABLE 5.2.1

FIG. 5.2

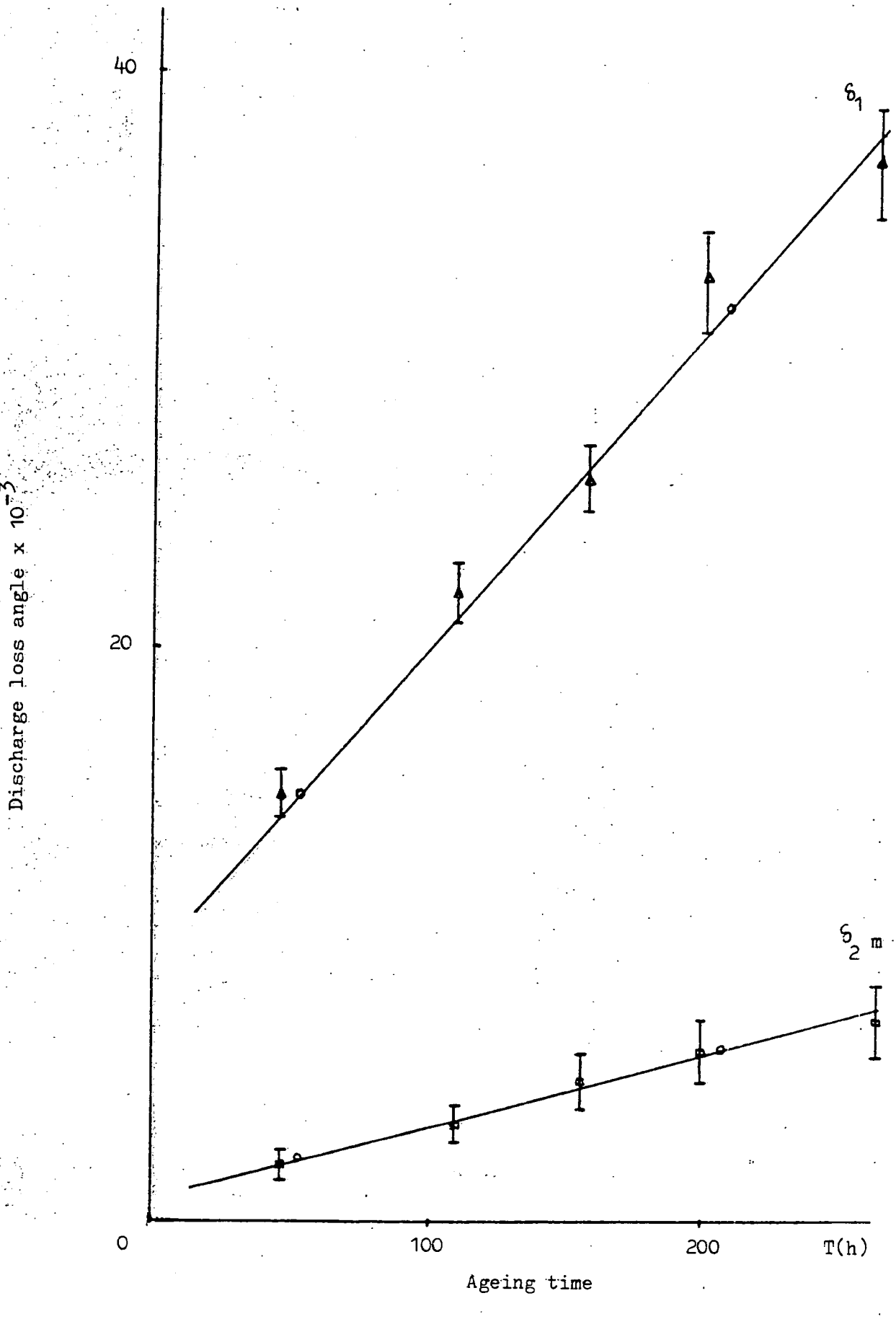

VARIATION OF δ_1 and δ_2 m WITH AGEING TIME (T)

OF SPECIMEN C - SEE TABLE 5.2.2

FIG. 5.3

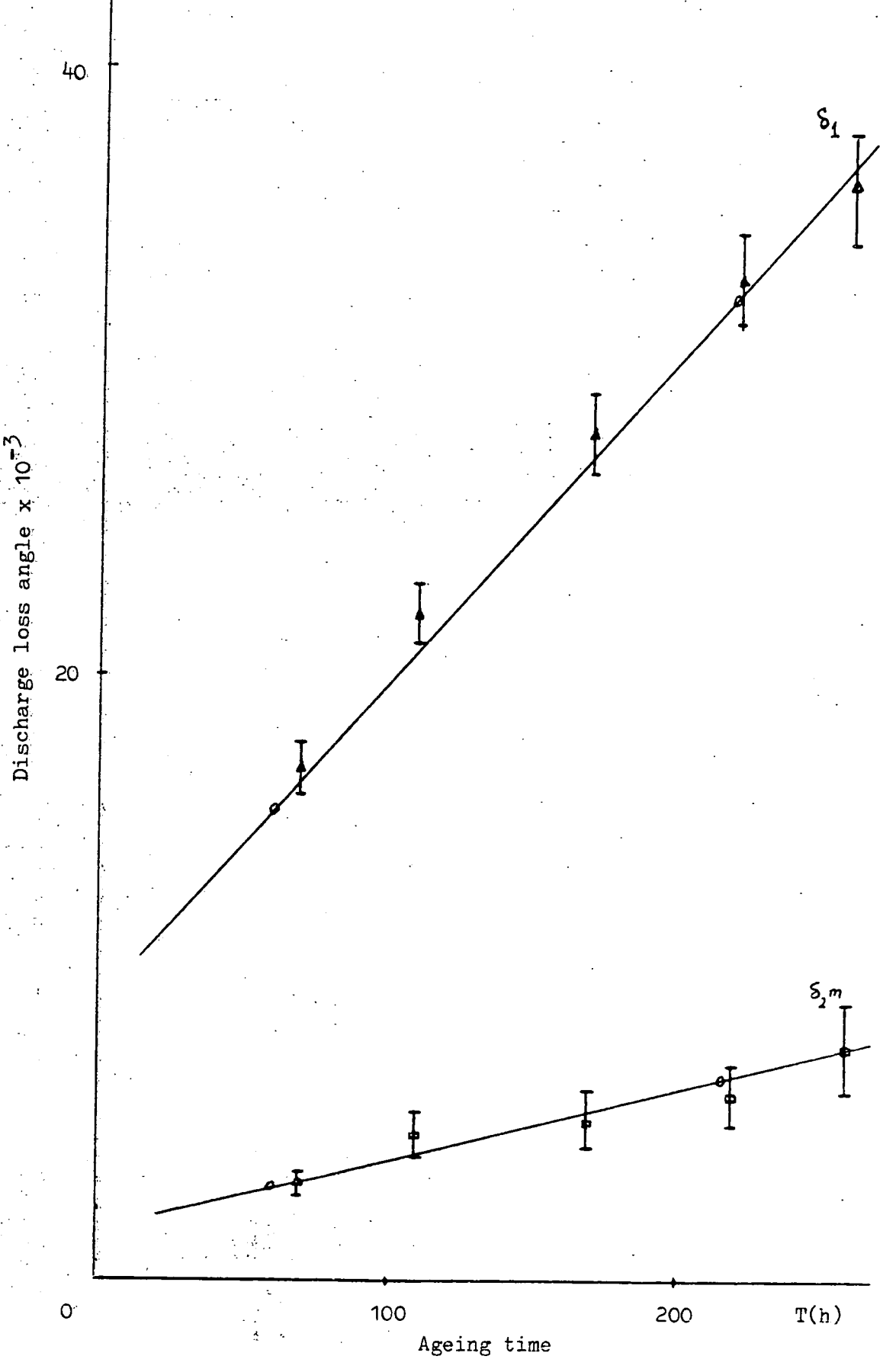

VARIATION OF δ_1 AND δ_2 m WITH AGEING TIME (T) OF SPECIMEN D - SEE TABLE 5.2.2

FIG. 5.4

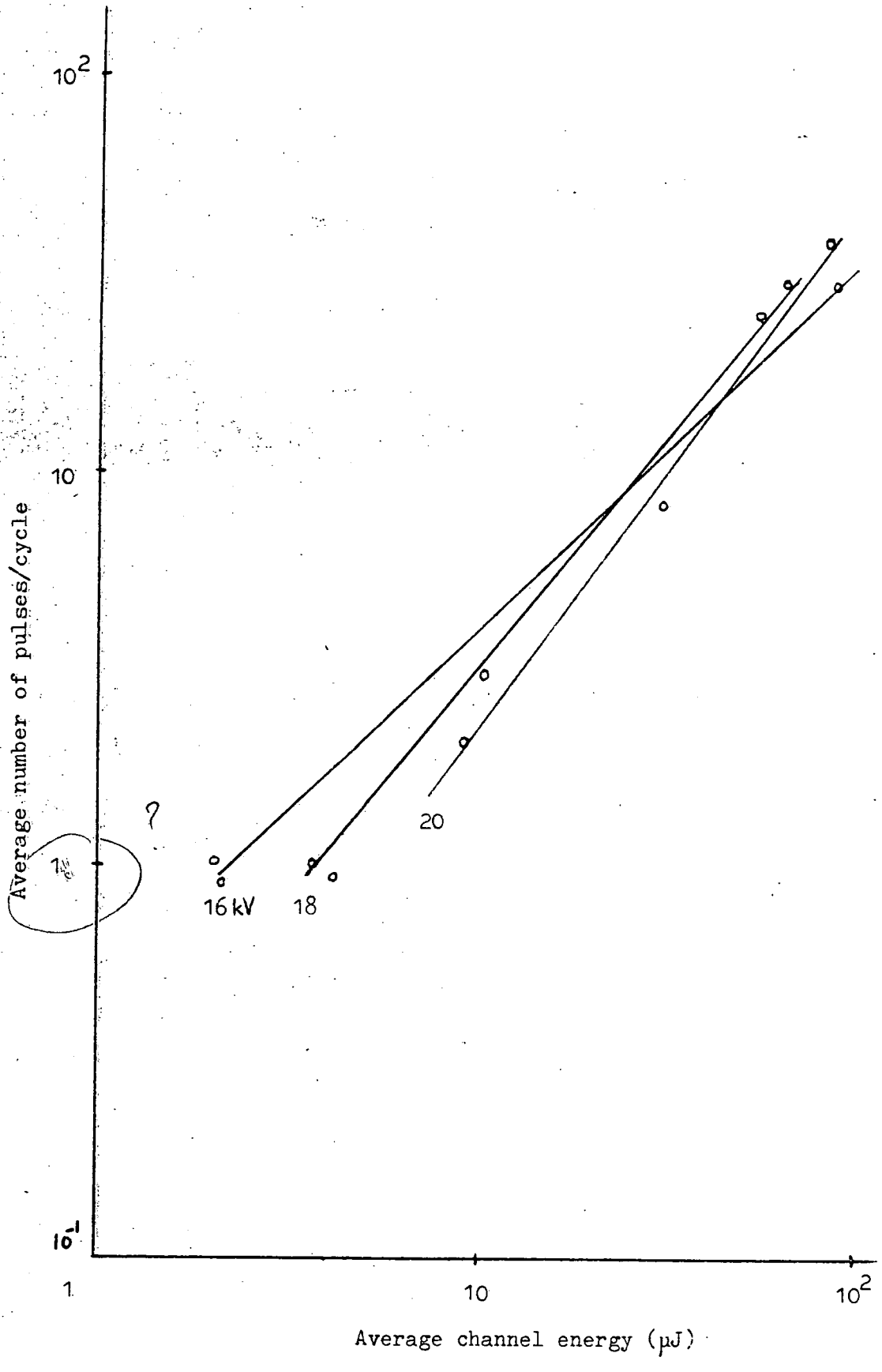

VARIATION OF DISCHARGE ENERGY PULSES/CYCLE WITH APPLIED VOLTAGE BEFORE THERMALLY AGEING SPECIMEN C - SEE TABLE 5.7.1

FIG. 5.5

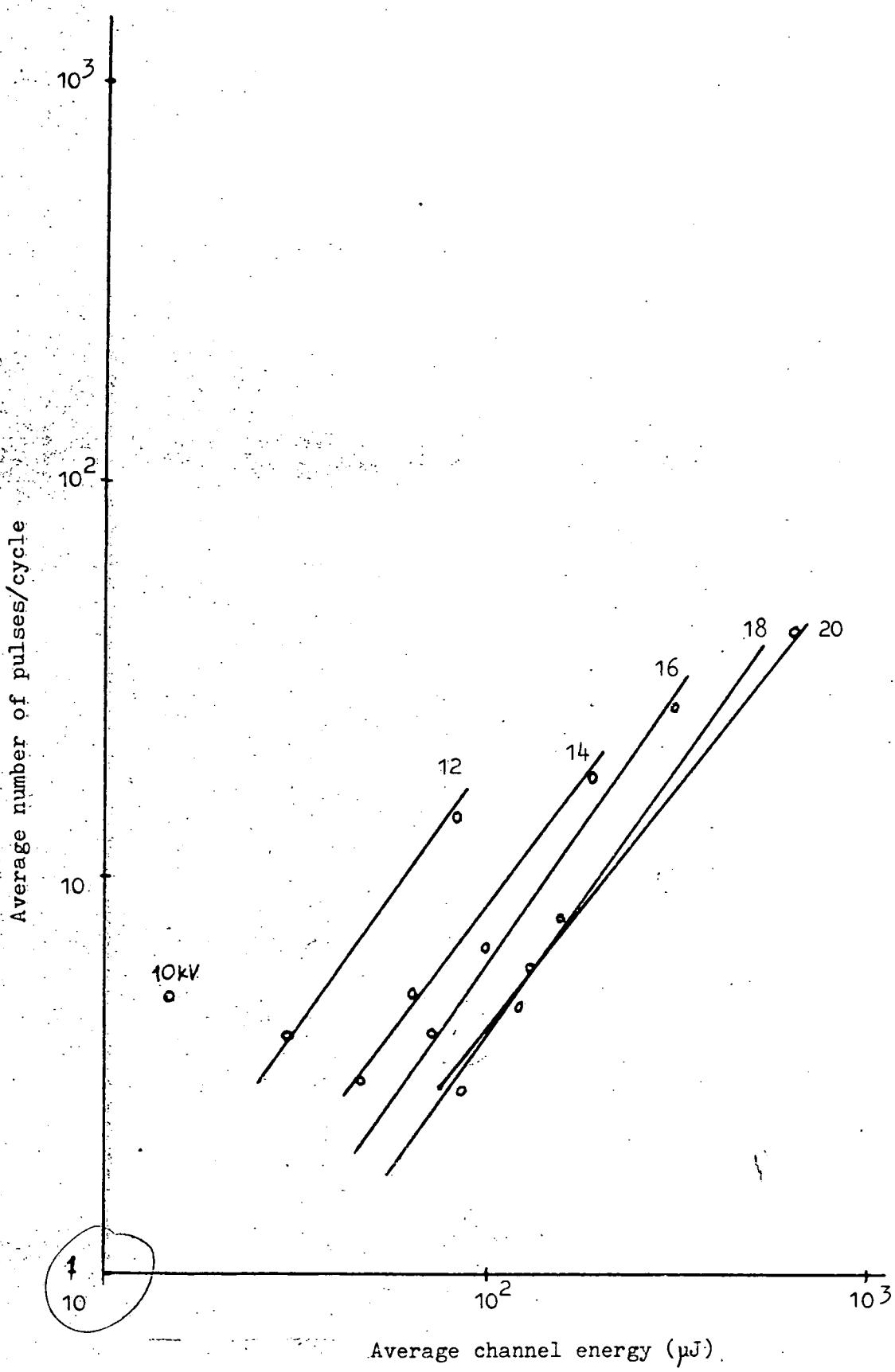

VARIATION OF DISCHARGE ENERGY PULSES/CYCLE WITH APPLIED VOLTAGE AFTER THERMALLY AGEING SPECIMEN C - SEE TABLE 5.7.1

FIG. 5.6

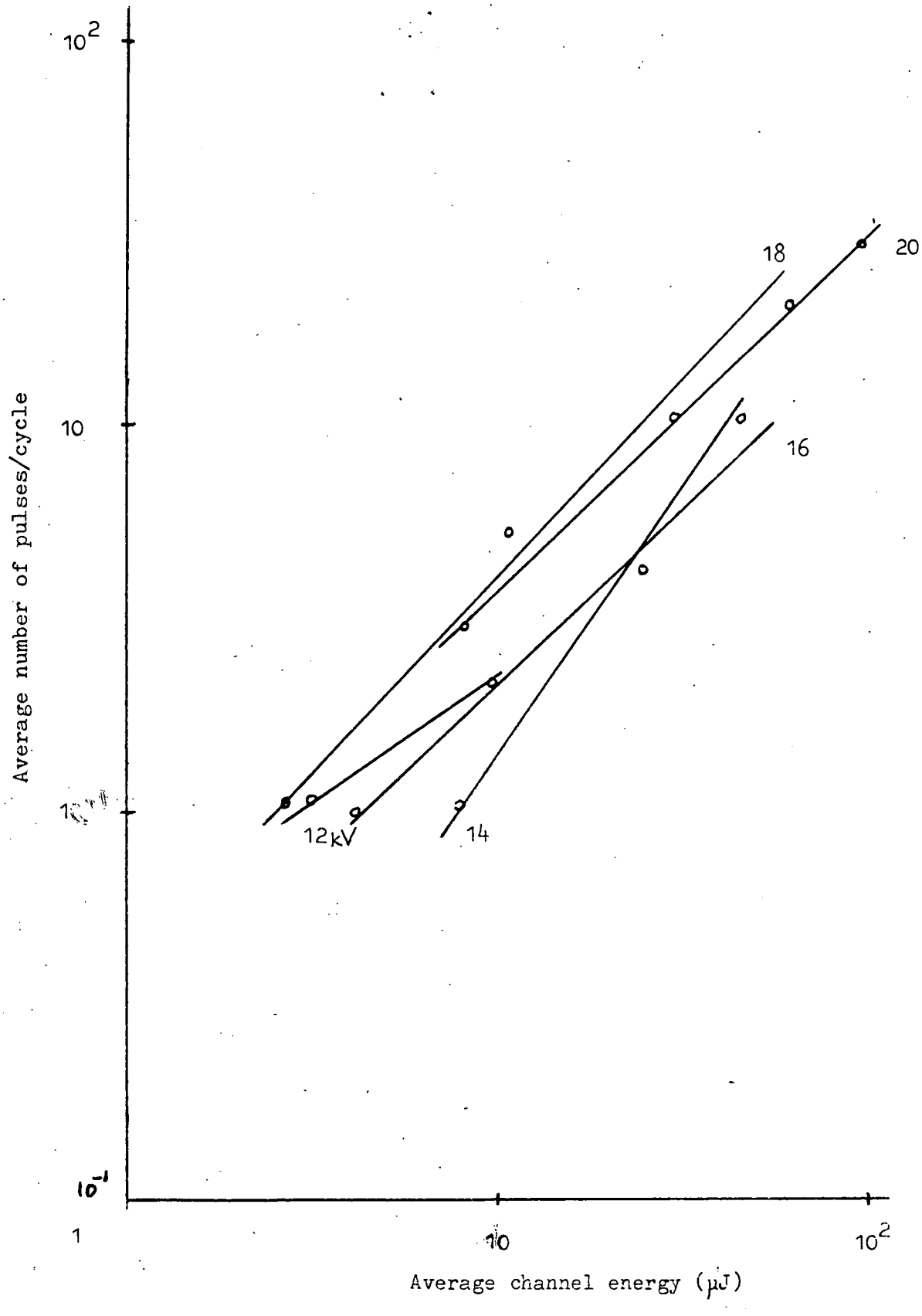

VARIATION OF DISCHARGE ENERGY PULSES/CYCLE WITH WITH APPLIED VOLTAGE BEFORE THERMALLY AGEING SPECIMEN D - SEE TABLE 5.7.2

FIG. 5.7

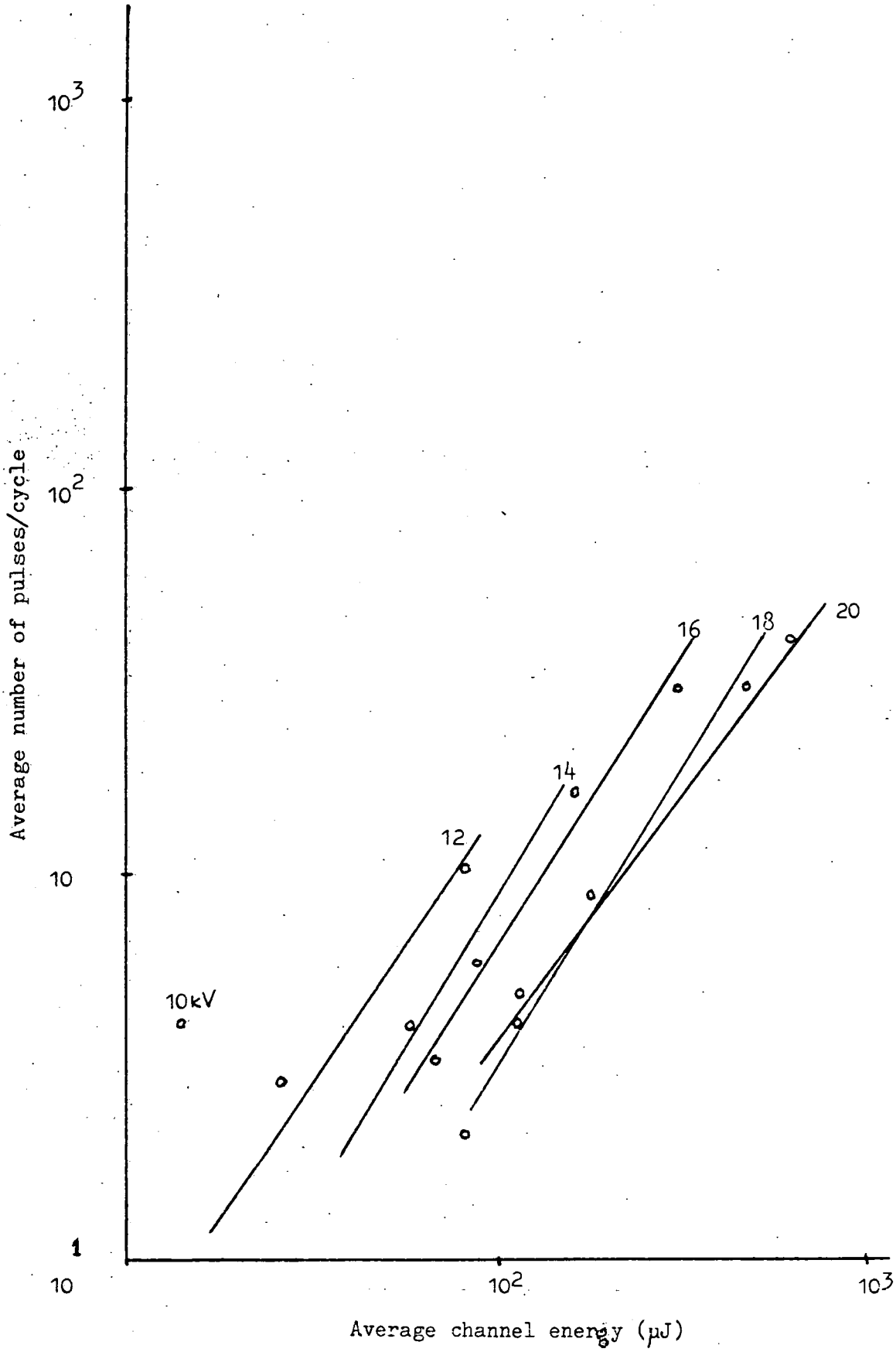

VARIATION OF DISCHARGE ENERGY PULSES/CYCLE WITH APPLIED VOLTAGE AFTER THERMALLY AGEING SPECIMEN D - SEE TABLE 5.7.2

FIG. 5.8

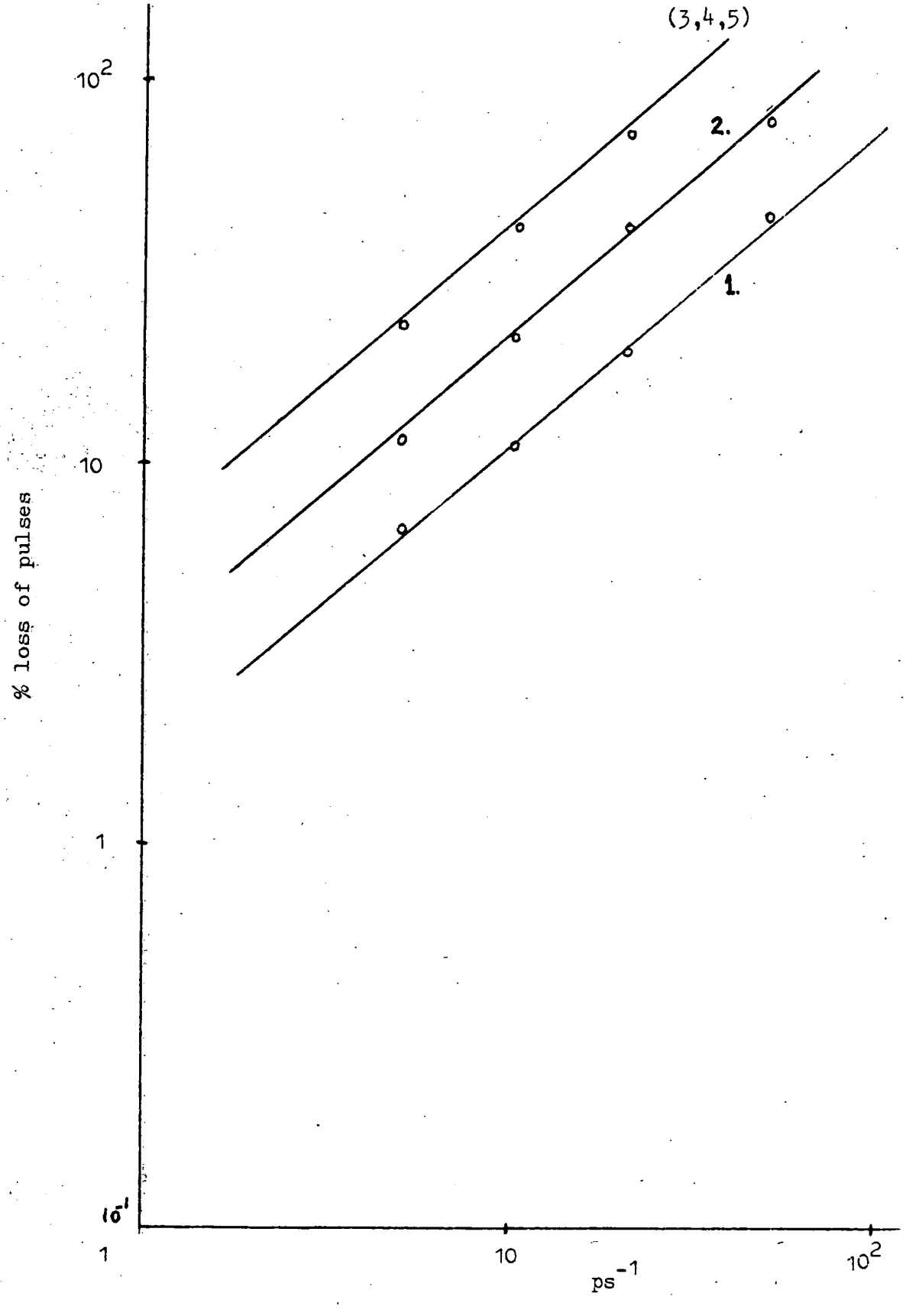

GRAPH GIVING THE STATISTICAL LOSS OF PULSES DUE TO THEIR RANDOM NATURE.

RESOLUTION TIME OF THE COUNTERS: (1) = 6 mS, (2) = 12 mS, (3,4,5) = 25 mS

FIG.5.9

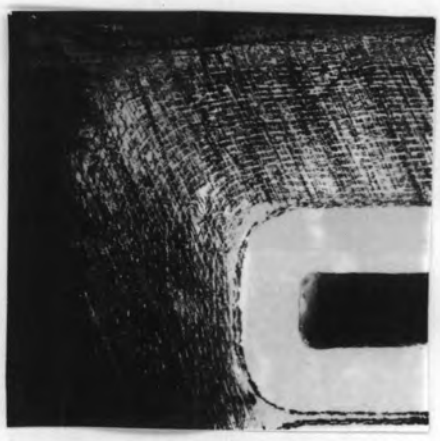

(a)

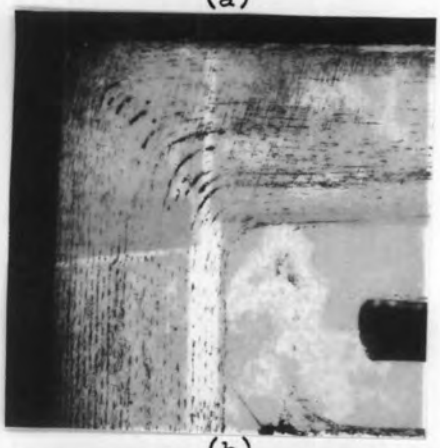

(b)

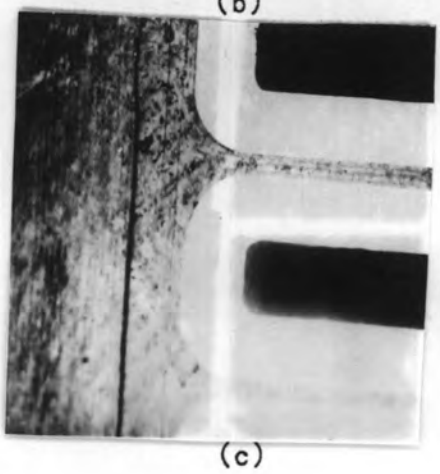

(c)

PHOTOGRAPHS SHOWING CUT-AWAY SECTIONS OF THE AGED AND NON-AGED SPECIMENS. (a) NON-AGED SPECIMEN, (b) and (c) AGED SPECIMEN C.

FIG. 5.10

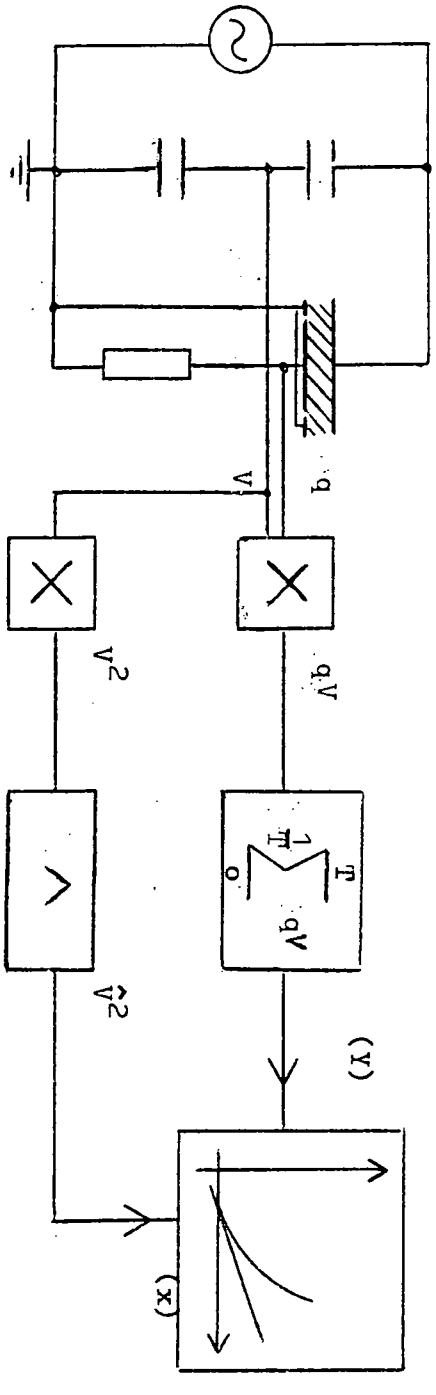

BLOCK DIAGRAM OF PROPOSED 0.1 Hz INSULATION DISCHARGE ANALYSER

FIG.6.1

REFERENCES

1. Lacotta, M.J., and Fozard, B. Electronics and Power, June 1976, pp.352-355.
2. Cooper, R. Brit. J. App. Phys. 1966, 17, pp149-16; 63.
3. Stark, K.H., and Garton, C.G., Nature, 1955, 176 p.1225; 63.
4. Whitehead, S. Dielectric breakdown of solids (Clarendon), 1951.
5. Garton, C.G., J.I.E.E., 88, Pt. 3 pp.23-40; 60, 229 (1941).
6. Garton, C.G. CERL international conference on gas discharges, (Butterworth), 1962.
7. Mole, G. ERA Report V/T115, 1952.
8. Dakin, T.W., and P.J. Malinaric. AIEE, Trans, Oct. 1960, pp.648-653.
9. Simons, J.S. IEE conference on dielectric and insulating materials, 1964, p.22.
10. McHenry, B.L. IEEE Conference Paper No. 31FP66-126, Nov. 1965.
11. IEEE, Standard No. 25, Dec. 1962.
12. Virsberg, L.G. and Kelen, A. CIGRE., 1964, Report No. 108.
13. Kreuger, F.H. 'Discharge detection high voltage equipment' (Heywood), 1964.
14. Mason, J.H. Proc. IEE, 1951, 98 Pt. 1, p.399.
15. Thomas, A.M. J IEE, 91 Pt. 11, 549 (1944).
16. Robinson, D.M. 'Dielectric phenomena in high voltage cables' (Chapman and Hall), 1936.
17. Ryder, D.M., Wood, J.W. and Hogg, W.K. IEEE Trans T-75-214-2
18. Ogilivie, K.W. ERA Report L/T 352 (1956).

19. Davis, R., Austen, A.E.W., and Jackson, W. J IEE Pt. 111 94 154 (1947).

20. Rogers, E.C. J IEE, 4, 621 (1958).

21. Denham, J.A., Hawley, R., Richardson, P., Douglas, J.L., and Lacotta, M.J. CIGRE, Paris, Paper 15-01, 1972.

22. Meek, J.M. and Craggs, J.D., 'Electrical breakdown of gases'. (Oxford Clarendon Press) 1953.

23. Halleck, M.C. Trans. Amer. IEE 95 (April 1956).

24. Dakin, T.W., Philosky, H.M., and Divens, W.C. Elect. Engr. London 73, 812 (1954).

25. Mason, J.H. ERA Report L/T 379 (1958).

26. Veverka, A. Acta Technica, No. 5 (1956).

27. Hickling, G.H., and Hawley, R. C.A. Parsons & Co. Publication.

28. Hall, H.C., and Russek, R.M. Proc IEE Pt. 11 101, 47 (1954).

29. Pelzer, H. ERA Report L/T207 (1948).

30. Bossi, A., Mirra, C., and Reggiani, F. ENEL, Research and Design Management, Rome (1967).

31. Standards project No. 433. IEEE. Dec 11, 1972.

32. Miller, R., Black, I.A., and Gray, V.N. J of Physics E. Scientific instruments, 8 Sept, 1975, pp.748-750.

33. Virsberg, L.G. ASEA pamphlet 8323E.

34. Miller, R., and Black, I.A. IEEE. Electrical insulation group. Montreal, Quebec, June 1976.

35. Black, D.F. et al. IEE Conf. Publ. 129. July 1975.

36. Widmann, W. AEG. Mitteilungen. Vol. 55, 1965, No. 1 pp.28-39.

37. IEC Publication 270, 1968.

38. Hogg, W. University of Newcastle upon Tyne, 1966. PhD Thesis.

39. Weber, E. 'Linear transient analysis', Vol. 11 (John Wiley).

40. Mole, G., and Robinson, F.C. Co-operative Electrical Research, 1963, 21 pp.8-12.

41. Widmann, W. ERA Translation 1B 1889.

42. Nigol, O. IEEE Trans. on power Apparatus and Systems, 1964, 33, p.524.

43. ASA Specification C63.2 (1963).

44. CISPR. Specifications for CISPR radio interference measuring apparatus for the frequency range 0.15-30 MHz.

45. Gelez, J. ETZ A. 1960, 81, p.129.

46. Veverka, A. and Kreisinger, V. Acta Technica, 6, 1961, p.508.

47. Dixon, H.S. Trans AIEE May 1959, p.207.

48. Goodman, R. 'Statistics' (English University Press) 1973.

49. Widmann, W. ETZ. A. June 1965, Vol. 86, No. 14, pp.458-463.

50. Black, I.A. International High Voltage Symposium, Zurich 1975. pp.239-243.

51. Franke, E.A., and Czekaj, E. IEEE Trans on electrical insulation, Vol. E1-10, No. 4, Dec 1975. pp.112-116.

52. Reynolds, P.H., and Saile, C.J. Proceedings of the 11th Electrical Insulation Conference, IEEE. Publ. No. 73cH0777-3E1-73E.

53. Buffler, C.R. and Helszajn, J. IEEE. 1968, Cat. No. 680, 38, p.231-247.

54. Mason, J.H. PPGp. Conf. 2 Dec 1976. South Bank Polytechnic London. p.18.

55. Thomas, A.M. ERA. Report. L/T 232 (1950).